Modelling construction phases of bored tunnels with respect to internal lining forces

A comparison of Finite Element Programs

D.J. Kunst

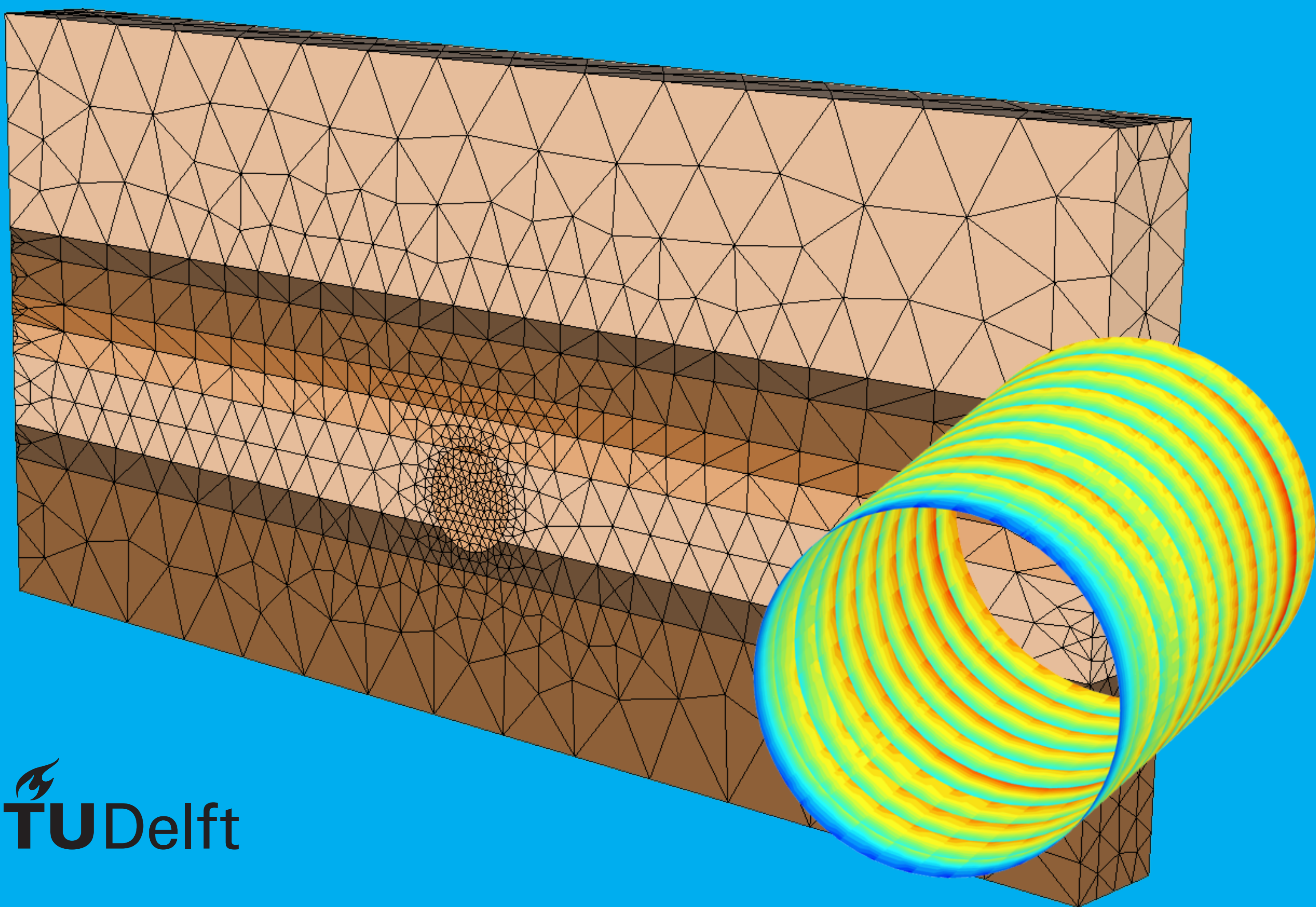

TU Delft

Modelling construction phases of bored tunnels with respect to internal lining forces

A comparison of Finite Element Programs

by

D.J. Kunst

to obtain the degree of Master of Science
at the Delft University of Technology,

Student number:	4135393	
Project duration:	October 1, 2016 – July 19, 2017	
Thesis committee:	Dr. ir. W. Broere,	TU Delft, chairman
	Dr. P. J. Vardon,	TU Delft
	Dr. ir. C. B. M. Blom,	TU Delft
	Ir. B. Safari,	Arthe Civil and Structure bv

Preface

Before you lies the thesis "Modelling construction phases of bored tunnels with respect to internal lining forces: A comparison of finite element programs".

This will be the final document in completion of the master programme Geo-Engineering at Delft university of Technology. I have worked on the research and writing from October 2016 until July 2017.

Together with Arthe Civil and Structure I have found this interesting topic in which much was to learn for both parties. It proved to be more difficult than initially expected. Days of battelling with the computer programs, only to come as winner occasionally. Fortunately, with some dedication and mostly perseverance I have been able to win a sufficient amount of times in order to answer the determined question. The sparring and joined modelling sessions together with Mr. Liem have really helped in understanding the issues and finding correct solutions. His input has helped shape this thesis.

I would like to thank Messrs. Hoffmann and Partovi of DIANA for their support with the program. With their help, I managed to create the models I could not do without in this research.

Furthermore I would like to thank Mr. Safari and my other committee members whose input during our meetings was very welcome. My other colleagues at Arthe CS have made sure I saw the humorous side of some of my situations, which I am them thankful for.

Last but not least, I would like to thank my parents, girlfriend and friends for the motivational words every now and then. It has helped me through tough times.

Please, enjoy your reading.

D.J. Kunst
Delft, July 2017

Abstract

Areas are getting more and more populated causing new infrastructure lines to be constructed below the surface. A bored tunnel is one of the possibilities to create this subsurface infrastructure, but the construction process of a bored tunnel is a complicated one. Many loads and aspects are present in this construction process that can be divided into six phases. In each of these phases, different loads and aspects are acting on the tunnel lining or the surrounding soil which can cause the lining to deform.

The increasing complexity and demands of problems have led to the use of the finite element method. A computer based method which allows one to model the problem.

For finite element modelling, numerous programs are available of which several claim to be able to model bored tunnels. However, it is not yet clear what the exact differences between the different programs are. With many aspects to be modelled, many differences between programs occur, either in the soil, the tunnel lining or a combination of both.

This research has focussed on the possibilities of modelling the different construction phases of bored tunnels in two widely used programs: DIANA and Plaxis. Simple two dimensional (2D) models were created to which the different construction phases were added before continuing with three dimensional (3D) modelling. This approach has led to a good assessment of the possibilities and limitations within these two programs.

DIANA is not yet suitable for modelling the construction process of bored tunnels completely. The construction phases are modelled undrained to account for the relative short time they are acting. A consolidation phase in which the pore pressure can dissipate cannot be modelled in DIANA, which is essential for modelling the construction phases.

Plaxis, on the contrary, is not able to model joints in the segmental lining appropriate for 3D. In 3D, Plaxis only allows to model a joints as "fixed" or "free". In DIANA different theories can be applied to the joints, including Janssens. For 2D, both programs have a rotational springs besides the free and fixed connection for modelling the joints.

For the model in which the material models were changed, the difference with the main impact between the two programs occurred, especially for the bending moment. This means the Modified Mohr-Colomb material model in DIANA is different than the Hardening Soil model in Plaxis.

Including the construction phases leads to more favourable internal lining forces for tunnels, something of which clients should be convinced. However, not until the models have been benchmarked with measured data from a tunnel project.

While 3D models have been investigated in this research, they should be extended in order have a better understanding of the different 3D phenomena that are present in the construction of bored tunnels. This will both assess the possibilities of modelling this process and more potential differences between programs can be investigated.

Besides extending the 3D models, other programs should be investigated on their capabilities too. In order to come to a proper assessment of the possibilities, program experience is strongly recommended. These programs should also be compared with measured data for benchmark purposes.

Contents

List of Figures

List of Tables

1

Introduction

With the increasing population, less space is available for infrastructural constructions. Especially in densely populated areas, moving infrastructure lines underground is necessary. Multiple applications can be used to create tunnels for these lines. For a tunnel underneath waterways, immersed tunnelling can be used. Sometimes, the cut and cover application is used, where the ground is cut open and a tunnel is created before the ground being backfilled onto the tunnel. In the densely populated areas, there is not enough space to do cut and cover and therefore mechanized tunnelling is used. Mechanized tunnelling is done with the help of a tunnel boring machine (TBM). For soils which are considered to be too soft or fluid to be stable, like in the Netherlands, a tunnelling shield is used. In a TBM, the tunnel lining (figure 1.1) is constructed directly behind the excavation from segments. The tunnel lining is the support erected in a tunnel to maintain the dimensions of the excavation. These segments are transported from the surface towards the TBM where they are placed. Concrete is a much used material for these segments, usually reinforced with steel.

Figure 1.1: Constructed tunnel where the tunnel lining is still clearly visible [39].

The design of this lining used to be done analytically. The increasing complexity of the calculations that have to be done in engineering to guarantee stability and safety has led to a new method. This method makes use of computers in order to do the calculations and is called the "finite element method." In order to decrease the complexity, a problem is divided into small elements (discretization) which are then modelled. Zienkiewicz et al. [81] provided a short and strong description about the finite element method: "a general discretization procedure of continuum problems posed by mathematically defined statements."

FEM has made it easier to model tunnel lining design and include more tunnel construction features. This has caused many tunnels to be designed with FEM. Nowadays, 2D models are used as well as 3D models. Both for tunnel lining and ground, there are many programs which can be used.

1.1. Problem Description

These many FEM program do not work the same and approach the problems differently. Especially for a 3D-continuum model there are still uncertainties regarding some modelling approaches of the different tunnelling aspects. Chakeri and Ünver [13] note that many researches have been done regarding the surface settlement for bored tunnels in which different methods have been compared as well. For the internal forces of the tunnel lining, there has been much less research about the effects of the construction process.

It would be interesting to know the difference between the different programs. Two programs are in favour to be compared: Plaxis 3D and TNO-Diana. These two programs are already widely used by engineers and in both programs lining and ground can be inserted. However, both are not regarded completely adequate for modelling ground-lining interaction. Why this is, will be discussed in section 2.4.

1.2. Research Questions

So two programs are used frequently for designing lining and both have proven to be sufficient in doing so. However, both programs do not incorporate everything. One is more sophisticated in modelling the ground, the other in modelling the lining. Yet both have to model the interaction between the lining and the ground. Therefore the main question of this research becomes:

What are the possibilities for modelling the construction phases of bored tunnels with respect to internal lining forces in Finite Element Programs?

In order to come to a conclusion on this matter, the following sub-questions have been set. These questions will also be a guideline for the process of this research.

1. **What are the loads and forces acting on a tunnel lining at every construction phase?**
   Multiple phases exist during construction of a tunnel. For every phase, the loads and forces have to be determined. The definitions and calculations of these loads will be incorporated in the answer of this sub-question.

2. **What are the possibilities in Plaxis, DIANA and other FEM programs for modelling the different construction processes?**
   The possibilities in Plaxis and DIANA will be reviewed first in order to get an idea of what is actually possible in those programs. Other FEM programs that could model ground-lining interaction and the possibilities in those programs will be discussed as well.

3. **What aspects are being modelled in order to compare Plaxis and DIANA?**
   Which loads, forces and other features will be included in the models in Plaxis and DIANA?

4. **How should the joints in the tunnel lining be modelled?**
   A major influence on the tunnel lining are the joints. How these will be modelled in Plaxis and DIANA will be discussed.

5. **What is possible in Plaxis for modelling the tunnel boring process as close to reality?**
   Out of all the different loads on the lining and the features of the program, what is possible in Plaxis. This includes the possibility of using different models and methods.

6. **What is possible in DIANA for modelling the tunnel boring process as close to reality?**
   Out of all the different loads on the lining and the features of the program, what is possible in DIANA. This includes the possibility of using different models and methods.

7. **What features are present in the model which is approximately the same for Plaxis and DIANA?**
   In order to compare the two programs, approximately the same model has to be created in both programs. Therefore it has to be known which features can be modelled in both programs.

8. **What is the difference between Plaxis and DIANA for modelling the ground-lining interaction of a bored tunnel for every step in the process?**
   The steps in the process will be explained in chapter 3. For every step, Plaxis and DIANA will be compared. This way there will be early comparison results and will make it easier to assess whether the modelling is accurate.

2
Literature Review

In this chapter, a summary will be given of the literature that has been reviewed. First, multiple aspects of the tunnel lining design will be discussed. In section 2.2, the loads that have to be included in a design will be discussed. Section 2.3 discusses the different aspects of the lining and the different theories behind the design. These theories will be elaborated as well. Multiple finite element programs are reviewed in section 2.4 which have been used by other authors to model the construction process of a tunnel. They are also graded based on the documentation found of the programs on features that are important for modelling this process. Different parameters of the ground, lining and grout are discussed on their influence of the structural forces in the lining in section 2.5. Section 2.6 reviews the different material models for soil and lining. The method for including ground-lining interaction is also described. Finally, in section 2.9 the properties are discussed of the final model. It is the intention to create this model and it will include all the different aspects of the tunnelling process so a realistic model is created and a good comparison can be done between the two programs.

2.1. Design procedure

According to the I.T.A. [42], a tunnel shall be designed according to the following steps:

1. **Adhere to code, standard or specification**
   Every tunnel that will be designed has to follow an appropriate code, standard of specification. In the Netherlands the "Richtlijnen ontwerpen kunstwerken" can be used which are largely based on the European Code, the Eurocode. Which codes, specification or standard to follow is decided by the people who are in charge of the project.
2. **Decide on inner dimension of the tunnel**
   The inner diameter of the tunnel depends on the functions that are needed in the tunnel. For example, for traffic it is the number of lanes needed, for water tunnels the required discharge affects the tunnel diameter.
3. **Determine load conditions**
   The loads and forces that may be acting on the lining are discussed in section 2.2. Which of these loads have to be included in the design, has to be decided on.
4. **Determine lining conditions**
   Also a decision has to be made about the lining. The thickness, the reinforcement etcetera all have to be decided on.
5. **Compute member forces**
   Based on the previous steps, member forces have to be calculated. The member forces are the bending moment, axial and shear force. These forces have to be calculated by using the appropriate material models for soil and concrete but also the appropriate calculation method.
6. **Safety check**
   The tunnel lining has to be checked for safety against the calculated member forces.
7. **Review**
   If the safety check came out as unsafe, the design has to be altered. If the safety check came out as incredibly safe, the design may want to be altered as well for a more economical design.

8. **Approval**
   When the designer judges that he has met all the requirements and the design is safe, the person in charge has to approve the design.

At step five, it states that the right design model has to be chosen. The first distinguishment that can be made for design models is analytical and numerical. Analytical models use mathematical techniques in order to find the exact solution of an equation while in numerical models an approximate solution is to be found. Most problems are so complex that an analytical solution is not possible. Analytical models are still used to get insight in the equation and the effects of the parameters [58]. More about design models will be discussed in section 2.3.

2.2. Loads, forces and deformations

In the design of this tunnel lining, the following loads should be taken into account [18, 42]:

- tunnel weight
- ground pressure
- water pressure
- subgrade reaction
- grout pressure
- surcharge
- construction loads
- temperature load
- traffic loads
- installations
- adjacent tunnels
- special loads

Tunnel weight
With tunnel weight, the weight of the concrete segments is meant. It is a vertical load which acts on the underlying soil. It is determined by the density of the reinforced concrete (2500 kg/m^3) and the volume of the tunnel lining [18].

Ground pressure
All the ground above the tunnel provides a pressure on the tunnel lining. This pressure should act radially on the tunnel lining or it should be divided into a vertical component and a horizontal component. The vertical component (vertical earth pressure) works at the crown of the tunnel and is equal to the overburden pressure. The horizontal component is called the lateral earth pressure and can be determined by multiplying the vertical earth pressure with a lateral earth pressure coefficient (fig. 2.1a). It can also be defined as an uniform load (fig. 2.1b) or as uniformly varying load (fig. 2.1c) [42].

Water pressure
In the Netherlands, it is common that the tunnel is constructed underneath the water table. Therefore a water pressure will act on the tunnel lining (figure 2.2). This water pressure depends on the hydraulic head of the

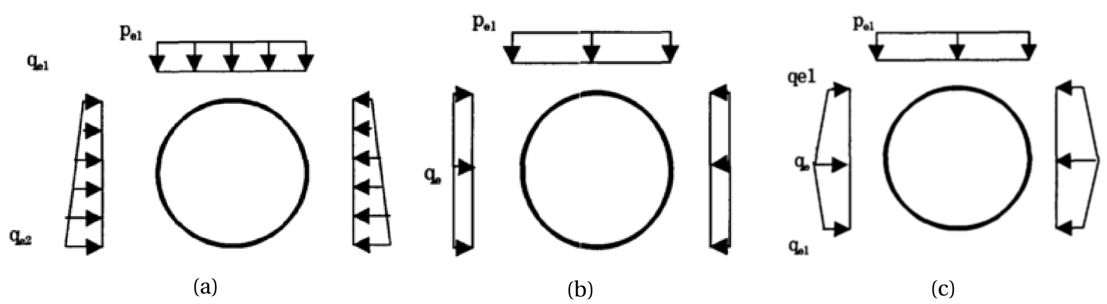

Figure 2.1: Three different ways to evaluate ground pressure load acting on tunnel lining [42].

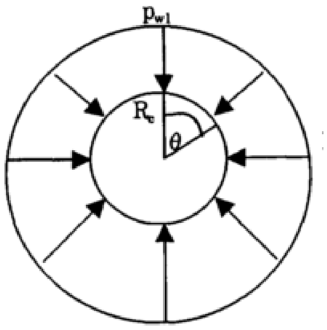

Figure 2.2: Water pressure load acting on tunnel lining [42].

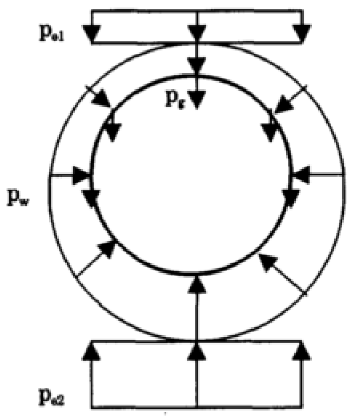

Figure 2.3: Vertical subgrade reaction on the tunnel lining [42].

layer the tunnel is in [18]. The water pressure at the bottom of the tunnel is usually higher than the pressure at the top due to a larger hydraulic head and this upward resulting pressure on the lining is called buoyancy [42].

Subgrade reaction
If the earth pressure and tunnel weight combined are greater than the buoyancy there will be a soil reaction called "subgrade reaction". This subgrade reaction is any soil reaction, either vertical or horizontal (fig. 2.3) [42].

Grout pressure
Grout is injected under pressure into the tail void behind the TBM to prevent any deformations of the soil. To prevent the deformations, the grout needs to withstand the pressure and it therefore needs to be larger than the pressure of of the ground and the water combined. Since the grout pressure distribution is not exactly known, the tunnel lining is designed by using multiple excessive values given by COB-L500 [18]. This grout pressure is not used in every tunnel design. In the calculation method proposed by COB-L500 [18], this grout pressure is the main difference compared to other methods.

Surcharge
Surcharge is made up out of loads or weights that increase the earth pressure on the lining. The following can act as a surcharge [18, 42]:

- Traffic (traffic; railway) load
- Weight of buildings
- Landfill loads

These loads and weights may results in an asymmetrical pressure on the lining, depending on where the loads are located.

While excavations at the surface decrease the earth pressure instead of increasing, thus not a surcharge, it should be included in the design. Loss of ground pressure reduces the subgrade reaction and might cause it to become negative. This means the buoyancy will be larger and the tunnel will start floating.

Construction loads
A TBM jacks itself forwards to excavate more soil for the construction of the tunnel. Apart from this, more forces and loads are present during the construction stage [18, 42]:

- Loads during transportation and handling of segments
- Load by operation (steering, jacking)
- Pressure in front of TBM
- Weight of TBM

Temperature load
Temperature may vary throughout the year due to the influence of the seasons. This leads to temperature changes in the ground and tunnel as well. Both have an influence on the tunnel lining and should therefore be taken into account. Variations for the temperature of the inside and outside wall of the tunnel lining are given in COB-L500 [18]. Within the tunnel lining, it is allowed to assume a linear gradient between the inside and outside wall. During the construction of the tunnel, the TBM produces heat. For the Netherlands, the temperature during construction is set at 25°C.

Traffic loads
Traffic (train, road) inside a tunnel induces a load on the lining. Multiple guidelines for both types of traffic are available and can be used for deducting the loads to be used in the design [18].

Installations
Non-traffic loads are also present inside the tunnel and they can influence the design as well. Facilities hanging on the ceiling may create an extra load for example.

Adjacent Tunnels
Sometimes a tunnel project involves constructing two tunnels next to each other. One large tunnel is too expensive to construct or there is not enough space for such a large tunnel. However, a smaller tunnel does not provide the required extra space for infrastructure and therefore two tunnel are constructed. In two different ways, an adjacent tunnel influences the loads:
1. Loads during drilling of adjacent tunnel
2. Loads due to presence and use of adjacent tunnel

During drilling of the adjacent tunnel, the shape of the TBM and the grouting of the tail void cause an additional load. The size of the TBM and the grouting procedure influence the quantity of the load. The distance between the tunnels is also of important for assessing whether the adjacent tunnel influences the tunnel loads. Whether the distance is sufficient depends on various factors:
1. depth
2. soil structure
3. TBM shape
4. grouting pressures
5. strength of lining
6. already acting forces in tunnel lining

If the distance between the two tunnels is more than 1/4 of the diameter, the influences are negligible [18].

Special Loads
Apart from the loads mentioned above, there are some special loads [18]:
- Explosion
- Fire
- Earthquakes
- Incomplete grouting

2.2.1. Construction phases
The loads discussed in section 2.2 do not act at the same time, a distinction can be made between loads during construction and during use. Even the construction stage of the tunnel can be divided into several phases. Each of these phases is important to include since other loads may act and therefore the phases have to modelled separately. Bernat and Cambou [5] distinguished four different phases in their research on settlements caused by tunnel construction.
1. Before and during excavation
2. Passing the TBM
3. Escaping the tail
4. Consolidation of grout

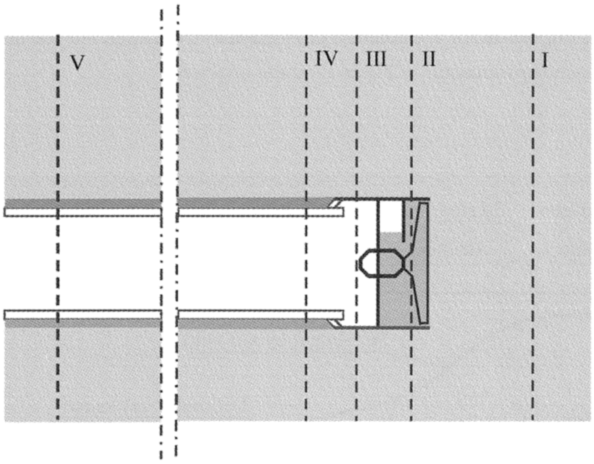

Figure 2.4: The first five construction phases distinguished by Bakker [4], the sixth phase is long term effects.

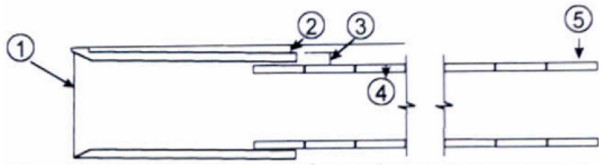

Figure 2.5: The five construction phases determined by Mair and Taylor [60] after Cording [25].

When passing the TBM, the TBM is supporting the ground. With "escaping the tail", the zone behind the TBM with liquid grout is meant. With regard to ground movement, Bakker [4] separated the first phase of Bernat and Cambou [5] into **1.** Before **2.** after excavation. For modelling the construction of a tunnel, Bakker [4] also adds a sixth phase: long term effects. Excessive pore pressure may dissipate and creep may occur as part of the long term effects (fig. 2.4).

For the grouting process, COB-L500 [18] determined three phases: **1.** Lining in TBM **2.** Wet grout **3.** Hardened grout. These three are the same as mentioned by COB-L520 [20] and they coincide with the phases found by Bakker [4] and Bernat and Cambou [5].

Finno and Clough [33] and Mair and Taylor [60], have categorized five construction phases, they coincide with the six phases from Bakker [4] but leave out the first phase (before excavation).

Concluding, there are six phases in constructing a tunnel:

1. Before Excavation
2. During Excavation
3. TBM passage
4. Tail void with liquid grout
5. Consolidated grout
6. Long term effects

2.2.2. Loads during construction phases

As mentioned in section 2.2.1, not all the loads act on the same time and it can differ for each construction phase. Therefore, it will be described in which phase, which load is acting. To classify every load mentioned in section 2.2 in a phase, the phase when the tunnel is in use has been included. Ground loads are acting in every phase of the tunnel. Water loads are acting in every phase as well when a tunnel is being constructed close to the water table. Surcharge and an adjacent tunnel may act in every phase of the tunnel. In the tail void phase, these four mentioned loads are not acting on the lining.

Before excavation

The ground and water in this phase are used to calculate the initial stresses in the ground [4], in case there is no surcharge or adjacent tunnel. Otherwise those have to be included in the stress calculations. Loads other than these four are not present in this phase.

During excavation

While excavating, a construction load is added. Since the TBM is pushed forward, it puts a load on the ground in front of the TBM and the ground puts a load on the TBM face.

TBM Passage
When the TBM passes, excavation has taken place. The tapered shape of the TBM leaves a void behind after the bore front has passed. This void is filled with grout adding a grout pressure load on the ground. The void may allow the soil to contract, adding the possibility of a subgrade reaction. The TBM itself is now present, which results in some additional loads. The weight of the TBM is one, but the heat that the TBM produces, poses an extra temperature load as well.

Tail void with liquid grout
In the tail void, the tunnel lining has left the TBM. This means the weight of the TBM is not present in this phase. The backup train attached to the TBM is present and therefore its weight. Jacking by the TBM on the tunnel lining is now added as a construction load. The tunnel weight itself is also present, posing an additional load. The ground and water pressure are present but they are acting on the liquid grout. The same accounts for surcharge and subgrade reaction. The grout pressure takes all the pressure coming from outside the tunnel and exerts those onto the tunnel lining. Therefore ground, water, surcharge and subgrade reaction are present, but when considering the lining, only the grout pressure is acting.

Consolidated grout
In this phase, the grout has completely consolidated and therefore no grout pressure is active any more. The gap can now be considered closed and from now on the ground and water pressure (and surcharge) will be acting on the hardened grout and thus the lining.

Long term effects
For the long term effects, the ground and water pressure may alter. If the boring has caused excessive pore water pressures, these will now dissipate [33]. Creep effects may also occur in this stage [4]. The TBM has now moved forwards so much that no construction loads are present any more, also not from the follow carts. The temperature load has switched from being caused by the TBM towards being caused by seasonal temperature changes. Long term is a statement which may consume a large timespan. Therefore the line between the long term and 'in use' phase cannot be specified clearly.

In use
Finally the tunnel can be taken into use and the traffic, special and loads from inside have to be taken into account. Long term effects described at phase 6 may also still occur.

		Phases						
		1 before excav.	2 during excav.	3 TBM passage	4 tail void	5 consol. grout	6 long term	7 in use
Loads	tunnel weight			x	x	x	x	x
	ground pressure	x	x	x		x	x	x
	water pressure	x	x	x		x	x	x
	grout pressure			x	x			
	surcharge	x	x	x		x	x	x
	subgrade reaction			x		x	x	x
	loads from inside							x
	construction loads		x	x	x	x		
	temperature load	x	x	x	x	x	x	x
	traffic loads							x
	adjacent tunnels	x	x	x		x	x	x
	special loads							x

Table 2.1: Overview of the loads present for each phase of the tunnel construction.

2.2.3. Lining deformations

All these loads cause the tunnel lining to deform or displace and multiple types are possible [18]:

1. global deformation of tunnel axis
2. ovalisation
3. displacement of rings
4. buckling

With regards to the global deformation of the tunnel axis, the realised alignment deviates from the planned one. Vertical or horizontal displacement of the tunnel lining causes this deviation. The vertical displacement can be caused by settlements underneath the tunnel, but "negative" settlements also may occur. This is caused by buoyancy as described in section 2.2. At the start and receiving shaft, the tunnel is fixed and no displacement can occur, only rotations. If vertical or horizontal displacement of the tunnel occurs, the tunnel lining is bended, causing additional loads in the tunnel lining. This phenomenon will be discussed in section 2.3.3. Moreover, if the alignment differs, it may not satisfy the requirements any more.

This settlement or buoyancy may also cause the rings to displace relative to each other. This will happen when the local shear resistance of the joints is exceeded, more about this will be discussed in section 2.3.4.

The most important deformation type is ovalisation. This is applicable to a tunnel ring. For ovalisation, the vertical loads at the crown and bottom of the tunnel are the largest while the horizontal loads at the sides of the tunnel are smaller (fig. 2.6a). This deforms the tunnel into an oval with the sides of the tunnel moving outward laterally and the crown and bottom move inward vertically (fig. 2.6b). This happens since the tunnel lining needs to find the right ground reaction in order to reach an equilibrium between the loads [2]. This deformation leads to bending of tunnel segments and rotations of joints about which will more be discussed in section 2.3.4. In the rare case of larger horizontal than vertical loads, vertical ovalisation can occur as well. Blom [7] discusses the ovalisation loads and how they migrate through the joints in his thesis.

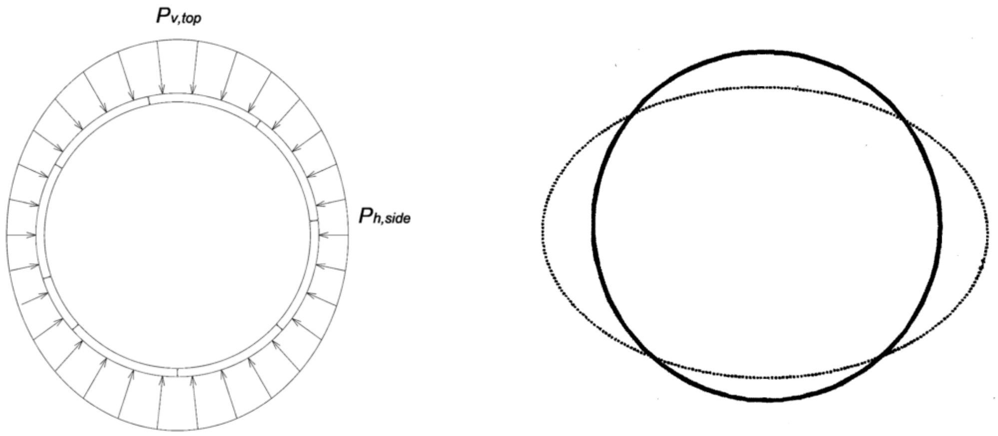

(a) Ovalisation load [2]

(b) Ovalisation deformation [18]

Figure 2.6: Ovalisation load (a) and the deformation caused by this load (b).

There is one more deformation type and it is called buckling. It happens when the tunnel lining is not able to withstand the forces any more due to large deformations of the lining [7]. There are three ways for buckling to happen [18]. **1.** folding of beam: The global deformations may lead to bending which cause the tunnel the fold. If the lining is unable to withstand the generated force, this may cause the lining to snap trough. This is very unlikely to happen due to the favourable ratio of lining thickness and tunnel diameter. **2.** Snap through: In a tunnel ring, the segments cannot withstand the normal force and cause them to snap through. **3.** Joint shearing: The shearing resistance cannot withstand the forces on the lining and one segment buckles through shearing along a longitudinal joint. This is more common to occur for special loads like explosion or collision loads.

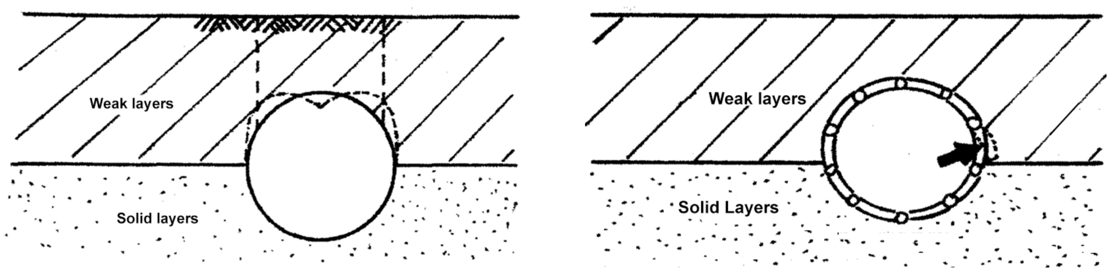

(a) Snap through (b) Shear buckling

Figure 2.7: Two types of buckling deformation of tunnel lining [18].

2.2.4. Slip or bonded ground-lining interaction

These deformations depend on how the load is acting on the tunnel lining. The interaction between the ground and lining plays an important role. For modelling this interaction, two extremes can be chosen for the boundary of the tunnel lining with the soil. These extremes provide two boundaries between which the actual stress state of the lining can variate [21]. The tunnel lining is fully bonding with the surrounding ground, so at the interface between the ground and the lining there is friction. There can also be no bonding at all which means there is no friction at the interface between the lining and the ground. These two options are called "bond" or "slip" modelling respectively. For bond modelling, the ground is perfectly attached to the lining. This may cause shear stresses to develop between the ground and lining. With slip, these tangential stresses will not be transferred between the soil and the lining [65]. Slip may be caused by grouting, ground water and temperature differences. This will lead to a reduction of the effective stress below the tunnel [18]. Modelling slip or bond translates into a difference in bending moment for different calculation methods. For bond, all the calculation methods have approximately the same bending moment results. While for slip, the different calculation methods differ in moment results [16].

2.3. Tunnel lining design

For designing a tunnel, different design approaches are available. The internal forces in the tunnel lining can be calculated by using analytical or numerical methods. These methods are used for different calculation models which are divided into ring and beam action models.

2.3.1. Schulze-Duddeck method

One of the first methods developed was the method by Schulze and Duddeck [71]. Many German bored tunnels have been constructed based on this theory and even nowadays it is still used in preliminary designs. While trying to approach reality as close as possible, the complexity of the models and calculation was kept as low as possible. Therefore, assumptions have been made in this method:

- Soil only supports the tunnel in a radial direction. The soil and tunnel can move free from each other in the tangential direction [18].
- The surrounding soil behaves linear elastic and deforms under plane strain conditions [18].
- The soil loading on the lining is determined from the initial soil loads of untouched ground at the depth of the tunnel axis [18]. This also assumes that the ground wants to return to the same state as it was before the construction of the tunnel [32]. From the converted loads, the forces in the lining are determined from ground-lining interaction graphs proposed by Schulze and Duddeck [71].
- Clay and peat have not been included in the graphs and therefore it is questionable whether this method can be used in Dutch conditions [58].
- The hydrostatic pressure is not increased along the tunnel depth. This is assumed in other to meet a load equilibrium [18].
- The depth is of great importance with this method. Three different areas can be distinguished based on the height of the overburden and the diameter of the tunnel.
  - height < two times the diameter
  - two times the diameter < height < three times the diameter
  - height > three times diameter

For the overburden height smaller than two times the diameter, support is only applied on the part of the lining where it deforms outward. This mean than 90°along the crown of the tunnel is unsupported by the soil. When the overburden height is larger than three times the diameter, the entire ring will be supported by the soil. If the overburden height is between two and three times the diameter, it is depending on the cohesion of the soil whether the top of the lining is supported or not [9, 18, 56].
- One homogeneous soil layer is located around the tunnel lining. So this method is not applicable when the tunnel crosses multiple soil layers [1, 18].
- The tunnel is made of an homogeneous ring. Joints are not applied in this method [58].
- The force distribution by Schulze and Duddeck [71] does not apply for liquid grout. It can be used for consolidated grout, but this approach does not take into account the liquid grout circumstances [8].

While many assumptions have been made, this method is still widely used. As can be deducted from the different assumptions, different phenomena are present in the structural behaviour of a segmental tunnel lining. The complexities of these phenomena cannot be taken into account with this method. A few of these phenomena and its complexities are described in sections 2.3.2, 2.3.3 and 2.3.4. These complexities can be modelled in finite element programs.

2.3.2. Ring action

In the ring action model, it is assumed that along the axis the loads are the same or deviations are too small to be included. Therefore, one ring of the tunnel lining is schematized together with the surrounding soil and only circumferential directed lining stresses are included.

Within a ring model, the ground is either schematized as discrete springs, two-dimensional or three-dimensional elements.

Discrete Springs

When using the discrete springs, the tunnel is modelled as a elastic supported ring which is stiff for both bending and strain. The discrete springs are the support of the tunnel. The tangential and radial stiffness for the springs are not connected and can be developed separately. The radial and tangential loads from the ground are directly attached to the lining. Furthermore, it is a one-dimensional model and therefore spatial effects cannot be taken into account. These discrete springs models can be calculated by using an analytical method [56].

2-dimensional continuum

The schematization of the problem with two-dimensional elements is a finite element method in which a continuum model is discretized. These finite element methods are more complex than the discrete spring model. For a preliminary design, analytical methods are often used. For final design or special effects, finite element methods are used. Some effects, for example the influence of soil layering, cannot be modelled with the discrete spring model described in section 2.3.2. However, the complex behaviour of the ground can be described by using material models for the soils in the finite element programs [56], including the influence of soil layering.

3-dimensional continuum

Tunnel excavation is a three dimensional problem [35]. Especially in the Netherlands the third dimension in tunnel lining design plays an important role. Because of the soft soils in the Netherlands, of which the properties can vary significantly, differential settlements may occur. If this happens, the tunnel lining is loaded differently along the axis of the tunnel. This non-uniform loading over the tunnel axis causes a change in internal forces in the tunnel lining. When modelling the problem with three-dimensional elements, both the ring action as well as the beam action are included, more about beam action will be discussed in section 2.3.3.

2.3.3. Beam action

As described in section 2.3.2, the load conditions in axial direction on the tunnel lining may vary. This can happen for various reasons [9]:

1. Difference in support
   While the tunnel load may be distributed equally, differential settlements can be caused by differences in stiffness for the supporting soil underneath the tunnel. The differential displacements cause a change in internal forces in the tunnel lining;

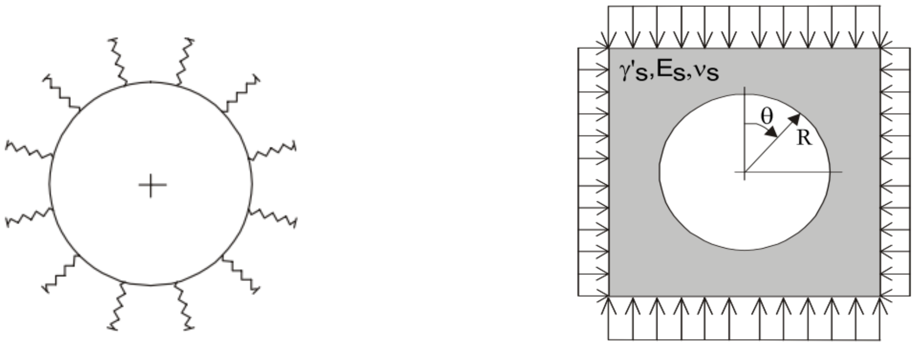

(a) (b)

Figure 2.8: A spring model (a) and a continuum model (b) for radial action [58].

2. Unequal soil loading
   The soil above the tunnel can be unequally loaded. Either by another tunnel that crosses the new tunnel or at the surface by buildings and roads. This unequally loaded soil can result in differential settlements of the soil and therefore unequal loading on the tunnel lining;

3. Consolidation
   This may cause differential settlements over time and therefore create a change in internal forces;

4. Fixated start and end
   At the start and end shaft, the tunnel is fixated. No vertical displacement will occur while rotating is possible. This can also lead to a change in internal forces;

5. Construction loads
   During construction, there is the load of the tunnel boring machine and everything that follows. Furthermore, a tunnel boring machine can also change course. Both bring an extra load on the ground and tunnel lining and may cause differential loading as well;

6. Buoyancy
   The tail void is injected with liquid grout. While the grout is liquid, the tunnel may suffer uplift until the grout is solidified. The uplift can cause a change in internal forces [18].

The analysis of these load conditions is called the beam action [58]. These loads can cause the tunnel to bend (figure 2.9a). Apart from the three-dimensional model described in section 2.3.2 in which both beam action and radial action are included, there is also a one-dimensional beam action model (figure 2.9b). In the one-dimensional model, the mechanics of the tunnel and the supporting ground can be set. Like with ring action, the ground is schematized by discrete springs [56]. In the three-dimensional model, the effect of the variation in load conditions in the axial direction can only be modelled by using multiple rings.

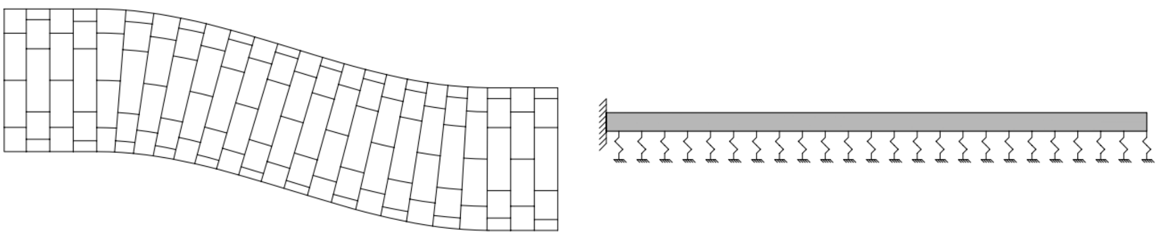

(a) (b)

Figure 2.9: Bending of the tunnel lining (a) and a simplified one-dimensional model of beam action (b) [58]

Types of beams
Bending of the tunnel causes an internal bending moment. Besides this moment, another internal force may occur in the tunnel lining for beam action, shear force. Therefore a tunnel can be considered as two types of beams or a combination of those types, a shear and a bending beam (figure 2.10). A nice explanation of the structural theory behind these beams is given by Bouma [10].

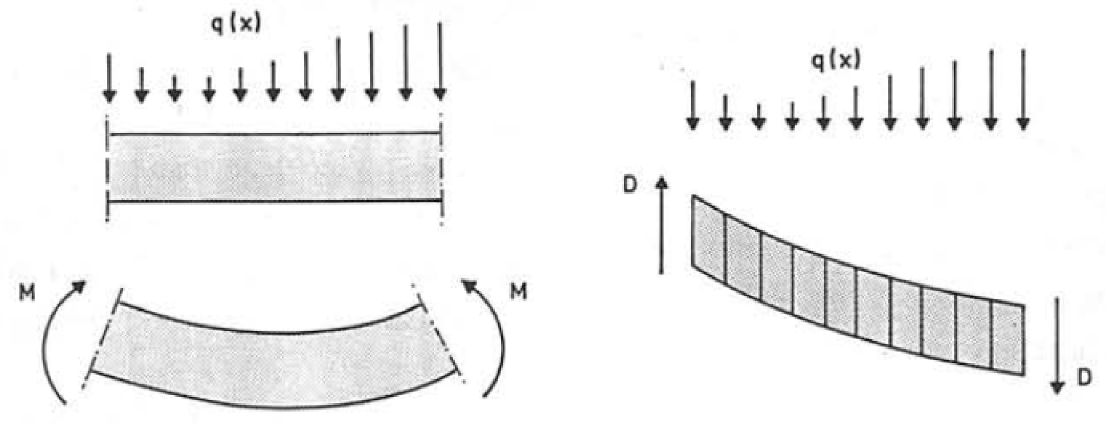

(a) (b)

Figure 2.10: A bending beam (a) and a shear beam (b) [10]

2.3.4. Joints

Both for radial and beam action, a critical issue has to be included in the lining design. In shield tunnelling, the lining is constructed in segments, as previously mentioned in chapter 1. Erecting the lining from segments has the consequence that a ring is a structure with multiple hinges. Furthermore, placing rings next to each other creates an extra hinge in the tunnel lining as well. These hinges are called joints and two types can be identified: longitudinal and circumferential joints. The longitudinal, radial or segment, joint is located between two segments in one ring. The circumferential, lateral or ring, joint is located between two consecutive rings (figure 2.11).

To ensure longitudinal joints are not continuous, usually a staggered configuration of the segments is applied, the so called masonry layout. Multiple elements can be present in a joint [56]:

1. Bolts (non/temporary/permanent)
2. Connection system
3. Packing material
4. Water seal

Bolts are applied to connect the segments and increase the bending stiffness of the tunnel, on which will be elaborated in section 2.3.4. Bogaards [9] shows different types of bolting.

Connection systems
There are also different kinds of connection systems between segments. The most used systems are:

1. Flat
2. Tongue-groove
3. Dowel-socket
4. Convex
5. Cam-pocket system

For a flat connection system, it can either be flat over the entire thickness of the segment (figure 2.12a) or it can have a reduced contact area (figure 2.12b). With a flat joint, the coupling between segments is only through friction and it supports itself without purposely interacting with other segments [59]. The flat surface does allow rotation and therefore can transfer bending moments. The tongue-groove is usually applied in the circumferential joints and consists of a groove in one of the rings while the connecting ring has a tongue

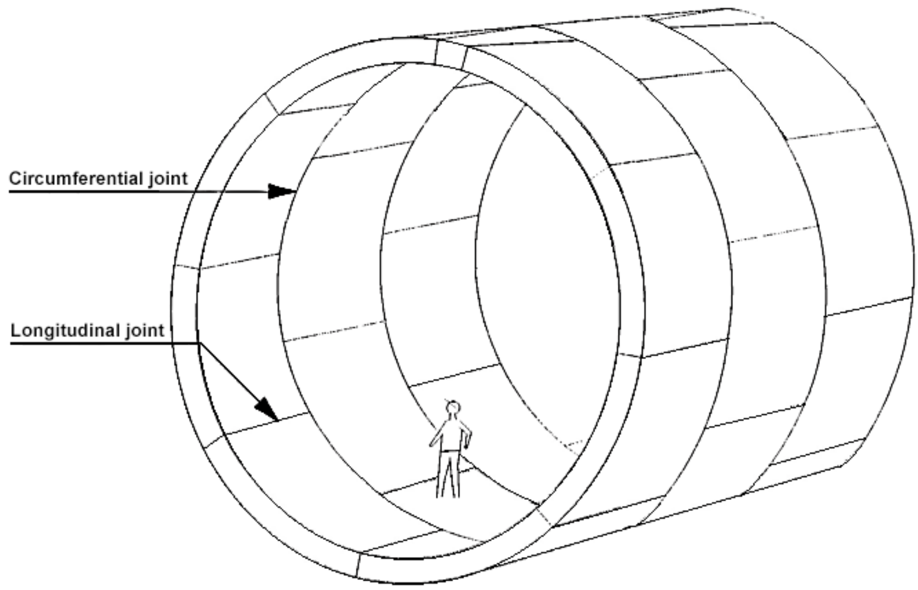

Figure 2.11: Definition of circumferential and longitudinal joint [24].

shape that fits with the groove (figure 2.12c). The dowel-socket system is a variant on the tongue-groove system but the groove is deeper and the tongue is higher. This allows it to be reinforced [24]. Another variant to the tongue-groove system is the convex-concave system (figure 2.12d). Another connection system is the cam-pocket system which is a point coupling system (figure 2.12e). The loads in this system are more locally restricted compared to distributed over the entire ring joint in the tongue-groove system. The last four systems help to centre the segments during placement and also limit the displacement differences between segments [7].

These systems cause two rings to come in contact. An un-smooth surface may lead to local peak stresses for concrete-to-concrete contact. This can be countered by using packing materials. These packing material types will introduce the internal forces into the next ring and two types are commonly used: plywood and kaubit. A shear force may develop in the plywood when different deformations occur in adjacent rings. This friction with the concrete will establish a cooperation between the two rings. Long term effects of the plywood, however, are unknown in terms of durability [58]. Koek [53] mentions that if the plywood totally deteriorates, the axial normal force may disappear completely. Kaubit is a bituminous material and has a very low stiffness. The transfer of internal forces by kaubit is unknown [24]. In compression, the kaubit will deform and increase the contact area. When compression is increased, at one point the kaubit is thinned out and concrete-to-concrete may occur again [58].

A tunnel needs to be watertight. The segments itself ensure watertightness, the joints do not. Therefore, a water seal is included that has to ensure watertightness even during deformations of the lining. The seals are made of neoprene or hydrophilic rubber. The neoprene profile will ensure watertightness when it is loaded by internal forces. The hydrophilic rubber will increase in volume when in comes in contact with water and thus ensure watertightness [9].

Bending stiffness

These joints decrease the bending stiffness of the tunnel. In the axial direction, the circumferential joints and the tunnel rings work in series. For a ring, the stiffness is also reduced because of the longitudinal joints. The bending stiffness of the joints is depending on the connection system as described in section 2.3.4. It depends on the geometry, its mechanical properties and the properties of the packing material [56].

The decrease in bending stiffness, caused by the joints, has a large influence on the structural behaviour of the tunnel lining [30, 52, 54, 58, 78]. In order to include this decrease in bending stiffness, a reduction can be given to the bending rigidity. This can vary between 0.5 and 1.0 [17, 54].

Another way to include the joint in the tunnel lining is by approaching the joint as a hinge with or without

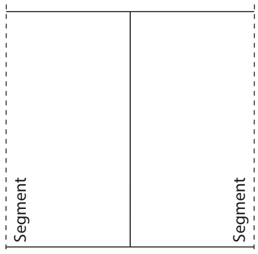

(a) Flat joint

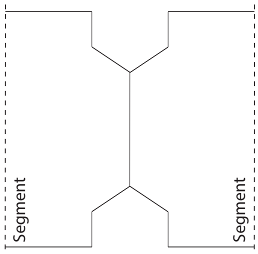

(b) Reduced flat [7]

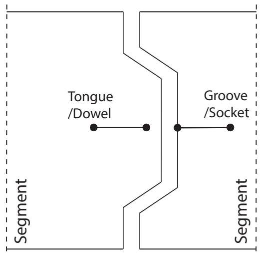

(c) Tongue-groove (dowel-socket) [7]

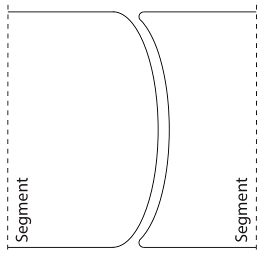

(d) Convex-concave [58]

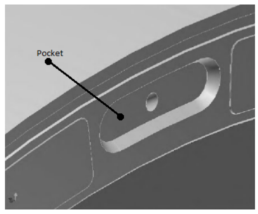

(e) Cam-pocket [61]

Figure 2.12: Five connection systems for construction of segmental tunnel lining.

a rotational stiffness. This is done for longitudinal joints in which the segments rotate relative to each other. In the case of an uniform radial pressure on the tunnel lining, a normal force will be acting in the joint. The joint height is the contact area between the segments. When this is small compared to the thickness of the segment, the forces will be transferred in a concentrated way. The hinge has a resistance to rotating, which causes a bending moment to occur. The rotating stiffness is derived from the theory of Janssen [45] and depends on contact area, tangential normal force and the rotation [7]. A small contact area may lead to additional curvatures and therefore rotations. This is applicable when the joints are still closed, also called the linear branch of the joint behaviour. The joint can also open, this is called the non-linear branch. The opening of a joint leads to a decrease in rotational stiffness of the joint. A joint can only open up when the pressure on the outer side of the contact area becomes zero. Bogaards [9] elaborates on the gaping of joints.

Janssen's theory is a theoretical model which describes the relation between the moment and rotation of a joint in segmental tunnel lining. It is based on the theory of concrete hinges. Janssen schematized the longitudinal joint as an equivalent concrete beam with the same properties. This beam is loaded by a bending moment and simulates the rotation and the additional curvatures in the adjoining segments. These curvatures are caused by the introduction of the concentrated force into the segments. Equation 2.1 & 2.2 give the relation between moment and rotation for the linear and non-linear branch respectively [58].

$$\phi = \frac{Mh}{EI} = 12\frac{M}{Eh^2b} \tag{2.1}$$

$$\phi = \frac{8F_n}{9bhE(\frac{2M}{F_nh} - 1)} \tag{2.2}$$

Janssen's method was the first, widely used method for including joints in tunnel lining. Since, other analytical solutions have been presented. Gladwell [37] also presented a moment-rotation relation. Blom [7] presented an adaptation to Janssen's method. These three methods are compared briefly by Luttikholt [58].

The circumferential joints have to be approached when the tunnel is discussed along its axis. In this joint, rotation and translation may occur. When no packing material is applied, a shear force may develop caused by the concrete-on-concrete contact that will counteract the mutual radial and tangential deformations. This also gives a resistance against rotations. The shear force is dependent on the normal force in the joint, the contact area and its smoothness. Moreover, an unsmooth surface may results in high speak stresses. With packing material two shear deformations may occur. The mutual deformations may be counteracted by the shear force developed because of the friction between the packing material and the concrete. It can also be counteracted by the shear deformation occurring in the packing material [58].

These joints are approached by using coupling springs. The dowel and socket connection system is the most approached connection system for circumferential joints. Coupling springs describe the behaviour of this system and also describe the lateral friction between the concrete and the packing material, as described above. These linear springs can only handle normal force and are radially orientated [7]. The approach by-Blom [7] starts with equation 2.1 and continues on the deformations induced by rotation in the longitudinal joints. He further elaborates on these deformations by adding the bending stiffness and the soil. Eventually the circumferential joints are included and coupled rings are acquired. The influence of coupled rings is significant [52]. Finally, an elastic soil continuum is added to the coupled system and the approach is completed.

While the joints are discussed by using analytical models, in FEM the joints are sometimes also modelled as springs. Either as rotational springs for the longitudinal joints or lateral springs for the circumferential joints. The non-linear behaviour as discussed can also be applied to those springs in FEM modelling [52]. More about modelling of the joints in finite element programs will be discussed in section 2.4.

2.4. Finite Element Method Programs

In this section, a short overview is given of the different programs that have been found suitable to model the construction of a tunnel. This overview has been created by examining the website and manuals of the programs as well as articles in which the program is mentioned. The advantages and disadvantages will be discussed and a verdict will be given for each program on its tunnel modelling capabilities. The comparison criteria searched for in the documents are:

- **Soil Models**: Availability of soil models on which will be elaborated in section 2.6;
- **Concrete Models**: Availability of concrete models;
- **Joints**: Modelling of joints;
- **Slip and Bond**: Modelling of slip and bond;
- **Interfaces**: Closely related to the above two points; modelling and use of interfaces;
- **Elements**: Availability of element types;
- **Phases**: Modelling of phased construction;
- **Results**: What can be calculated and how it can be plotted;
- **Specific tunnel application**: If is advertised or mentioned that tunnelling is one of the applications;
- **Ease to work with**: Interface or programming input and available documentation;
- **Design approaches**: Extra features for design, for example designing with a Eurocode;

2.4.1. Plaxis

Plaxis is well known for its modelling of the subsurface. This can also be seen in the amount of constitutive soil models that are present in the program, more than any other program discussed in this section. With regards to the lining, Plaxis does not have specific concrete models but it does have linear models that can be applied with concrete properties. In the 2D version of the program, segmental joints can be modelled as hinges. For the 3D version, no solution for modelling the joints has been found in the documentation except for reducing the stiffness to account for the joints. The contact between lining and soil can be modelled with an interface that consists of joint elements with its own friction angle and adhesion. With regards to the elements used in the model, for soil many high-order volume elements are available and for the lining, plate and beam elements. With these structural elements, the structural forces can be measured and displayed. The same accounts for the displacements. Different types of plots are available for displaying the results, for example vector and contour plots. Phases can be implemented in which elements can be activated as well as de-activated. This way, a staged construction can be modelled. Plaxis has a tunnel designer module inside the program, which makes modelling a tunnel more simple. Besides this module, Plaxis works with a user interface for input and a lot of documentation is available. Different manuals for reference of the program features are available as well as a manual for the scientific base for all the different calculations in the program. The constitutive models are also explained extensively and there is a tutorial manual. For many geotechnical issues, a tutorial is available on how to model this in Plaxis, this includes tutorials for tunnelling. Furthermore, an extra feature in Plaxis is able to define a coherent set of parameters and partial factor according to ultimate limit state design methods, apart from the serviceability limit state calculations [12].

2.4.2. DIANA

Many constitutive models are available in DIANA. Furthermore, it also has some concrete models that can be used for lining, besides the linear elastic models. These concrete models can model non-linear behaviour and incorporate cracking as well. For the modelling of the joints, special elements are available called contact and interface elements. A Janssen characteristic (as shortly described in section 2.3.4) can be applied to these elements. Also for the interaction between the lining and the soil, interface elements can be used with non-linear behaviour. A few special elements have already been mentioned, but there many other types available in DIANA, including shell and solid elements. Phased construction can be applied. For displaying the structural forces results, different plot types are available. Tunnelling is a major focus of DIANA, as can be deducted from DIANA FEA BV [27]. This also shows from the amount of tutorials available. While there are many, they are not all for the same pre-processor. DIANA has multiple pre-processors of which one uses a programming input and another uses a user interface. For the latter, DIANA is currently creating the tutorials so there are not a lot available yet. Besides the tutorial, a large amount of documentation can be found in their online manual, this includes user guides and reference material. Designing according to the Eurocode is an extra mentionable feature in DIANA [27].

2.4.3. CESAR-LCPC

CESAR has many constitutive soil models: several linear and non-linear elasticity models and many plasticity soil models. Besides for soil, there are also some plasticity models for other materials available, including early age concrete [44]. Whether lining joints can be modelled remains unclear. There are interface and spring elements available, but it is not highlighted they can be used for lining joints. The interface elements are able to model slip and bond. Three contact models are available for these interface elements: Coulomb's friction, bonding, perfect slippage. Besides the interface and spring elements, there are volume elements available for the soil and trusses, beams and shells as structural elements. Phased construction is available by removal or addition of clusters, the confinement forces are also automatically generated. From the beam and shell elements the structural forces can be shown in a 3D view. Furthermore, there are cross sectional planes and iso-surfaces available [43]. While tunnelling is one of the main applications of CESAR, other geotechnical and structural issues can also be modelled. This is done through an input interface. With regards to documentation, information about the constitutive models [44] and a brochure about the programs features [43] area available. There is also a user guide available but that does not contain much more information than in the before mentioned documents. Tutorials, however, are scarce. There are some tutorial videos but these do not contain complicated problems. Factor of safety calculations can also be donein CESAR [43].

2.4.4. GTS NX

GTS NX is a program developed by Midas and can be bought as a pre- and post-processor for DIANA or a standalone program, which will be discussed here. It has both elastic and plastic material models, but mostly for soil and no specific concrete models. There are also interface models available: Janssen and Coulomb friction. This Janssen model can be used on the interface elements that represent the joints, while the Coulomb friction can be used for the soil-structure interface elements. Other element types are also available, for example truss, beam and shell elements [63]. Phases can be implemented as well, it is emphasized this can be used for shield TBM analysis in which the structural forces are obtained for every phase [62]. These forces can be displayed through cross-section and contour plots amongst other display options [64]. It is obvious that tunnelling is an application for GTS NX. This can also be seen from the amount of tunnelling tutorials. Both for 2D and 3D there are tutorials, there is even a tutorial for shield TBM analysis. Besides the tutorials, there is also documentation for reference and verification and a user guide. As input, GTS NX uses a user interface. It is not clear whether extra features like the factor of safety calculations or Eurocode designing are present in GTS NX.

2.4.5. Other

These five programs are not the only finite elements programs that have been used for tunnelling. These are the five however that have been deemed to be the most suitable based on the criteria given at the beginning of this section. There are some programs however that should be mentioned and explained why they were not further reviewed.

Abaqus
Abaqus is a multipurpose finite element program. While tunnels can be modelled in this program as done by [51, 57, 68], Abaqus itself does not promote or mention it. Therefore no tutorials for tunnel modelling in Abaqus can be found. There is one document on their website about a tunnel plugin for Abaqus. In this document Fioranelli Jr et al. [34], discusses that the Abaqus interface is not user friendly for tunnelling analysis and that therefore the plugin has been developed. Abaqus only has two plastic constitutive soil models as well. Further elaboration on Abaqus has not been done based on these criteria.

Ansys
Ansys is excluded from further elaboration for almost the same reasons as Abaqus. Multiple authors [7, 8, 16] have modelled tunnels in Ansys. Nowadays, little documentation by Ansys can be found with regards to tunnelling. Many tutorials are available but none of them are about geotechnical issues. Lengkeek [56] already stated that Ansys is more focused on structural than on geotechnical. issues. Another program called "CivilFEM" can be used to make working on geotechnical issues in Ansys easier.

Tochnog Professional
This program has many soil constitutive models but lacks the structural approach. Joints cannot be modelled and no information can be found about whether the structural forces in the lining can be modelled. The available tutorials are not for tunnelling problems either. Based on these criteria, Tochnog Professional is not further reviewed.

RS^3
This program has been developed by Rocscience. The ground can be modelled by many different constitutive models, only the lining cannot be modelled correctly. Joints cannot be modelled and it is unclear whether the structural forces in the lining can be measured in this program. Therefore it is not further reviewed.

Flac3D
Flac3D is also a program which can model geotechnical issues including tunnelling. However, it is a program which uses the finite difference method instead of finite element. This is the reason is has not been included in further reviewed since only FEM will be investigated.

2.4.6. Conclusion
Table 2.2 provides a summary on how the different programs score on the criteria. It is clearly visible that based on these criteria, DIANA is considered the best program for modelling the tunnelling process, followed by GTS NX and Plaxis. This has only been based on the available documentation of the different programs. A real conclusion on these programs can be given when the program is used for modelling the tunnelling process and results have been compared. It has been decided to assess the possibilities of modelling the construction phases of bored tunnels in DIANA and Plaxis. DIANA comes out as the most suitable program based on the available documentation and Plaxis, while not being second, is widely used in the geotechnical, and thus tunnelling community, in the Netherlands. Therefore the Plaxis is favoured for assessing the possibilities over GTS NX.

2.5. Parametric studies
In tunnelling, many different parameters are present and require input when modelling the soil and lining. However, not all parameters have the same influence on the problem. This section elaborates on parametric studies that have been performed on the influence on the tunnel lining forces.

2.5.1. Soil parameters
First, the influence of soil parameters on the lining forces will be discussed.

Young's modulus
For a stiff ground, thus a high Young's modulus, a circular excavation in the ground will lead to less convergence of the soil into the excavation. When the soil is less stiff, more convergence will occur. This will lead to more loading on the lining. An increase in Young's modulus will result in a decrease in the internal forces of the lining [2, 30, 55, 66, 70]. This includes the shear force [46].

		Plaxis	DIANA	CESAR-LCPC	GTS NX
		Programs			
Criteria	Soil Models	++	+	+	+
	Concrete Models	+/-	++	+	+/-
	Joints	+/-	++	-	++
	Slip and bond	+	++	++	+
	Interfaces	+	+	+	++
	Elements	+	++	++	++
	Phases	++	++	+	++
	Results	++	++	++	++
	Specific tunnel application	++	++	++	++
	Ease to work with	++	+	+/-	++
	Design Approaches	+	++	+	-

Table 2.2: Summary of the different FEM programs and their scores on the criteria.

Lateral earth pressure coefficient
The bending moment is the lowest when the lateral earth pressure coefficient is at unity. Moving away from unity, either increase or decrease, leads to an increase in bending moment [30, 66, 70]. When the lateral earth pressure coefficient is at unity, the vertical and horizontal load are equal. Moving away from unity, the difference between vertical and horizontal load increases and therefore the bending moment in the lining will increase as well. An increasing lateral earth pressure coefficient will lead to an increasing normal force [30, 70].

Poisson's ratio
While the Poisson's ratio does not have an influence on the normal force in the tunnel lining, it does affect the bending moment. An increase in Poisson's ratio leads to a slight decrease in bending moment [70] and shear force [46].

Cohesion
Cohesion does not have an influence on the bending moment. An increase in cohesion does lead to a slight decrease in normal force [66, 70]. More cohesion means less convergence in a circular excavation, therefore the normal forces in the lining will decrease.

Friction angle
With more research needed, Möller and Vermeer [66] state that the friction angle has little influence on the internal lining forces. Kasper and Meschke [50], Palassi and Mohebbi [70] state that with an increase in friction angle the normal force will decrease. A higher friction angle means more load is taken by the soil itself, this causes the radial loading to decrease and therefore the normal forces in the lining. For the bending moment, they are in disagreement. Kasper and Meschke [50] state that an increase in friction angle will lead to a slight increase in bending moment while Palassi and Mohebbi [70] states that the bending moment will slightly decrease.

Overconsolidation ratio
An increase in overconsolidation ratio leads to a slight decrease in normal force in the lining. With a low overconsolidation ratio, plastic deformations of the soil around the tunnel are large. The reduction of this plastic deformations when increasing the overconsolidation ratio, causes the lining pressure to decrease as well and therefore the normal force. The bending moment is hardly influenced by the overconsolidation ratio [50].

Permeability
The permeability has little influence on the bending moment and normal force in the tunnel lining. Whether these forces slightly increase or decrease with increasing permeability depends on the location at the tunnel

ring. The pore pressures around the tunnel are influenced by the grouting pressure, the support face pressure and the buoyancy [50].

2.5.2. Tunnel parameters

Apart from the soil parameters, the project (or tunnel) parameters also have an influence on the tunnel lining.

Cover depth

Kasper and Meschke [50], Katebi et al. [51], Palassi and Mohebbi [70] state what many authors state: an increase in depth for the tunnel leads to an increase in internal forces. The increase in overburden height and hydrostatic pressure with the depth cause an increase in the lining pressure. The difference between the pressure at the crown, bottom and sides of the tunnel also increases, which increases the bending moment. The increase in depth also leads to an anticipation of pressure in the excavation chamber. More pressure is needed in that chamber to resist the soil and therefore the jacking forces and the axial loading will increase [50].

Tunnel radius

The tunnel radius is usually already set in the project, but it does have an influence on the internal forces of the lining. When the tunnel radius increases, the bending stiffness of the lining decreases. This leads to a decrease in bending moments as well. Furthermore, because the radius increases, the pressure on the lining increases. This leads to an increase in normal force in the lining [70].

Face support pressure

This pressure has already been mentioned discussing two other parameters and their influence on the internal forces of the lining. An increase in face support pressure causes the stress release in front of the TBM to decrease. Therefore there will be a slight increase in the lining pressure and thus the normal force in the lining. The difference in pressure surrounding the tunnel decreases so the bending moment decreases as well. For the axial loading, the same accounts as discussed with the influence of the tunnel depth [49].

Grouting pressure

Grouting pressure causes the same type of soil response as the face support pressure. When it is increased, the stress release of the soil is decreased. The lining pressure and the normal force increase, the bending moments decrease [49].

Hydration characteristics grout

Grout hardens towards a final strength and stiffness. The final values of this strength and stiffness are important, but not as important as the time it takes to get to that values. When the grout hardens quicker, there will be less time for the soil to release the stress. The lining pressure will increase causing the normal force to increase as well. When the hardening time is short, there will still be some upward movement from the soil below the tunnel caused by the TBM passage. Combined with the reduction in stress release, this will lead to an increase in pressure at the bottom of the tunnel. This causes the bending moments to increase [50]. More about the grouting and its characteristics will be discussed in section 2.8.1.

TBM weight

The TBM is located in front of the lining, so it does not exceed a pressure on the lining directly apart from jacking forces and this axial pressure. However,the weight does have an influence on the radial pressure on the lining. Underneath the TBM, the ground settles under the weight. This results in a heave of the soil as soon as the TBM has passed. Behind the TBM, the lining is already in place. So the heave results in a radial pressure on the lining. An increase in weight will results in more settlement and therefore more heave. The increased lining pressure due to the heave will cause the normal force and bending moments to increase slightly [49].

TBM length

Apart from the weight, the TBM also causes deformation through frictional interaction between the shield skin and the soil. Softening occurs at the sides of the tunnel and increases with increasing TBM length, which leads to a decrease in lining pressure at that location. With little changes at the crown or bottom, an increase in bending moment and decrease in normal force occur. For a longer TBM, the friction increases as well. That causes the jacking forces, and thus the axial loading, to increase. The analyses in which this phenomena is investigated used overconsolidated soils in the model [49].

TBM taper

If the taper is increased, the shape of the TBM becomes more conical. This leads to an increase in stress release of the surrounding soil. The lining pressure decreases causing the normal force to decrease and the bending moment to decrease slightly. The friction resistance is also decreased by an increasing taper and therefore the axial loading is decreased [49].

Trailer weight

The trailer following the TBM has a weight and therefore has a pressure on the lining. This load is not distributed evenly since the trailer is on wheels. In between two trailer loads, the pressure that the trailer exceeds on the lining has a negligible influence on the lining forces. Kasper and Meschke [49] did not elaborate on the influence of one trailer load directly on the lining. The trailer weight does counteract the buoyancy, an increase in trailer weight would decrease the buoyancy.

2.5.3. Lining parameters

The lining is the last part in which different parameters can have an influence on the internal lining forces.

Stiffness

Just as with the soil, the lining can have a stiffness. An increase in this stiffness leads to an increase in bending moment. The normal forces are not influenced by the lining stiffness [70]. Do et al. [30] also state that a tunnel which deforms less has higher structural forces.

Thickness

The thickness of the lining is related to the bending stiffness. When the thickness increases, the bending stiffness increases.

Number of joints

A joint can decrease the lining stiffness depending on the joint's stiffness, which will be discussed below. Therefore, the number of joints influence the lining as well. According to Do et al. [30] and Nikkhah et al. [69], this is only the case for the bending moment, which decreases with an increasing number of joints. This only accounts for more than four joints.

Orientation of segment joints

The orientation of the joints only influences the bending moment of the lining [30, 55]. The bending moment however also influences the influence of this joint. The joint's influence is the largest when it is located at the largest bending moment location [30].

Rotational stiffness of joint

As stated previously, a stiffer lining will result in higher internal forces. This is again applicable for the rotation stiffness of a joint. If this increases, the internal lining forces also increase [30, 55, 69].

Radial and axial stiffness of segment joint

Apart from the rotational stiffness, there are also the radial and axial stiffness of a joint. Both, however, have a negligible influence on the lining forces according to Do et al. [30].

2.6. Soil models

The soil can be modelled with different models, as previously mentioned in section 2.4. In this section, a couple of soil models will be described briefly. These soil models have been encountered in studies about modelling the tunnelling process. The main reason for the different models is that not all soil types can be represented by one model. The difference in behaviour is related to differences between soils but also the application is important with regards to choosing a soil model. Long term behaviour may be very different than short term behaviour for example.

2.6.1. Mohr-Coulomb

The Mohr-Coulomb model is a simple model and is used to get a first approximation of the soil behaviour. This soil model is used in many studies [3, 5, 13, 14, 36, 46, 51, 79]. It is a linear elastic perfectly plastic model thus no hardening or softening will occur [72]. Hooke's law of isotropic elasticity is the basis for the elastic part of the Mohr-Coulomb model. The perfectly plastic part is based on failure criterion by Mohr-Coulomb. With plastic behaviour, irreversible strains develop while with elastic behaviour, the strains will be reversed when unloading. The boundary between this elastic and plastic behaviour is given by the yield function which is a function of the stress and strain. Since it is a perfectly plastic model, this yield function is fixed and only defined by its model parameters. This means that straining will not affect the yield function. Elastic behaviour will occur with stress states that are located within the yield function and plastic behaviour will occur for the stress states outside this yield function [12].

The Mohr-Coulomb requires five input parameters. An explanation about these input parameters is given by Brinkgreve et al. [12]. The five input parameters are:

E	Young's modulus
$\boldsymbol{\nu}$	Poisson's ratio
c	Cohesion
$\boldsymbol{\phi}$	Friction angle
$\boldsymbol{\psi}$	Dilatancy angle
$\boldsymbol{\sigma_t}$	Tension cut-off and tensile strength

2.6.2. Hardening Soil

A more advanced soil model compared to Mohr-Coulomb is the Hardening Soil model and is also used in many studies [40, 41, 67, 73]. First, in this model the stress-strain relation for primary loading is a hyperbola. Second, the yield surface is not fixed and plastic strain can cause it to expand which is called "hardening plasticity". Two types of hardening are included in the model. Shear hardening for the irreversible strains caused by primary deviatoric loading and compression hardening for the irreversible strains caused by primary compression in isotropic and oedometer loading. The shear hardening causes a decrease in deviatoric loading and the compression hardening causes plastic compaction in primary compression and a difference between primary loading and unloading and reloading. An elaborate explanation on this is given by Brinkgreve et al. [12]. With these differences, different input parameters are also needed. The last four parameters discussed for Mohr-Coulomb in section 2.6.1 are also in the Hardening Soil model since the Mohr-Coulomb failure criterion is still applied. The other parameters that are needed are [12]:

$\boldsymbol{E_{50}^{ref}}$	Secant stiffness in standard drained triaxial test
$\boldsymbol{E_{oed}^{ref}}$	Tangent stiffness for primary oedometer loading
$\boldsymbol{E_{ur}^{ref}}$	Unloading/reloading stiffness
m	Power for stress-level dependency of stiffness

It can be seen from the list that one stiffness in the Mohr-Coulomb model (Young's modulus), has been replaced by three different stiffnesses. These three cover the effects of the shear and compression hardening. E_{50}^{ref} is used for the plastic strains caused by primary deviatoric loading (shear hardening). E_{oed}^{ref} is used for the plastic strains caused by primary compression (compression hardening). Besides the plastic strains, compression hardening also included the difference between loading and unloading/reloading stiffness. This is cover by the parameter E_{ur}^{ref}. The three stiffnesses are also related to a reference pressure because the Hardening Soil model also accounts for the stress-dependency of these stiffness-moduli. This is covered by the power "m". For some soft soils, other parameters may be used to calculate the stiffness parameters [12]. Conversion guidelines for Mohr-Coulomb parameters to Hardening Soil parameters are given by CUR [26]. The E_{oed} parameters have to be converted to the reference oedometer parameter E_{oed}^{ref} by using the effective vertical stress at the middle of the soil layer and converting that to a reference stress of 100 kPa. The conversion includes the factor "m" of which indication values are given by CUR [26] as well. From the E_{oed}^{ref}, other conversion rules are available for both clay and sand to acquire E_{50}^{ref} and E_{ur}^{ref}. The "m" chosen in the conversion also has to be used in the Hardening Soil model for the corresponding soil layers.

The differences mentioned above are also mentioned by multiple authors [18, 72]. In other tunnelling projects it is also mentioned that Hardening Soil might give better results on the structural forces in the lining than Mohr-Coulomb, just because of the stress-dependency and the different stiffness for unloading/reloading compared to primary loading [15, 23].

2.6.3. Hardening Soil small strain

The unloading/reloading behaviour in the Hardening Soil model is assumed to be elastic. However, this is only the case for a very small strain range. The soil stiffness actually declines non-linearly with increasing strain amplitude. Figure 2.13 shows the stiffness of the soil against the strain and shows a S-curve that reduces with increasing strain. For the very small strains, the stiffness changes significantly. This can be taken into account by the Hardening Soil small strain model.

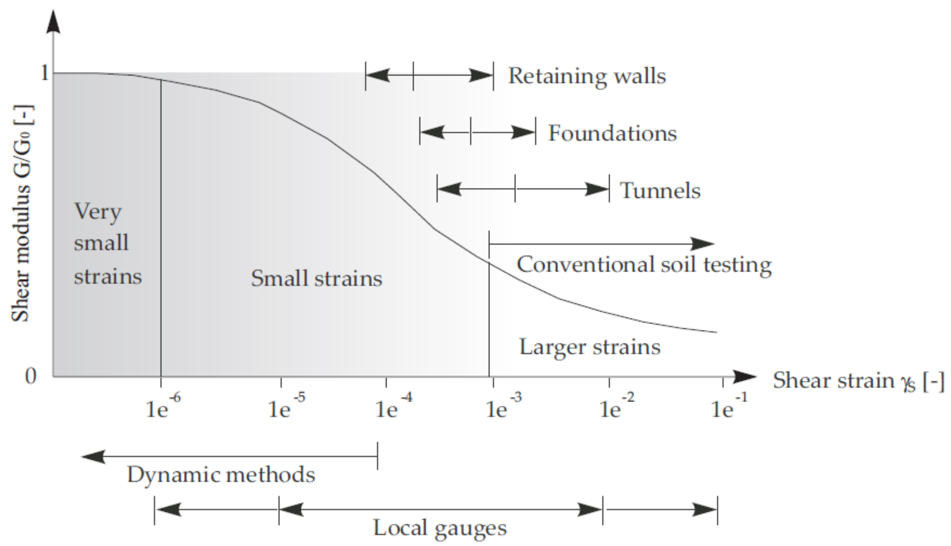

Figure 2.13: Stiffness-strain behaviour of soil. Strain ranges for different structures have been indicated as well [12].

Since it is an extension on the Hardening Soil model, all its features will remain and so are its parameters. Two extra parameters are needed for the small strain stiffness.

G_0	Very small-strain shear modulus
$\gamma_{0.7}$	Shear strain level when secant shear modulus is reduced to 70%.

2.6.4. (Modified) Cam-Clay

(Modified) Cam-Clay is used by Finno and Clough [33] and Kasper and Meschke [48] for modelling soft cohesive soils, like clay, in there tunnelling model. It predicts the softening when dilatant plastic strains occur and hardening when contractant plastic strains occur. These two types of strains occur depending on the stress state of the soil. The boundary between these two stress state areas is called the critical state line. Therefore, this line gives a relation between the mean principal stress and the deviatoric stress in state of failure. As with Hardening Soil, unloading/reloading does not follow the same relation as primary loading. This is caused by the compression that may occur in soft, cohesive soils during primary loading and during unloading/reloading. A more elaborate explanation is given by Brinkgreve et al. [12], Kasper and Meschke [48]. The input parameters needed for the Modified Cam-Clay model are [12]:

ν_{ur}	Poisson's ratio
κ	Cam-Clay swelling index
λ	Cam-Clay compression index
M	Tangent of critical state line
e_{init}	Inital void ratio

κ determines the compressibility of the soil during unloading/reloading while λ determines the compressibility of the soil during primary loading.

It is, however, recommended to not use this soil model for practical applications. Extremely large shear stresses may be allowed for particular stress paths, as well as softening may occur for particular stress paths.

This leads to practical problems like mesh dependency and convergence problems for iterative processes in the finite element programs [12].

Hypoplastic
The hypoplastic model has been created for describing state changes of granular materials and is an extension to the critical state concept to which the Modified Cam-Clay models also belongs. These granular materials are characterized by the current stress and void ratio. Instead of a Mohr-Coulomb or Drucker-Prager failure criterion, the hypoplastic model has a failure criterion created by Matsuoka-Nakai. Within the hypoplastic model, the stiffness for unloading is not equal to the stiffness for loading and it therefore is irreversible. These stiffnesses are non-linear as well and are dependent on the stress level as well as the void ratio. Since it described the state changes of granular materials, it includes intergranular strains. This means the small strains stiffness is described as well, just like in the Hardening Soil small strain model. The following parameters are required for the hypoplastic model [11]:

$\boldsymbol{h_s}$	Granular hardness
$\boldsymbol{n}$	Exponent of compression law
$\boldsymbol{\phi_c}$	Critical state friction angle
e_{d0}	Void ratio at maximum density for p=0
$\boldsymbol{e_{c0}}$	Void ratio at critical state for p=0
$\boldsymbol{e_{i0}}$	Void ratio at minimum density for p=0
$\boldsymbol{\alpha \& \beta}$	Pycnotropy exponents
$\boldsymbol{m_R}$	Stiffness multiplier for initial or reversed loading
$\boldsymbol{m_T}$	Stiffness multiplier for neutral loading
$\boldsymbol{R_{max}}$	Small strain stiffness limit
$\boldsymbol{\beta_r \& \chi}$	Parameters adjusting stiffness reduction curve slope

These parameters have to be acquired through multiple lab tests: oedometer compressionn index, biaxial, cyclic shear and monotonic or cyclic triaxial tests. The amount of parameters that are required and the difficulty to determine these parameter are a disadvantage of the hypoplastic model. Undrained behaviour is not captured well either with the hypoplastic model. The set of parameters needed, is only valid for a specific stress range. When this stress range changes, the parameters have to be modified. However, there is only one set needed for a particular material type. Only the void ratios have to adjusted for different densities. All the other advantages have already been mentioned earlier: stiffness dependent, failure criterion and a critical state model [11].

2.6.5. Concluding remarks

Other constitutive soil models have been found in the literature as well. They have not been reviewed for various reasons. The first reason is that they have only been used by the one person who created the model. While this might be a suitable model, little extra information was available about these models and therefore no conclusions could be drawn. Furthermore, the likelihood that these models could be implemented in the finite element programs is low and would be time consuming. The second reason is that the models are called differently but are equal to the already discussed models. Other models have not been reviewed since they are complex and require input parameters that have to be acquired through specific and extensive testing. The likelihood that extensive soil testing will be done for a project is small.

Based on the differences between the models and the application, a provisional conclusion can be drawn on the most suitable soil model. Hardening soil is more complex than Mohr-Coulomb, but the stress dependency and the different stiffness for unloading/reloading are two major advantages considering the soil in tunnel construction is unloaded and reloaded in the process (2.2.1). In previous researches on the construction of tunnel lining Mohr-Coulomb was used and it was also recommended to do the same modelling with Hardening Soil [23]. In later researches, it is used since it is the most accurate model for stress-depending stiffness in unloading/reloading [15]. It is closer to reality than the Mohr-Coulomb material model especially regarding excavations [73]. The disadvantage on the other hand is the increased amount of parameters that is needed for this model. The conversion from Mohr-Coulomb to Hardening Soil parameters is useful in this case, but the acquired values might not be accurate. This disadvantage also accounts for Hardening Soil small strain against Hardening Soil. The advantage of the Hardening Soil small strain is the correct modelling of the very small strains, but it can be seen from figure 2.13 that strains for tunnels are not considered very small. It can also be seen that the stiffness-strain curve over the tunnel strain range is approximated well by a linear relation. Figure 2.13 shows that these small strains usually occur in dynamic loading, which will not be the case in this research. The (Modified) Cam-Clay is said to be for soft cohesive soils. While the Dutch subsurface consists of many soft cohesive soils, this also depends on location. In section 2.9 the subsurface that will be modelled will be discussed and only then it can be concluded whether there are many soft cohesive soils and the (Modified) Cam-Clay model will be used. However, it is recommended that the Modified Cam-Clay model should not be used for practical applications. The Hypoplastic model has many advantages which are suitable for tunnelling problems, like the stiffness dependency and the critical state characteristics. The many parameters however are a major disadvantage. Since they are hard to define, it is not likely these parameters will be acquired in a real tunnelling project and therefore the practical applicability of this model is not high.

Therefore, the preferable soil model will be Hardening Soil. A comparison of the results between Hardening Soil and Mohr-Coulomb will be made.

2.7. Concrete models

Throughout all the researches found about modelling tunnel lining, the concrete has always been modelled with a linear elastic model. Even in programs that are considered to model concrete accurately (see section 2.4), the segments and lining have linear elastic properties. Therefore a linear elastic model will preferably be used in the model as well.

2.8. Ground-lining interaction methods

As mentioned before, the construction of a tunnel is a three dimensional problem. In order to incorporate these 3D phenomena into a 2D finite elements analysis, ground lining interaction assumptions have to be adopted. Many methods are mentioned throughout the literature to incorporate this interaction between the ground and lining: convergence-confinement, volume loss control, stiffness reduction, gap method etc [47]. Some methods are applicable to both NATM and TBM tunnelling, others only for either one of them. While specific for TBM tunnelling, an important issue during the tunnelling process was not modelled in the methods: grout. The grouting behind the TBM is difficult to model but should not be neglected since it can have a large influence on the lining forces [18, 31, 50, 65]. Therefore a new method was created called the "grouting pressure method", which incorporated the grout behind the TBM.

This method is a combination of elements from the gap method and the stress reduction method [67].

2.8.1. Grouting pressure

Most pressure changes and deformations in the soil occur during and after TBM passage. These tail effects are countered by injecting grout, as mentioned in section 2.2. The grout is injected under a certain amount of pressure that withholds the soil from contracting. Grout is a fluid form of concrete, it has a complex behaviour which includes a fluid form and a hardened form. The fluid form of grout can be approached as a Bingham plastic with time dependent rheological properties [6, 75, 76]. A Bingham plastic is viscoplastic material, which means that for low stresses it behaves like a rigid body, while for high stresses it behaves like a viscous fluid. This means it can withstand shear stresses without flow. A specific amount of stress has to work on the grout before it starts flowing. This amount of stress is called the yield stress. Because it does not flow for shear stresses below the yield stress, the vertical pressure gradient in grout will be lower than a static pressure gradient. A model called DCgrout was created in order to calculate the grout distribution surrounding the lining in the tail void. A summary of the features in the DCgrout are given by Talmon et al. [75]. This model shows good results for the grouting pressure in the tail void when it assumed that there is a friction between the grout and soil that is equal to the internal friction of the grout. Some limitations are also mentioned by Talmon et al. [75].

- It is difficult to determine the rheological properties of the grout;
- The influence of the friction at the boundary between the grout and soil is unknown;
- About the rheological properties at the grout-soil boundary, as a function of compression and fluid loss, is unsufficiently known.

Due to compression and fluid loss, the resistance to flow may be increased. In the same report, Talmon et al. [75] also state that the number of grout injection points and its locations are of great influence on the grout pressure in the tail void.

Talmon et al. [76] continue with this DCgrout model and validated it with measurements taken from the

Botlek Rail Tunnel and the Sophia Rail Tunnel. It states some other limitations of the DCgrout model (it only models three rings) and lists some features in the grout which emphasizes the complex behaviour. During drilling of the TBM, the grout flows backwards, so away from the TBM. This leads to very little shear stress on the lining caused by the grout. Furthermore, the grout is usually approached as being homogenous, while quick dewatering may actually cause a soilskeleton to be formed in the grout. At the boundary between the soil and the grout, a groutcake may form which influences the friction. The grout does not consolidate completely, some parts remain a fluid until it is hardened. All of this has an influence on the grouting pressure distribution in the tailvoid. A distinction is made between the influence of the different factors on the vertical grout pressure gradient at two locations: close to the TBM and further behind the TBM. The vertical grout pressure gradient close to the TBM, is influenced by the following factors [76]:

- Rheology grout
- Time dependency of rheological properties of the grout
- Specific Weight
- Thickness grout layer

Further behind the TBM, it is influenced by these factors [76]:

- Rheology of grout when insufficient yield stress
- Specific weight of the grout
- Thickness grout layer
- Jacking forces
- Excentricity of lining position

The location of the transition between "Further behind the TBM" and "close to the TBM" has not been clearly defined yet. In order to assess this influence, Bezuijen et al. [6] investigated the pressure in the longitudinal direction by looking at the Sophia Rail Tunnel as well. It was again emphasized that of the rheological proeprties, the yield stress and viscosity are the most important regarding the grout pressure distribution. With time, both these properties increase as well. Bezuijen et al. [6] also noted that the measured gradient is influenced by the bending moment in the lining and combined with the buoyancy forces they govern the pressure during standstill and further away from the TBM.

Another important feature of grout is the hardening. Talmon and Bezuijen [74] investigated this behaviour and created a new model with regards to longitudinal grout flow, called DClong. This model can provide the length of the liquid grout phase and the vertical pressure gradient at the turning point between liquid grout and elastic grout behaviour. However, the DClong model mainly focusses on the grout behaviour while the soil behaviour and tunnel displacements are essential as well since they change geometry of the tail void. There is still too much uncertainty on these two factors.

The influence of some of the rheological characteristics of the grout have been assessed in section 2.5, but it becomes clear from this small summary of investigations on grout behaviour that it is a very complex problem. For which a complete solution has not been found yet. In order to account for the presence of grout in the construction process of a tunnel, the assumption has been made that for the entire grouting phase, the vertical pressure gradient is constant and that the rheological properties do no change over time. This is not completely realistic as described above and what also can been seen in the grout pressure measurements taken in various tunnelling projects [6, 74, 76, 77]. Otherwise, it would be too difficult to implement the grouting in this research and it would still be doubtfull whether the real grout behaviour has been captured.

For the hardening of the grout, it is assumed that the grout does not deform. After it has completely hardened, the borehole is fixed and the grouting pressure is removed. A water pressure is then applied on the borehole wall which may lead to a vertical translation [22].

When approaching the grouting with a vertical constant gradient, the "grouting pressure method" can be follow to model the different construction phases [22]. It allows for modelling stress changes and deformations in the soil surrounding a borehole.

With the grouting pressure method, the stress changes and deformations With those stress changes and deformations, the following aspects can be determined for a given grout pressure distribution [22]:

- Surface settlements
- Horizontal and vertical ground displacements around the tunnel
- Load on and support of the tunnel by the surrounding soil layers including the hardened grout layer.

Nonetheless, there are some aspects which are not suitable to be determined by the grouting pressure method [22]:

- jacking forces
- vibrations
- temporary special loads
- given ring displacement in axial direction

2.8.2. Concluding remarks

Since shield tunnelling is commonly used for bored tunnels, grouting is an important feature that has to be modelled in the construction process. While at first the grouting pressure method was used in a 2D model [18] or other construction aspects were left out because not enough computational power was available [19]. Now a 3D grouting pressure method for a 3D model which proceeds over time has been created [15]. This will be followed to ensure implementation of the grout in the 3D models for comparison of Plaxis and DIANA. As discussed previously, the exact grout behaviour is too complex and there are still too many uncertainties in order to be implemented in the finite element models.

2.9. Final model properties

For this research, an existing design case from Arthe CS is used for comparison of the created models in Plaxis and DIANA. In Mashhad, Iran, a new metro line is planned and Arthe CS has been asked to design the tunnel. In this design, four different sections have been identified along the alignment. Out of the four, the most interesting section has been chosen. The properties of this section that will be included in this research are summarised in this section. Not all the different loads described in section 2.2 will be modelled in the final model. Temperature, installation and special loads will not be included in this research and the same accounts for adjacent tunnels.

The properties of the tunnel can be found in table 2.3.

		value	unit
Dimensions	Depth tunnel axis	-35.4	m below surface
	Outer diameter	9.1	m
	Inner diameter	8.4	m
	Wall thickness	0.35	m
	Ring width	1.5	m
	Number of segments	7 + 1	-
	Water table	-38.5	m below surface

Table 2.3: Tunnel properties

The dimensions of the 3D model are determined by the dimension rules (equations 2.3 & 2.4) given by COB-L520 [22]. These rules are based on the overburden height (H) and the diameter of the tunnel (D) and ensure that all the soil that is influenced by the tunnelling is included in the model. With the rules, the boundaries of the model will not be influenced by the tunnelling.

$$\text{Width of model} = 3(H + D) = 3(30.7 + 9.1) = 120m \tag{2.3}$$

$$\text{Height of model} = H + 2D = 30.7 + 2 * 9.1 = 49m \tag{2.4}$$

The length of the model will be ten rings. Preferable, the model will be as long as possible, however, this results in a very large model with a large computational time. Besides the influence of surrounding soil, the height of the model is also dependent on the available soil data. From the soil investigation that has been done, eight soil layers have been identified that can be represented by three different soil types. The properties of these three types are given in table 2.4 and the layering of these soils are given in table 2.5.

		Properties									
		γ_{bulk} (kN/m^3)	γ_{sat} (kN/m^3)	c' (kPa)	ϕ' (°)	ν_{ur} (-)	$E'_{50;ref}$ (MPa)	$E'_{ur;ref}$ (MPa)	$E_{oed;ref}$ (MPa)	m (-)	K_0 (-)
Soil types	Clay	19.1	20.1	6.4	29.7	0.2	13.4	33.5	13.4	0.5	0.5045
	Silt	19.1	20.4	5.6	31.2	0.2	19.6	49	19.6	0.5	0.4820
	Sand	19.5	21.1	4.7	32.7	0.2	20.9	52.3	20.9	0.5	0.4598

Table 2.4: The three different soil types identified and their properties.

		top layer (m below surface)	bottom layer (m below surface)
Dimensions	Sand	0	19.7
	Silt	19.7	22
	Clay	22	26
	Sand	26	28.5
	Clay	28.5	31.5
	Sand	31.5	38.3
	Clay	38.3	41.5
	Sand	41.5	54.5

Table 2.5: Soil layering

		value	unit
Properties	Concrete type	C40/50	-
	Specific weight	25	kN/m^3
	Elastic modulus	35	GPa
	Poisson's ratio	0.2	-

Table 2.6: Lining properties

With the described soil layering, the model height becomes 54.5 meters, which is sufficient with regards to the proposed model height with equation 2.4. Besides the soil, the tunnel lining also has specific properties. The dimensions of the lining have already been discussed in table 2.3, the concrete properties of the lining can be found in table 2.6. The properties of the TBM that is used in Mashhad can be found in table 2.7.

		value	unit
Properties	Diameter front TBM	9400	mm
	Diameter back TBM	9350	mm
	Taper TBM	50	mm
	Weight TBM	1100	tons
	Steel class	S355	
	Elastic modulus	190	GPa
	Poisson's ratio	0	

Table 2.7: Properties of the TBM

The grout will also be modelled and the properties that will be followed are listed in table 2.8. The grout pressure at the top has been deducted by calculating the effective stress at the top of the tunnel, since the grout has to withstand this pressure in order to keep the borehole open. The gradient of the grouting pressure has not been specified yet, this since the behaviour of grout is complex. The grouting pressure gradient will be assessed during the research and based on those results, a decision will be made which gradient will be followed from then on.

In segment joints, no packing material is available and therefore concrete is in contact with concrete. The friction coefficient of this contact is guiding for the shear stiffness of these joints. The friction coefficient for concrete-to-concrete contact is 0.4 which is given by Gorst et al. [38] who have taken the value from British Standard 5975:1996. The rotation stiffness of these joints are governed by the Janssen theory.

Along the alignment of the metro line and also present at the chosen section are buildings. For the final model, four buildings will be included of which the properties are given in table 2.9.

		value	unit
Properties	Length liquid grout zone	9	m
	Grout pressure top	600	kN/m^2
	Reference depth	30.7	m below surface
	Gradient		kN/m
	Elastic Modulus	500	MPa
	γ	21	kN/m^3
	Poisson's ratio	0.3	

Table 2.8: Grout properties retrieved from effective stress at top of the tunnel.

	distance from tunnel axis (m)	width (m)	number of floors above surface (-)	number of floors below surface (-)	foundation depth (m)
Building 1	37.0	23	1	0	1
Building 2	20.0	5	1	0	1
Building 3	0.0	10	1	0	1
Building 4	20.0	40	7	2	7.5

Table 2.9: Properties of the surrounding buildings

After the tunnel has been constructed, it will be used. The train tracks constructed in the tunnel will need a flat surface and therefore a concrete aggregate will be placed in the bottom of the tunnel. The properties of this inlay and the loads of a train are given in table 2.10.

		value	unit
Properties	Height top inlay	38.4	m below surface
	Specific weight	23	kN/m^3
	Train load	145	kN per axle
	Width inlay at top	6.73	m

Table 2.10: Inlay properties for when the tunnel is in use.

3
Methodology

In order to come to the final model as described in section 2.9, a step-by-step approach will be followed. With the step-by-step approach more knowledge about the modelling is gained and flaws in the model can be spotted quicker. This due to the small steps that are taken and the short computation time the model will have in the beginning. The short computational time will also provide early comparison results in anticipation of the final model. As discussed in section 2.9 as well, not all the different loads described in section 2.2 will be modelled. A comparison will be made between the two programs, but also between the different phases in one program because it is also interesting to see the influence of the extra phases to the model. The difference between 2D and 3D modelling in the programs will be compared as well. A schematic overview of the different steps can be seen in Appendix A. The different models that will be used are discussed in section 3.1. The modelling technique of the different aspects of the tunnel construction process are discussed in sections 3.2 and 3.3 for 2D and 3D respectively. In this research versions 2016.01 and 2016 of Plaxis are used for 2D and 3D respectively. For DIANA, version 10.1 is used for both. More elaborate information on the models is given in appendix C.

3.1. Different models

The different models that will be used in for this research are described in this section, starting from the easy models to the more difficult models. A switch is made between the Plaxis and DIANA after every model and the results will be compared.

3.1.1. 2-Dimensional

Model One

First, a simple 2D model will be created with one soil layer and the ring composing of one segment. Mohr-Coulomb and linear-elastic material models will be assigned to the soil and lining respectively. For the interaction between the lining and soil, bonding is assumed. Two phases will be implemented in this model: The initialisation phase (figure 3.1a) and the phase in which the tunnel is in place (figure 3.1b).

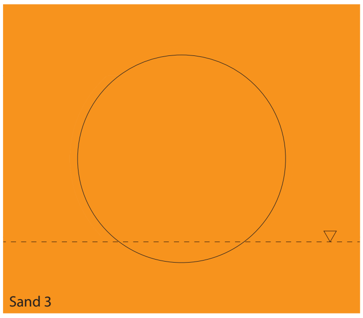

(a) Initial phase

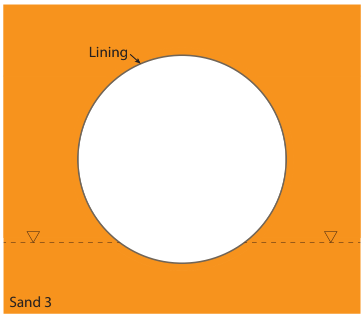

(b) Tunnel in Place

Figure 3.1: Close up of the two phases in the "Mohr-Coulomb One Layer" model

Model Two

For the next model, the number of soil layers will be increased from one to the eight soil layers which are defined in section 2.9. These soil layers all have Mohr-Coulomb as constitutive model. The phases are the same as in the previous model (fig. 3.2b).

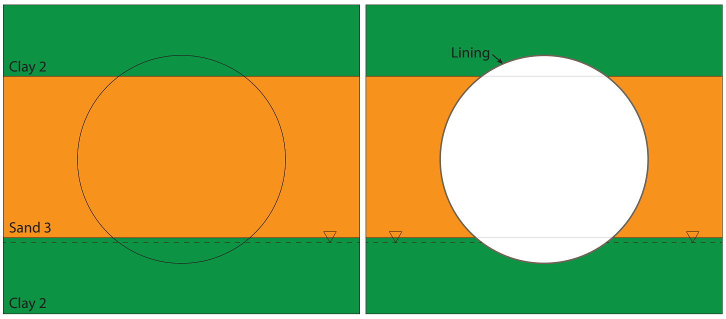

(a) Initial phase (b) Tunnel in Place

Figure 3.2: Close up of the two phases in the "Mohr-Coulomb Eight Layers" model

Model Three

While the previous models included complete bonding, this model will include slip. A reduction factor of 0.5 will be followed to account for partial slipping of the soil along the tunnel surface. How this factor will be applied will be discussed in section 3.2 and an elaborate explanation of the value of the reduction factor will be done in sections 5.1.3 and 5.1.4. The two phases remain the same, only the interface strength is adapted to account for slippage. The method for modelling bond and slip, is also discussed in section 3.2.

Model Four

After assessing the influence of the reduction factor, the material models for the soil will be changed to the Hardening Soil model. The set up as shown in fig. 3.2 will remain.

Model Five

From model four onwards, the different phases in the tunnel construction process are added. The first phase of this process to be added is the excavation of the soil. In this model, the constitutive models remain the same, only there has been added an extra phase. Instead of two phases, there are now three phases which are shown in figs. 3.3a, 3.3b and 3.3e. In the second phase a TBM has been included. Instead of the placing the tunnel directly in the soil in the third phase, a hardened grout ring around the tunnel will be modelled, since grout is used to fill up the tail void. The methods of modelling these features are described in section 3.2. While the hardened grout properties are given in section 2.9, the value for the stiffness is not always exactly known. The stiffness for this hardened grout is difficult to define since the hardening process is difficult to predict due to grout being a mixture of sand and concrete. Therefore, the influence of the hardened grout stiffness will be assessed with this model as well.

Model Six

The second construction phase to be added is the taper of the TBM. A new phase is created in the model in which this contraction is applied and therefore the model consists of four phases (figs. 3.3a to 3.3c and 3.3e). There are multiple methods for modelling the taper of the TBM, both for Plaxis and DIANA. Again, these methods are described in section 3.2. These different methods will be compared with each other and sensitivity of the model towards these methods will also be assessed.

Model Seven

In this model, the grouting phase is incorporated as well. Now there are five phases (figs. 3.3a to 3.3e). The modelling approach for the grout will be described in section 3.2.

Model Eight

After the grouting, the follow carts of the TBM apply a load on the lining. This first follow carts are driving on the lining itself before some inlay is placed on which the rest of the follow carts are driving. In this model, the first couple of carts are modelled since it is expected that they have a larger influence on the internal lining forces than the carts which are driving on a temporary inlay. The phase in which the tunnel is installed will be replaced by a phase in which the tunnel is installed and has an additional follow cart load (figs. 3.3a to 3.3d and 3.3f). This is partly based on the results of the previous models and will be discussed in section 4.1.8.

Model Nine

In this model, the last and final construction phase will be added to the model so it consists of all the construction phases. This final phase is the in-use phase where the load of the metro trains is acting on the inlay of the tunnel. Therefore this model will consist of six phases (figs. 3.3a to 3.3d, 3.3f and 3.3g).

Model Ten

Modelling these different phases leads to unloading and reloading of the soil. Therefore, as a side step, another model is created in which the soil models are changed back to Mohr-Coulomb in order to compare the results again with Hardening Soil. This will show the influence of the additional unloading/reloading stiffness parameter in the Hardening Soil constitutive model.

Model Eleven

For all the previous models, the lining is assumed to be made out of one ring, while in reality it is made out of segments. In this model, those segments (and thus the joints) are being modelled. All the phases will be included as with model nine and the soil will be applied with the Hardening Soil constitutive model. The methods for creating these segments are discussed in section 3.2. Figure 3.4 shows the location of the joints. The Janssen theory will be applied to these joints.

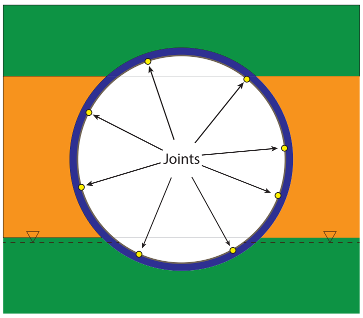

Figure 3.4: The lining with the locations of the joints

Model Twelve

The last 2-dimensional model that will be created is including the buildings located at the surface. Multiple buildings are present at the surface of which one even has multiple levels. The influence of these buildings on the tunnel lining will be assessed in this last model. The phases remain the same, the overal model will be slightly different (fig. 3.5).

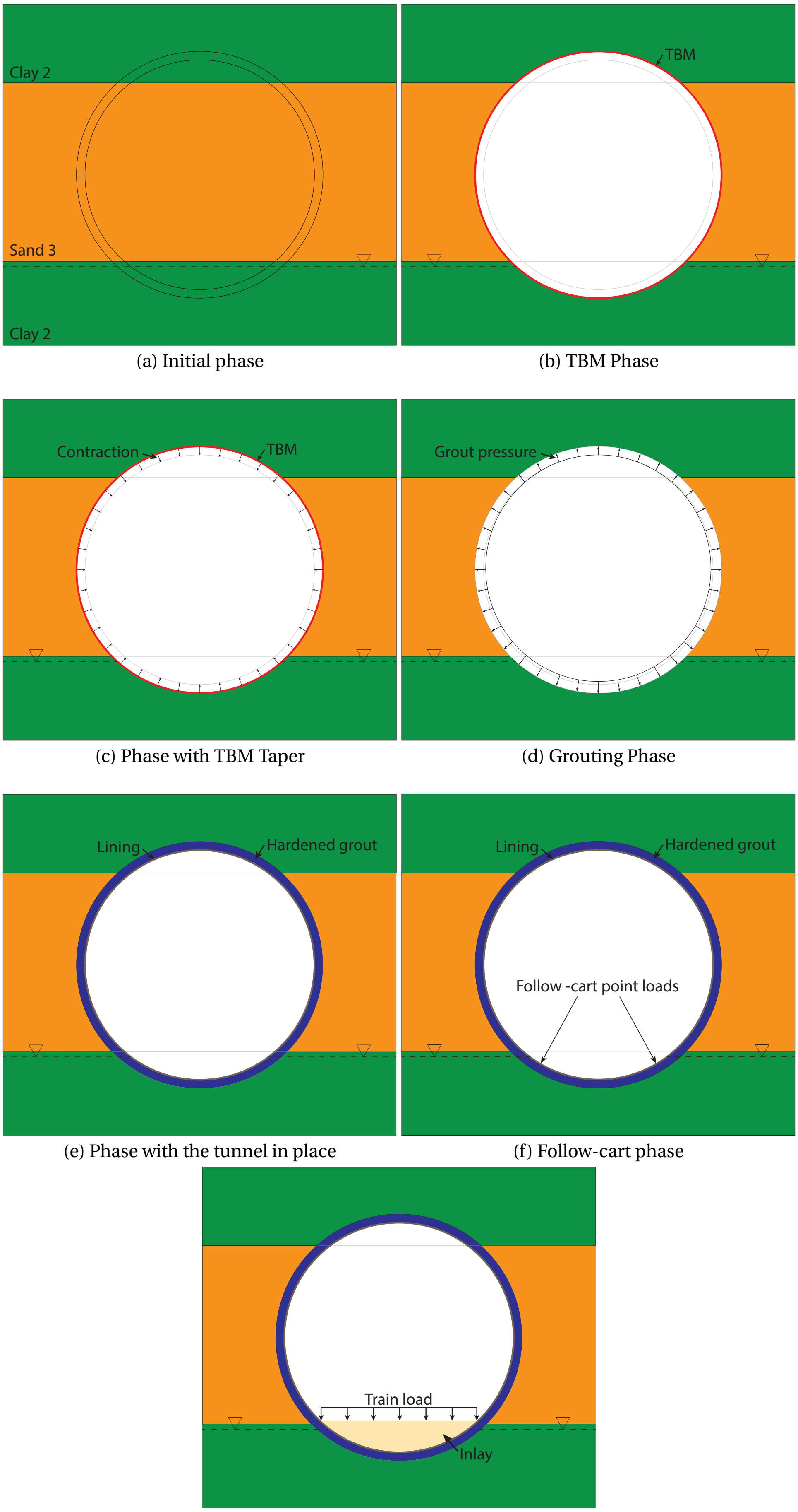

(a) Initial phase

(b) TBM Phase

(c) Phase with TBM Taper

(d) Grouting Phase

(e) Phase with the tunnel in place

(f) Follow-cart phase

(g) In-use phase

Figure 3.3: Close-up schematisation for the different phases that will be applied in the models

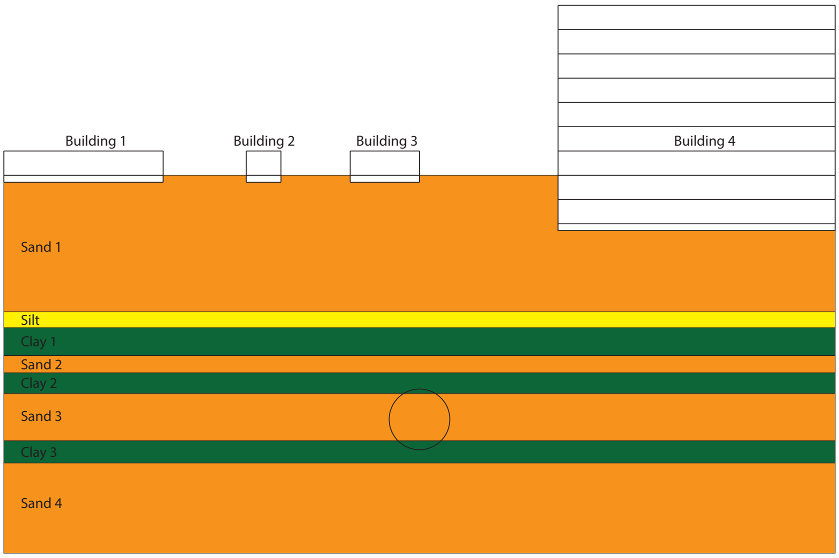

Figure 3.5: Overview of the model with buildings

3.1.2. 3-Dimensional

Three types of models are created in 3D. First, the models in which one ring is modelled will be discussed before moving on to the two models with multiple rings:

1. Without construction phases
2. With construction phases

One-Ring models

In Plaxis, the first three dimensional models that will be created exist out of one compelete ring of one and a half meters wide. This means the soil body has the same horizontal and vertical size as with the two-dimensional models, but is one and a half meters thick, so a thin slice of soil. An schematic view of this model is provided in appendix B. The same type of models will be created as the two dimensional models with the exception of the follow cart phase, the model with joints and the model with buildings. For the joints, an explanation is given in section 3.3.1. The exclusion of the follow carts and buildings will be discussed in section 5.2.1. These models with one ring will only be created in Plaxis, in section 5.2.1 an explanation is given.

Multiple rings without construction phases

After the models with one ring, more extensive models are created with multiple rings. The first is a model without the construction phases as seen in 2D and with the One-ring models. The reason behind not implementing the phases will be discussed in section 5.2.1.

Only two phases are included in these models: **1.** Initialisation **2.** Constructed tunnel. In the last phase, all the different rings are activated and placed at the same time. Between the rings and segments no joints are applied, thus it will be a monolithic tunnel. This issue on the joints will be discussed in section 3.3.1.

Multiple rings with construction phases

The second model with multiple rings includes the different construction phases. Except for the inlay and follow cart, this model will have the same construction phases as with the two dimensional and the one-ring models. The tunnel itself will consist of multiple rings without any joints. The exclusion of joints will be discussed in section 3.3.1. The model starts with an initialisation phase. For every phase after, the construction phases will progress through the soil. The TBM will be present on two rings, the same accounts for the grouting phase. So for the tunnel between not being excavated yet and the lining being constructed are four phases. This model is only created in Plaxis and the explanation is given in section 5.2.3.

3.2. 2D modelling techniques

With the different models described, a description of the different features that are applied in the model will be given in this section for the two dimensional models. First the techniques used in Plaxis will be discussed and after, the techniques in DIANA.

3.2.1. Plaxis

In order to model the construction process of the tunnel as close to reality as possible, multiple aspects have to be modelled. How these aspects are modelled in Plaxis is discussed in this section. This section will describe the 2D approach, the techniques in 3D will be discussed in section 3.3.1.

Soil

For the soil layers, the borehole tool is used in Plaxis. The top and bottom height of the different layers can be given and materials assigned to the different layers, so either Hardening Soil materials of Mohr Coulomb materials. For the first model, only one layer is specified while for all the other models, eight layers are specified with the borehole tool. The height of the hydraulic head can also be set in this tool. The Mohr-Coulomb parameters for the first models are converted from the Hardening Soil parameters given in section 2.9.

Lining

Modelling the tunnel is done through the tunnelling tool in Plaxis. In this tool a circle representing the tunnel is created from the axis location and radius as input. From that ring, plates and a negative interface are created. For the plates, the "lining" material model is selected which has the properties of the lining as given in section 2.9 and is an elastic, isotropic material. For the negative interface, a thickness of 0.01 m is applied. In order to input the stiffness of the concrete, Plaxis demands an axial stiffness, "EA" and a flexural rigidity, "EI". These stiffnesses have been deducted from the Young's modulus of uncracked concrete. Inputting specific weight of the material is done through entering a force per unit length per unit width. Table 3.1 shows the input values that have been used. The created negative interface is located on the outside of the tunnel and is used to model the lack of friction. This interface will receive its properties from the surrounding soil.

		value	unit
Properties	Axial stiffness "EA"	1.225e+07	kN/m
	Flexural rigidity "EI"	1.250e+05	kN m^2/m
	Specific weight	8.75	kN/m/m
	Poisson's ratio	0.2	-

Table 3.1: Lining input properties in Plaxis

Bond/slip

An interface is used in order to model relative movement of the lining with respect to the soil. Which means shearing material at the contact between the lining and the soil may occur. That contact can be somewhere between rough, so the soil is fully bonding to the lining, or smooth, the soil is slipping along the lining, as discussed in section 2.2.4. In Plaxis, the roughness of the interface is given in the material properties of the surrounding soil by setting a value for the strength reduction factor, "R_{inter}". The behaviour of the interface elements is an elastic-plastic model with a Coulomb criterion. When it is elastic, slipping and gapping or overlapping may occur. Which means relative movement parallel to the interface or displacement perpendicular to the interface may occur. The distinction between elastic and plastic behaviour is coming from the Coulomb criterion. With this criterion, a shear stress is calculated for which the interface behaviour remains elastic. When the shear stress on the interface is higher, the interface will behave plastic and thus permanent slip will occur within the interface. The input for the elastic-plastic model and the Coulomb criterion is coming from the surrounding soil parameters. By using the strength reduction factor and taking a value below one, these values can be decreased for the interface. This is done since usually the contact between soil and lining is weaker and more flexible than the soil [12]. The lowest value possible, to reduce most of the strength and therefore the friction, is 0.01. For modelling "slip" in this research, the strength reduction factor is set at 0.5. The strength reduction factor only works when there is an interface created at the lining or the TBM. The equations used in Plaxis for calculating the interface properties are given by Brinkgreve et al. [12], but are also discussed in section 5.1.4.

TBM

For the TBM, the same approach as with the lining is followed. So a circle is created in the tunnel tool in Plaxis, this time with a larger diameter than the tunnel but with the axis at the same location. From the circle, plates and a negative interface are created. The negative interface has a thickness of 0.01 m.

TBM taper

The taper of the TBM is modelled by applying a line contraction to the plates. This can be done in the tunnelling tool. The value for this contraction is "the area loss as a percentage of the total tunnel area" [12]. With a 9.4 m and 9.35 m as initial and final TBM diameter respectively, the contraction used is 1.06%. This method is the preferred method by Plaxis for modelling the taper of the TBM.

Another approach of modelling the taper is available however and can be done by creating a stress release of the soil surrounding the TBM. This can be achieved by modelling the total excavation but not applying the TBM in the model. Instead, the calculation phase in which this taper is acting is not entirely run. Plaxis can be forced to terminate early by setting a value for the total multiplier called "$\sum M_{stage}$". This total multiplier is set a 1.0 when the entire calculation phase is to be run. When it is to terminate early, this value can be reduced [12].

Grout

The effects of grouting are modelled by applying a hydraulic pressure in the excavated soil clusters equal to the properties given in section 2.9. The pressure at the top of the excavation is given by setting the pressure and the reference height. An increment with depth is also given. The value of this depth gradient will be assessed and discussed. This hydraulic pressure results in a radial pressure on the borehole. This approach is not realistic, as discussed in section 2.8.1. However, this is the preferred approach in Plaxis for modelling grout.

Follow-cart load

As already discussed in section 3.1, the first follow carts are driving directly on the tunnel lining. The other follow carts are driving on a temporary elevated platform which leans on the tunnel lining at the same location as the wheels of the first carts. Therefore the follow carts will be modelled by applying a point load at the location where the wheels drive and the elevated platform leans on the lining.

Inlay

For creating the loads during use, a volume is created in the bottom of the tunnel to represent the concrete aggregate. On this volume a line load is set to model the tunnel loads. The most conservative case is assumed when two train are passing each other and both axles are at the same points. So the line load will have the load of two train axles divided over the width of the inlay. This leads to a value of -45.5 kN/m/m.

Joints

For the joints, instead of creating a complete circle, eight curves are created, one for each segment. Together the eight curves are a complete circle. For all the curves, plates and negative interfaces are created. The actual joints are modelled by creating connections between these curves. For these connections, the rotation can be set fixed, free or as a spring. The joints will modelled as a spring on which the Janssen theory will be applied that is described in section 2.3.4. Plaxis requires a rotational stiffness as input for the joints. In order to apply the Janssen theory, iterations to assess this rotational stiffness are done manually. A starting rotational stiffness is used after which the normal force and bending moment are calculated by Plaxis. With these forces, the stiffness of the joints is back calculated by using equations eqs. (2.1) and (2.2). The used input stiffness in the joints is changed until it meets the calculated stiffness. This has to be done for every joint seperately. An overview of this procedure is given in fig. 3.6.

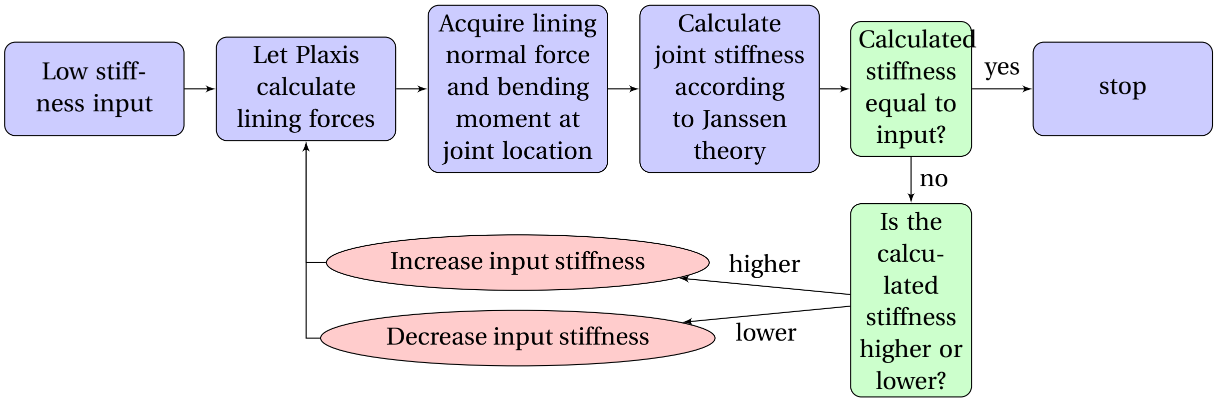

Figure 3.6: Manual Janssen iteration procedure

Buildings
The buildings are modelled by the use of plates. These plates have the same stiffness as the lining except for the weight, that has been put on zero. Instead a line load is applied to the bottom of the building, so at the foundation depth.

3.2.2. Modelling in DIANA

While the same construction process is trying to be recreated, not everything is modelled with the same approach in both programs. This section will elaborate on the modelling techniques used in DIANA for modelling the construction process of a tunnel as close to reality as possible.

Soil
The soil is modelled by creating a rectangular face for each soil layer. After which every soil layer is assigned to a material. These materials have been created beforehand or are created when assigning them to the faces. No property geometries are assigned to the soils. In order to ensure the stresses in the soil are calculated, a global dead weight load is assigned to all the soils. This global dead weight load will also be applied on the other features in the model.

Hydraulic head
A hydraulic head load is created to model the ground water level. This load requires the shapes on which it acts and the height of the hydraulic head. This approach of assigning the hydraulic head requires the mass density of the soil to be specified by the dry density and porosity. This can be assigned in the material properties. This load is included in the same load case as the dead weight. From the dry density and the porosity, the pore pressure are calculated in the soil.

Lining
The lining is modelled by creating a circle at the location of the tunnel. This circle is imprinted on the soil layers but the circle is kept. From the faces that have been created by the imprinting, the excavation face will be created through extraction. This excavation face will be subtracted from the soil. This will create soil layers with a hole which can be filled by the excavation faces. On the line the material properties are assigned with the lining properties given in section 2.9, the element geometry is assigned with the thickness of the lining: 0.35 m.

Bond/slip
On the face of the lining, and also the TBM, interface elements can be created. However, the lining and TBM are lines in the model. When selecting them for interface, an interface on either side of that line will be created while only one between the lining/TBM and soil is needed. Therefore the interface is created from the borehole wall. An interface material model can be assigned. A Coulomb-friction criterion is chosen to model the friction along the lining and TBM. When assigning the element geometry to this interface, a geometry with a thickness of 0.01 m is assigned. While it is possible to assign a thickness of zero and this is the case in reality, the interface properties cannot be determined with the guidelines explained below. While Plaxis determines the interface properties based on the soil and strength reduction factor itself, in DIANA, these properties are required as input:

- Normal interface stiffness;
- Shear interface stiffness;
- Cohesion;
- Friction angle;
- Dilatancy angle

The input properties for the element stiffnesses can be defined with the following guidelines [28]:

$$\text{Shear stiffness} = \frac{A^2}{t}\frac{E_{soil}}{2(1+\nu_{soil})} \tag{3.1}$$

$$\text{Normal stiffness} = f \cdot \text{Shear stiffness} \tag{3.2}$$

with:

A	Reduction factor
t	Interface thickness
E_{soil}	Young's modulus of surrounding soil
ν_{soil}	Poisson ratio of surrounding soil
f	Multiplication factor that can vary between 10 and 100.

For the Coulomb-friction input parameters, the following guidelines are followed [28]:

$$c = A \cdot c_{soil} \tag{3.3}$$

$$tan\phi = A \cdot tan\phi_{soil} \tag{3.4}$$

With c_{soil} and ϕ_{soil} the cohesion and friction angle of the soil respectively.

When using the highest values of the surrounding soils for the different properties, the following input is acquired for a reduction factor of 0.5 and a multiplication factor of 100 as a first assessment of the interface:

		value	unit
Properties	Normal interface stiffness	3.71e+07	kN/m
	Shear interface stiffness	3.71e+05	kN/m^3
	Cohesion	3.2	kN/m^2
	Friction Angle	17.8	degrees
	Dilatancy angle	0	degrees

Table 3.2: Interface input properties in DIANA

TBM

The TBM is modelled in the same way as the lining. A circle is created for the TBM itself and imprinted in the soils. The faces extracted from the imprinting are the tail void soil clusters. These shapes are subtracted from the soil layers again. The material model with the properties of the TBM given in section 2.9 is assigned to this circle and an element geometry with a thickness of 0.05m is applied.

TBM taper

The first method to model the taper of the TBM is by applying a stress release value. In order to do this, the calculation phase with the taper does not include the TBM. Instead, the stress release value will be applied to the TBM. A value of 1.0 means there is no stress release and a value of 0 means there is no support any more at all.

Assigning a prescribed deformation to the TBM is another way to model the taper. This displacement will only exist of translational deformations. Functions are created for the deformation in the vertical and horizontal direction. These functions ensure the prescribed displacement occur at the right location. For the top and bottom of the TBM, there will be no prescribed displacement in the horizontal direction while at the sides of the TBM, no prescribed displacements occur in the vertical direction. This load will be placed in a different load case than the dead weight and hydraulic head.

Grout
The grout is modelled by a line load on the borehole wall. This load coincides with the grout properties given in section 2.9 by creating functions for the grouting load in both directions. By using these functions it can be assured that the line load becomes a radial load. This load will be placed in a load case with self weight and will only applied in the phase with grouting.

Follow-cart load
In DIANA the load of the follow carts will be modelled with the same approach as used in Plaxis.

Inlay
For the inlay, an extra element cluster is created within the tunnel, located at the bottom. This cluster is given an inlay material model, with a high stiffness and a weight. On this inlay, a line load representing weight of the metro trains is applied. The properties of the inlay and train load are given in section 2.9. Again, the most conservative case is taken in which two train pass each other at the modelled lining ring.

Joints
In order to model the joints, the lining is modelled differently as well. A ring with the diameter of the lining is divided into 8 segments by imprinting points on the lining. The points have the location of the joints. The segments that have be formed are used to deduct the excavation clusters from the surrounding soil body. While DIANA has the possibility of creating point interfaces, it is not yet possible in DIANA to apply a point interface with the Janssen theory. Therefore a rotational spring will be modelled on which the same approach will be applied as with Plaxis, so the manual Janssen iterations.

Buildings
The buildings are constructed by creating lines. These lines are imprinted in the soil again. The created are extracted and subtracted from the soil again. A building material model is given to these lines without any weight. The weight of these buildings is modelled by applying a line load on the bottom plates of the building.

3.3. 3D modelling techniques

Some of the modelling techniques differ little between two and three dimensions, others might be different. This section will discuss the modelling techniques used for the 3D models in Plaxis and DIANA.

3.3.1. Plaxis

Soil
Creating soil in 3D in Plaxis is equal to that in 2D. The given model size at the start of the project will create the soil layers given in the borehole tool in three dimensions.

Lining
Again the tunnelling tool in Plaxis is used in order the create the lining. Everything is the same as in 2D except for modelling the length of the tunnel. In the tunnelling tool a ring size can be assigned and the number of rings can be set as well. Plaxis itself creates the different excavation clusters and the different lining rings.

Bond/slip
This approach is equal to the approach in 2D. In the tunnelling tool a negative interface can be assigned to the plates. When creating the extra rings, this negative interface is created along every part of lining as well.

TBM
This approach differs from the 2D approach that has been used, but is also available in 2D. In the tunnelling tool a "thick" lining is created. Plaxis creates another circle in the tool at the given "thickness" of the lining. From this circle, plates can be created and a TBM material can be assigned.

TBM taper
The taper is practically created the same, a line contraction is applied to the TBM plates. The contraction value also remains the same. However, when modelling the phases, this taper moves through the soil and the TBM taper is applied over multiple rings. Therefore, Plaxis requires a reference distance for every phase in order to assess how much taper should be applied for that part of TBM plates in that phase. This has to coincide with the right amount of taper over the total length of the TBM. A good explanation and example is given by Brinkgreve et al. [12].

Grout
The grout will be modelled in the tunnelling tool as a load on the outside circle, the TBM in this case. When the grout should be active, this load should be activated. The TBM does not have to be active in order to do so.

Follow-cart load
For creating the follow-cart load, a line load can be used. When creating this line load, the begin and end of the line is required as input and the loading in three directions. However, when creating the model, the mesh needs to very fine at the location of the line load to make sure it works on nodes. This very fine mesh causes the model to have a large computational time.

Inlay
In order to create an extra soil cluster to account for the inlay, a surface can be made to create a seperation in an existing soil cluster. The same approach as in 2D, but with the third dimension added. However, when following the height of the inlay as in 2D, the meshing also becomes a problem. The mesh has to be very fine in order to accept the location of the inlay and this causes a large computational time.

Joints
Joints have to be created in the analysis itself. In order to create the different segments, the same approach can be applied as in 2D by creating different curves. In the analysis, a connection can be made between the different segments. However, this connection can only set to "fixed" or "free" and no stiffness can be assigned, neither a rotational nor a translational stiffness.

3.3.2. DIANA
For the three dimensional models in DIANA, less modelling techniques will be discussed. An explanation on this matter will be given in chapter 5.

Soil
The soil in DIANA is modelled by creating a sheet, just like in 2D, but in order to add the third dimension, the sheets are extruded. This will create the solids that represent the soil. A dead load will also be applied in 3D.

Hydraulic head
The hydraulic head is modelled with the same approach as in 2D. A load has to be added on all the shapes that are influenced by the hydraulic head. A height of the head is required for input again.

Lining
The lining is modelled by creating a circlesheet at the location of the tunnel. This circlesheet is extruded as well for a length which is equal to the width of the lining ring. After, this ring will be copied five times so a total of six rings has been created. These circle sheets will subtracted from the soil layers and will results in an excavation solids and the soil layers. The lining is created by selecting the faces on the outside of the excavation solids and extract these, creating surfaces. While the material properties are assigned with the lining properties given in section 2.9, the element geometry is assigned with the thickness of the lining: 0.35 m. Regular curved shell elements will be used for the lining.

Bond/slip
As with 2D, the interface will be modelled from the face of the soil surrounding the lining. To these elements, an interface material model can be assigned. A Coulomb-friction criterion is chosen to model the friction along the lining and TBM. When assigning the element geometry to this interface, a geometry with a thickness of 0.01 m is assigned. The guidelines and values discussed in section 3.2.2 will be used again. The shear stiffness has to be used twice, for the extra third dimension.

Joints
In 3D, line interfaces can be created between shells in DIANA. These interfaces can be given a material model with the Janssen theorem and coulomb friction. DIANA does the iterations regarding the rotational stiffness of the interface itself.

4

Results

This chapter will discuss the results acquired from the different models. Just as with the investigation itself, the results will be discussed in the step-by-step approach. If any differences may occur, the cause of this will be discussed in chapter 5, which means the results in regard to the research questions will be given in that chapter. First the results of 2D will be discussed before moving on to 3D.

4.1. 2-Dimensional

4.1.1. Model One

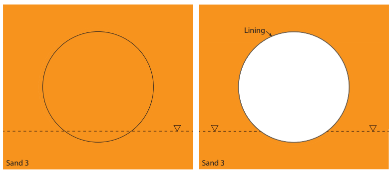

Figure 4.1: Phases in model one

Figure 4.2 shows the results of the normal forces and the bending moments for Plaxis and DIANA acquired from model one. This model only consists of one soil layer which has a Mohr-Coulomb constitutive model. Very little difference between Plaxis and DIANA is encountered for both the normal force and bending moment for this model as the lines in figs. 4.2a and 4.2b are not differing from each other. There is also little difference between the maximum and minimum values given in figs. 4.2c and 4.2d.

4.1.2. Model Two

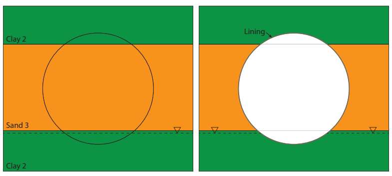

Figure 4.3: Phases in model two

Figure 4.4 shows the results of the normal forces and the bending moments for Plaxis and DIANA acquired from model two. This model has eight soil layers with a Mohr-Coulomb constitutive model. What accounted for the model one results, also accounts for these results. The values for both the normal force and bending moment are almost equal along the entire lining. The extreme values differ very little as well.

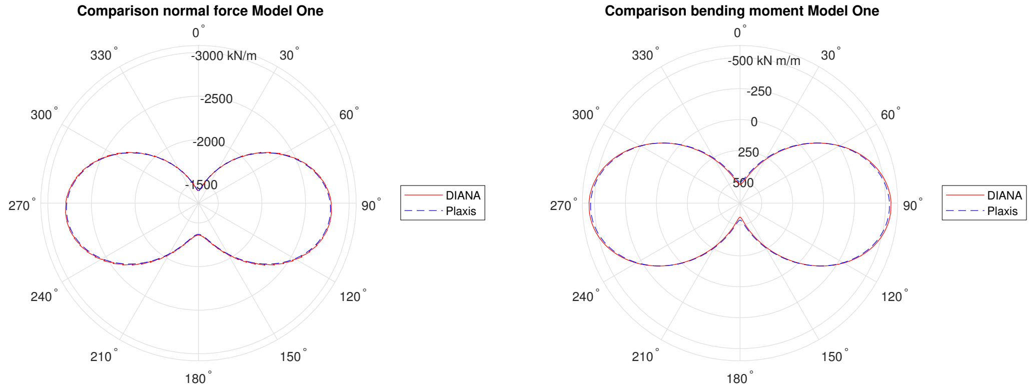

(a) Normal forces (b) Bending moments

	Max [kN/m]	Min [kN/m]
Plaxis	-1418	-2788
DIANA	-1415	-2800

(c) Extreme values for normal force

	Max [kN m/m]	Min [kN m/m]
Plaxis	538.4	-531.8
DIANA	562.7	-544.1

(d) Extreme values for bending moment

Figure 4.2: Results for the normal force and bending moment for model one

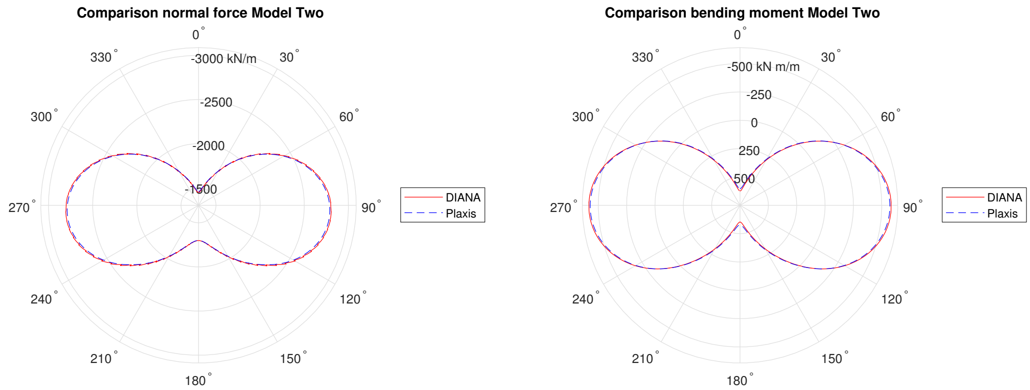

(a) Normal forces (b) Bending moments

	Max [kN/m]	Min [kN/m]
Plaxis	-1457	-2791
DIANA	-1447	-2807

(c) Extreme values for normal force

	Max [kN m/m]	Min [kN m/m]
Plaxis	603.3	-571.7
DIANA	625.0	-582.8

(d) Extreme values for bending moment

Figure 4.4: Results for the normal force and bending moment for model two.

4.1.3. Model Three

Figure 4.5 shows the results of the normal forces and the bending moments for Plaxis and DIANA acquired from model three. This model has a reduction factor of 0.5 for the interface strength instead of full bonding in the previous models. From fig. 4.5a it can be seen that the little difference between Plaxis and DIANA occurs at the sides of the tunnel. This difference is not that large when looking at fig. 4.5c. For the bending moment, the figure is less clear, but there is a difference which can be seen in table 4.5d. However, this is also a small difference.

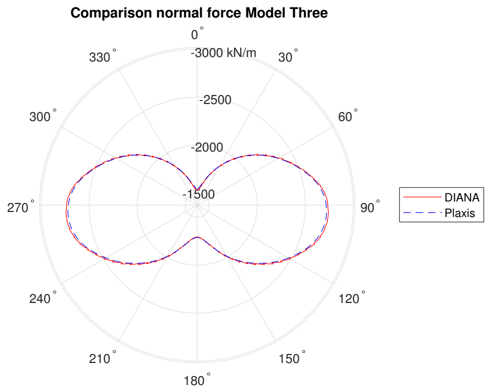

(a) Normal forces

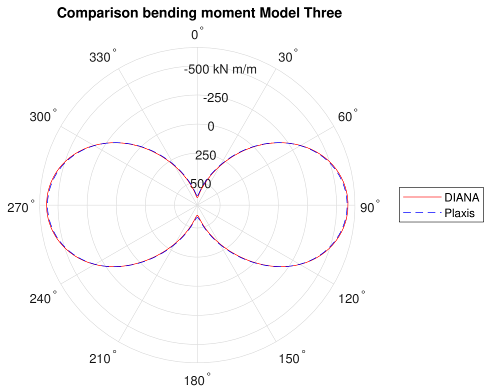

(b) Bending moments

	Max [kN/m]	Min [kN/m]
Plaxis	-1546	-2729
DIANA	-1527	-2743

(c) Extreme values for normal force

	Max [kN m/m]	Min [kN m/m]
Plaxis	626.2	-597.9
DIANA	632.6	-597.8

(d) Extreme values for bending moment

Figure 4.5: Results for the normal force and bending moment for model three

4.1.4. Model Four

The results for model four are presented in fig. 4.6. This models is a continuation of the previous model, so partial slipping along the lining is present in this model but the material models for the soil have been changed. When comparing the figs. 4.6a and 4.6b with the figs. 4.5a and 4.5b, it can be seen that the shapes of the different lines are not exactly the same. Compared to model three, the normal forces are approximately the same. The difference in bending moment between Plaxis and DIANA has become larger with a Hardening Soil material model for the soils (figs. 4.6b and 4.6d).

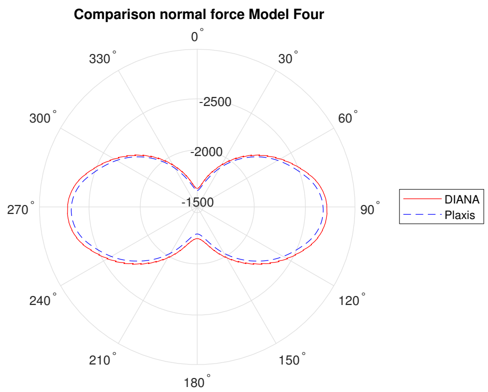

(a) Normal forces

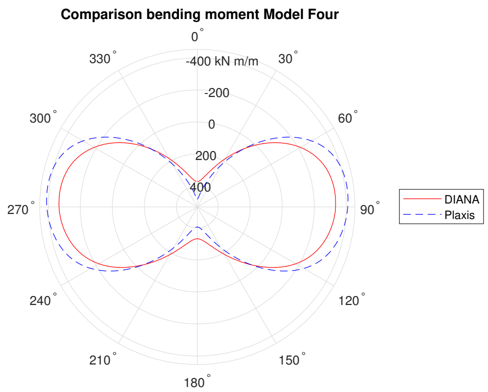

(b) Bending moments

	Max [kN/m]	Min [kN/m]
Plaxis	-1604	-2674
DIANA	-1623	-2713

(c) Extreme values for normal force

	Max [kN m/m]	Min [kN m/m]
Plaxis	482.1	-412.4
DIANA	372.4	-333.8

(d) Extreme values for bending moment

Figure 4.6: Results for the normal force and bending moment for model four

4.1.5. Model Five

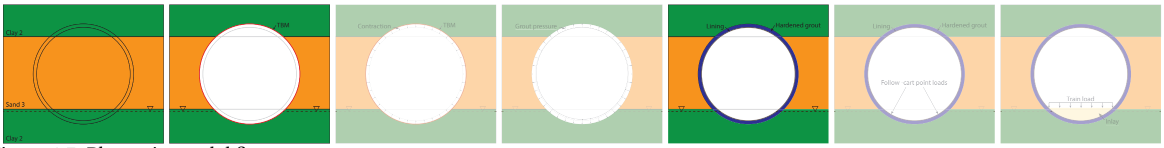

Figure 4.7: Phases in model five

The first construction phase in the process is the excavation phase which is added to create this model. The results of the internal forces of the lining are shown in fig. 4.8. When the lining is constructed after the excavation phase, the normal forces in the lining are larger for DIANA than for Plaxis at the top and bottom of the tunnel. For the sides of the tunnel it is the opposite: the lining force are larger for Plaxis than for DIANA. This is also the case for the bending moments (fig. 4.8b).

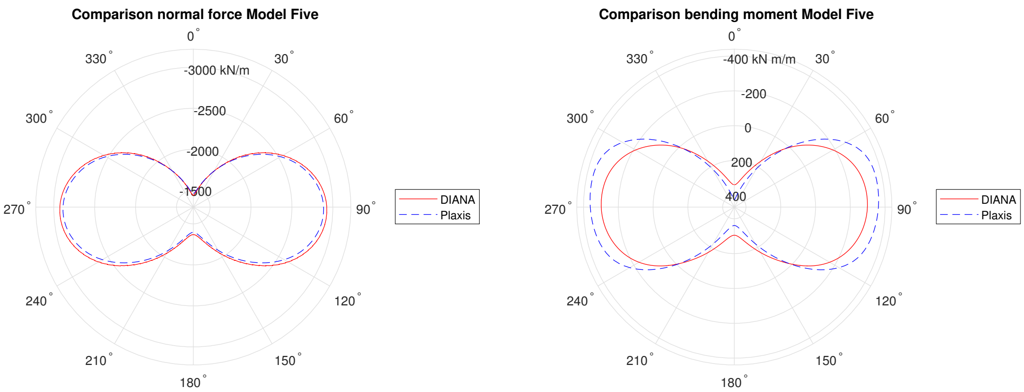

(a) Normal forces (b) Bending moments

	Max [kN/m]	Min [kN/m]
Plaxis	-1461	-2888
DIANA	-1439	-2927

(c) Extreme values for normal force

	Max [kN m/m]	Min [kN m/m]
Plaxis	424.6	-365.7
DIANA	338.9	-298.5

(d) Extreme values for bending moment

Figure 4.8: Results for the normal force and bending moment for model five

4.1.6. Model Six

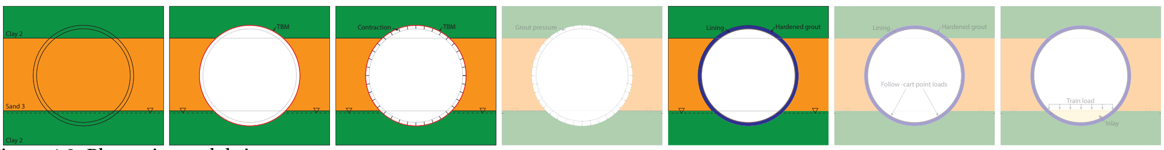

Figure 4.9: Phases in model six

In this model, the taper of the TBM, the second construction phase, is included. If the lining is placed after the taper of the TBM, the internal forces would have the values as presented in fig. 4.10. As described in section 3.2, the taper of the TBM can be modelled in different ways. For the results presented in fig. 4.10 the taper has been modelled as a contraction in Plaxis and a stress release in DIANA. The different modelling approaches and its influence on the internal lining forces are discussed in section 5.1.9. The choice for the approach that is shown in this section is also explained.

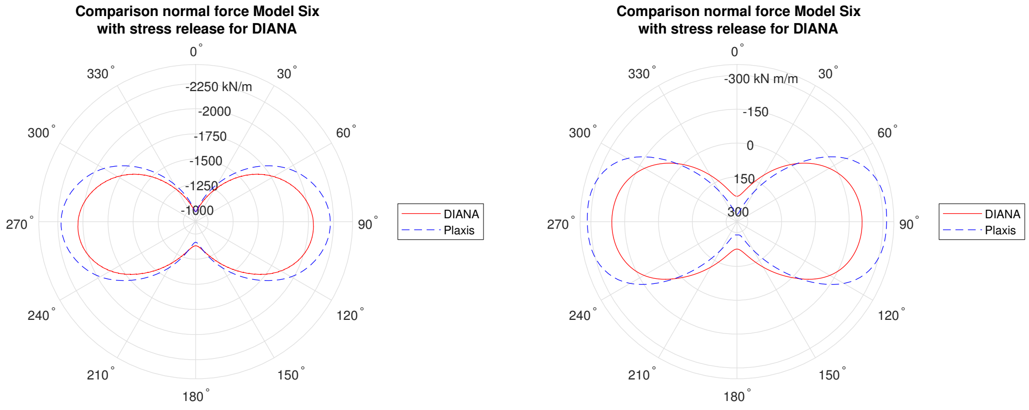

(a) Normal forces

(b) Bending moments

	Max [kN/m]	Min [kN/m]
Plaxis	-974.3	-2218
DIANA	-977.6	-2051

(c) Extreme values for normal force

	Max [kN m/m]	Min [kN m/m]
Plaxis	316.4	-316.4
DIANA	235.6	-207.0

(d) Extreme values for bending moment

Figure 4.10: Results for the normal force and bending moment for model six

4.1.7. Model Seven

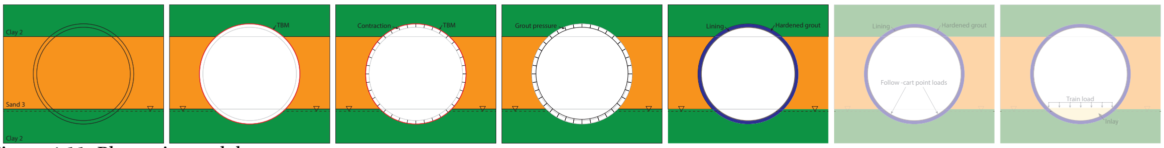
Figure 4.11: Phases in model seven

For model seven, the grouting phase has been added. When the construction process up to installation of the lining is conducted, by including the grouting phase, the results presented in fig. 4.12 are acquired. For both DIANA and Plaxis, the normal force values approach uniformity along the lining, for DIANA more than for Plaxis. This leads to very low bending moments. Since DIANA is more uniform than Plaxis, the bending moments in DIANA are lower than in Plaxis as well.

These results of almost uniform normal force and very low bending moment is caused by the drained analysis that has been used. More about this and undrained analysis will be discussed in section 5.1.10.

When having model seven with an undrained analysis and a consolidation phase after, the results in fig. 4.13 are acquired. The normal forces are not approaching uniformity anymore and thus are the bending moments not approaching zero anymore as well.

4.1.8. Model Eight

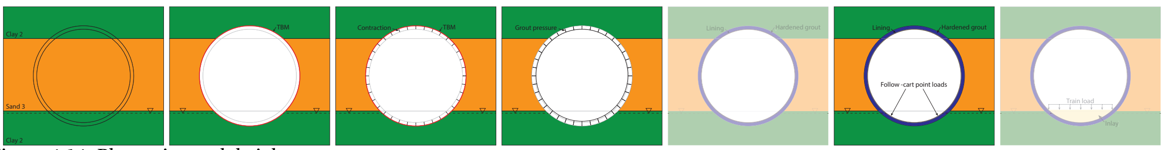
Figure 4.14: Phases in model eight

For this model, the follow-carts have been modelled. The consolidation phase has been modelled after the follow-cart phase and does not include the follow-cart load. The time the follow carts pass the modelled lining ring is very short. Therefore undrained behaviour is applicable for this phase. The results shown in fig. 4.15, are the lining internal forces after the consolidation phase.

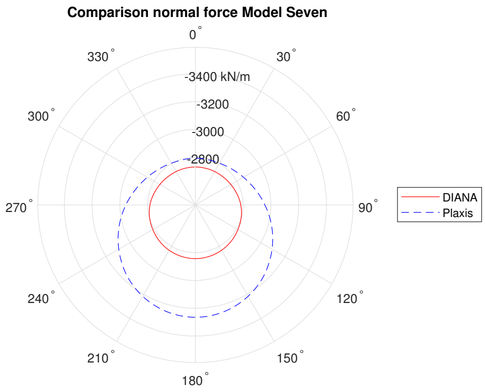

(a) Normal forces

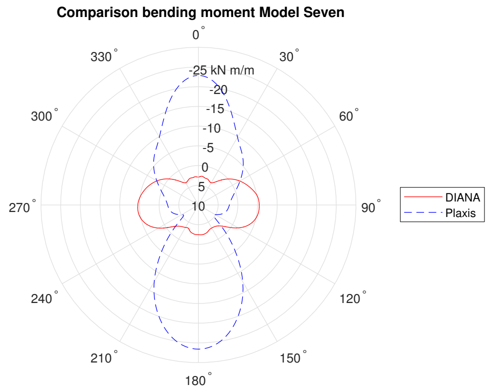

(b) Bending moments

	Max [kN/m]	Min [kN/m]
Plaxis	-2793	-3265
DIANA	-2730	-2843

(c) Extreme values for normal force

	Max [kN m/m]	Min [kN m/m]
Plaxis	5.42	-26.58
DIANA	3.60	-5.45

(d) Extreme values for bending moment

Figure 4.12: Results for the normal force and bending moment for model seven

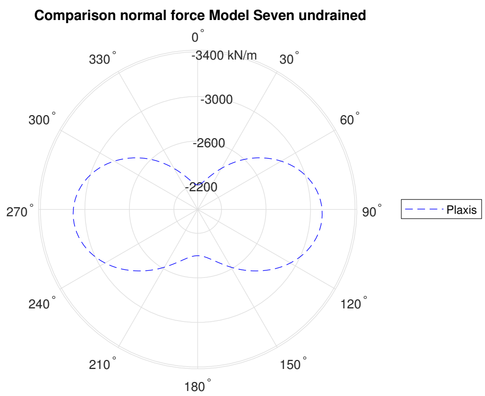

(a) Normal forces

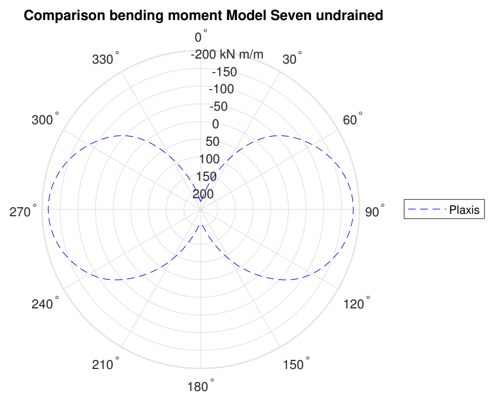

(b) Bending moments

	Max [kN/m]	Min [kN/m]
Plaxis	-2207	-3106

(c) Extreme values for normal force

	Max [kN m/m]	Min [kN m/m]
Plaxis	225.5	-183.5

(d) Extreme values for bending moment

Figure 4.13: Results for the normal force and bending moment for undrained model seven

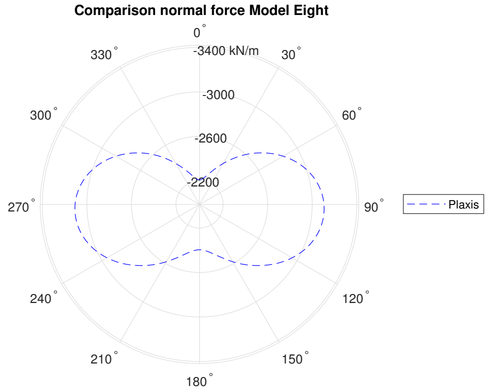

(a) Normal forces

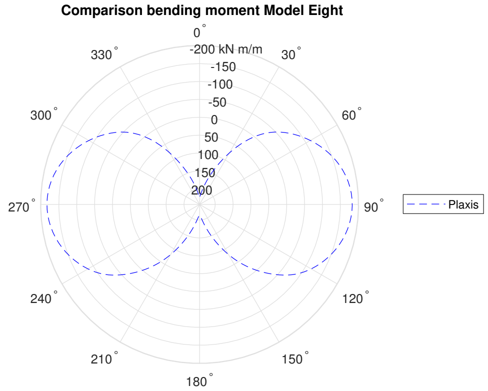

(b) Bending moments

	Max [kN/m]	Min [kN/m]
Plaxis	-2209	-3108

(c) Extreme values for normal force

	Max [kN m/m]	Min [kN m/m]
Plaxis	221.5	-183.2

(d) Extreme values for bending moment

Figure 4.15: Results for the normal force and bending moment for undrained model eight

4.1.9. Model Nine

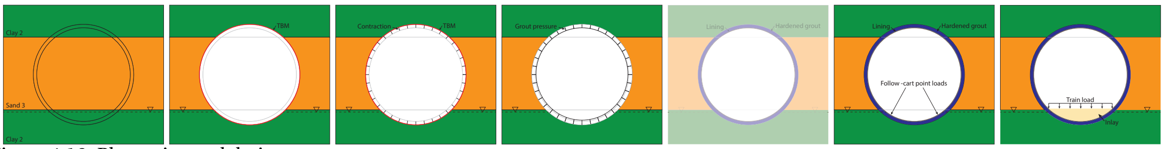

Figure 4.16: Phases in model nine

Finally, the tunnel will be taken into use. The metro train will now be driving through the tunnel in an extra phase. In this model, the consolidation phase has been placed after the follow carts have passed and before it is taken into use. During this consolidation phase, the inlay is already present. When it is in use, the analysis is also undrained. The time for which a train passes the modelled section is very short. Therefore undrained analysis suffices for this phase in the construction process. The results presented in fig. 4.17 are acquired from the undrained phase of the train passage. Compared to the previous models, the normal force at the bottom of the tunnel differs. This also results in a lower bending moment at the bottom of the tunnel.

4.1.10. Development throughout construction process

In order to assess which phase is causing changes in the internal lining forces, the extreme values of these forces have been plotted in figs. 4.18a and 4.18b. The results from Plaxis and DIANA show the same trend for both the maximum and minimum values. This is the case for the normal force results as well as the bending moment results. With regards to the normal force, Plaxis and DIANA differ very little. The different modelling approaches for the taper have some influence on the minimum value. For the bending moment, it is clearly visible that the difference between Plaxis and DIANA is created in model four. This is when the material models are changed from Mohr-Coulomb to Hardening Soil. With regards to the overal trend, it shows that when including more construction phases, the bending moment decreases.

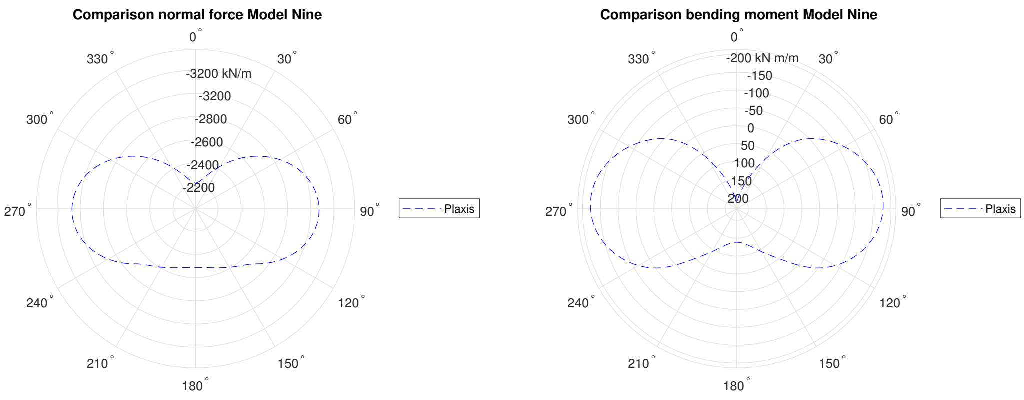

(a) Normal forces (b) Bending moments

	Max [kN/m]	Min [kN/m]
Plaxis	-2229	-3072

(c) Extreme values for normal force

	Max [kN m/m]	Min [kN m/m]
Plaxis	211.5	-178.1

(d) Extreme values for bending moment

Figure 4.17: Results for the normal force and bending moment for model nine

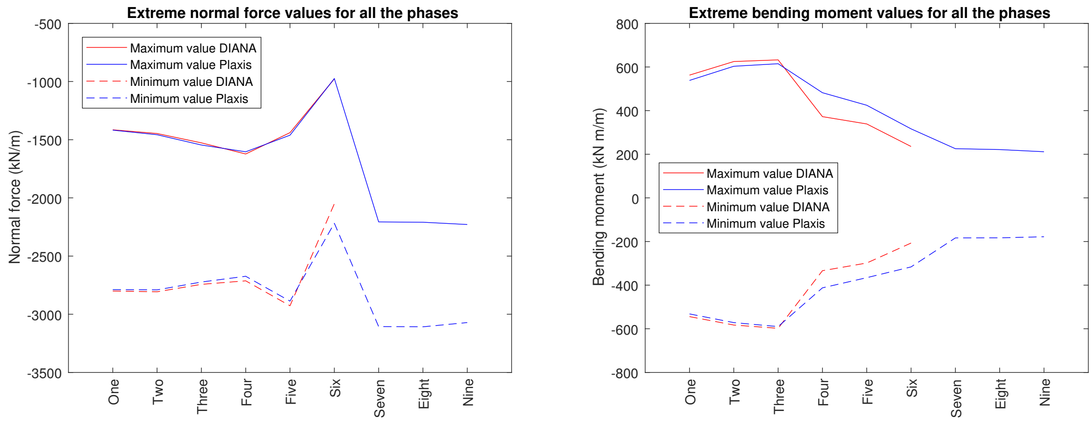

(a) (b)

Figure 4.18: Development of the internal lining forces over the complete construction process

While the trend for Plaxis and DIANA have the same shape with regards to the development of the internal lining forces, there are some differences. These differences have been plotted as a ratio and a difference in fig. 4.19 for the normal force and bending moment. For the normal force, the ratio between Plaxis and DIANA differs very little throughout the different models since they are almost equal for every model. Only the minimum normal force value difference increase with model six. However, when looking at the ratio between Plaxis and DIANA, it can be seen that this difference is not very large compared to the total minimum normal force. The ratio stays below 1.1 which means the difference is less than ten percent. As shown above, the difference in bending moment between Plaxis and DIANA originates in model four, which is the change in material models. From there on, the ratio of the maximum values remains at approximately the same level. As for the minimum values, the ratio changes, because the difference increases, but also because the actual bending moment values decrease, resulting in a higher ratio difference.

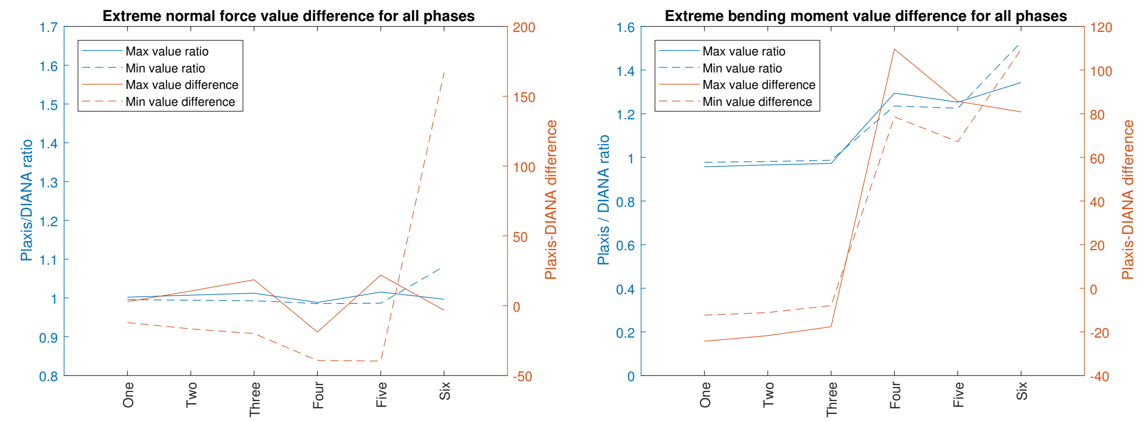

(a) Normal force (b) Bending moment

Figure 4.19: Ratio and absolute difference between Plaxis and DIANA

4.1.11. Model Ten

In order to assess the difference between the Mohr-Coulomb and Hardening Soil material models again, all the different phases in the construction process have been carried out with Mohr-Coulomb material models as well. Figure 4.20 shows the normal force and bending moment for all the models in the construction process with Mohr-Coulomb and Hardening Soil material models.

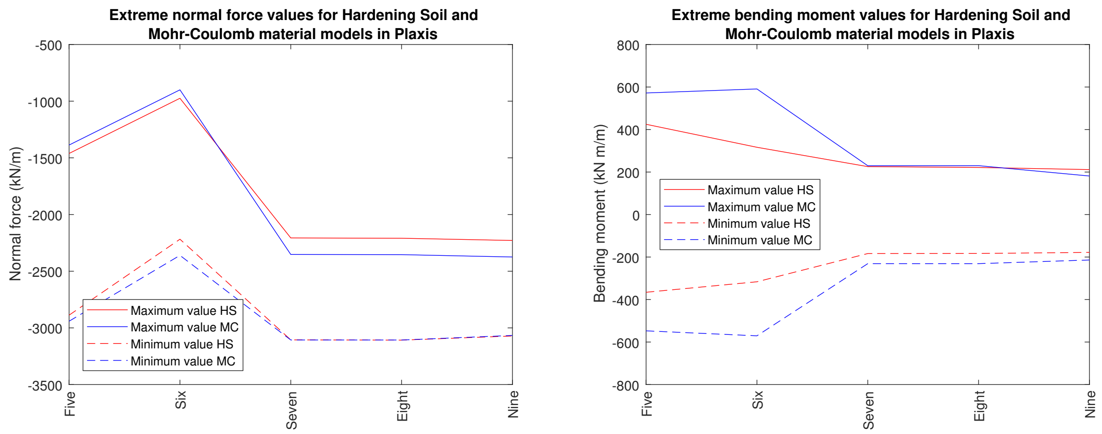

(a) Normal force (b) Bending moment

Figure 4.20: Lining forces for Hardening Soil and Mohr Coulomb material models for models five to nine

The figures show that for the different models, the normal forces are approximately equal for Hardening Soil and Mohr-Coulomb. The difference in bending moment between Hardening Soil and Mohr-Coulomb could have already been spotted by looking at the results of model three and four (figs. 4.5 and 4.6). It can also be spotted by looking at the bending moments for all the different models shown in fig. 4.18b. In these models, no excavation phase has been added yet.

The phases in which the soil is excavated and the TBM taper is modelled add to the difference between Hardening Soil and Mohr-Coulomb. This difference is nullified by the grouting phase which is added in model seven. The last construction phases with the follow carts and the train load do not lead to a difference between Hardening Soil and Mohr Coulomb.

4.1.12. Model Eleven

The stiffness for every joint as a results of the manually performed Janssen iteration is shown in fig. 4.21. Almost all the joints are closed and for the joints which are gaping, the stiffness is close to that of a closed joint.

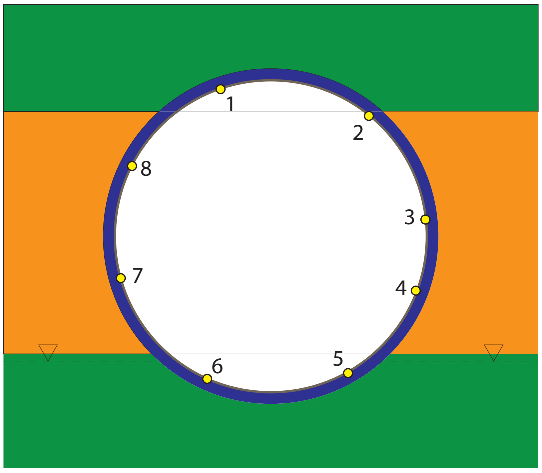

(a) Joint numbering

Joint	Rotational stiffness [kN m/m/rad]	Open/closed
1	1.32e+05	open
2	1.44e+05	closed
3	1.43e+05	open
4	1.44e+05	closed
5	1.44e+05	closed
6	1.44e+05	closed
7	1.44e+05	closed
8	1.44e+05	open

(b) Rotational stiffness for each joint

Figure 4.21: Joint numbering and accompanying rotational stiffness

With these stiffnesses for the different joints, the results shown in fig. 4.22 have been acquired.

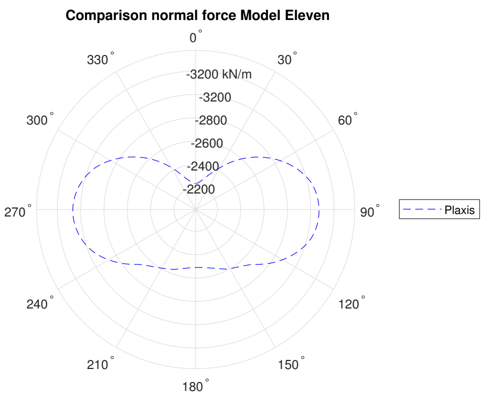

(a) Normal forces

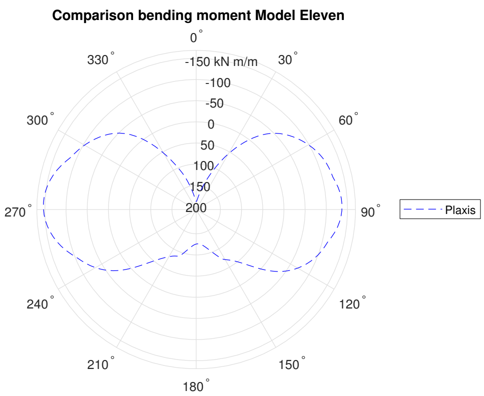

(b) Bending moments

	Max [kN/m]	Min [kN/m]
Plaxis	-2237	-3071

(c) Extreme values for normal force

	Max [kN m/m]	Min [kN m/m]
Plaxis	188.3	-153.5

(d) Extreme values for bending moment

Figure 4.22: Results for the normal force and bending moment for model eleven

4.1.13. Model Twelve

In this model, the buildings have been added. As discussed in section 3.1 the buildings are included after the initialisation phase and before the tunnel construction commences. The results are shown in fig. 4.23.

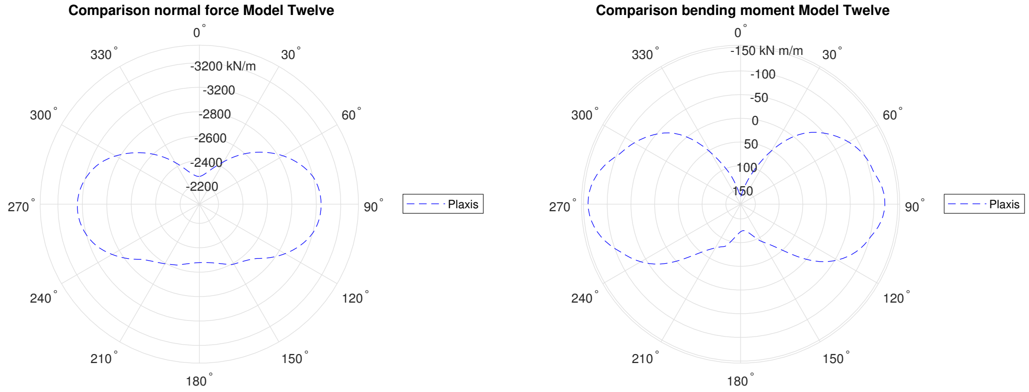

(a) Normal forces (b) Bending moments

	Max [kN/m]	Min [kN/m]
Plaxis	-2270	-3041

(c) Extreme values for normal force

	Max [kN m/m]	Min [kN m/m]
Plaxis	164.6	-140.3

(d) Extreme values for bending moment

Figure 4.23: Results for the normal force and bending moment for model twelve

4.2. 3-Dimensional

The results of the three dimensional models will be presented in this section. First the one-ring models in Plaxis will be presented before moving on to the multiple ring models in Plaxis and DIANA.

4.2.1. One-ring models

When comparing the different one-ring models with the two dimensional models, fig. 4.24 is acquired. The forces over the entire lining for every model in two and three dimensions are attached in appendix I. It can be seen that the normal forces are almost equal in two and three dimensions for the different construction phases. The bending moment is almost exactly the same in two and three dimensions.

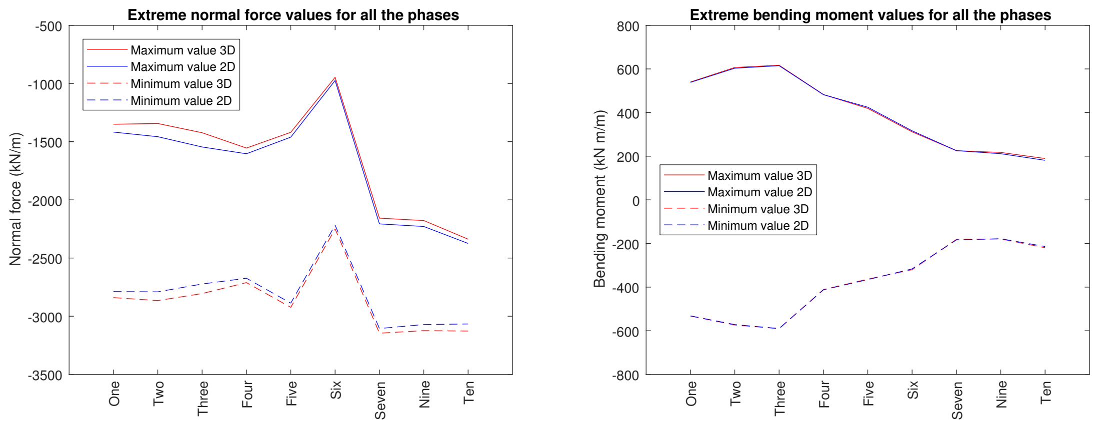

(a) (b)

Figure 4.24: Development of the internal lining forces over the different models in 2D and 3D

4.2.2. Without construction phases

When not modelling the construction phases or the joints, the results in fig. 4.25 are of a cross section through ring six of the ten ring model in Plaxis and the fourth of six rings in DIANA. The results for Plaxis look very strange with many peak forces. In order to acquire the results of a ring in 3D, a cross section is made in the center of ring six after calculation has been done. This section does not cross every element exactly at a node. Since it is done after the calculation an interpolation between nodes provides the value at the location of the cross section. However, these are still interpolated values. This is the cause of the irregular curve, mainly in fig. 4.26a. The results for DIANA on the other hand are smoother. While cross sections are easy the create in DIANA, the data from that cross section cannot be exported. Instead, an extra ring is created in the model before the analysis, a so called "composed line". This ring does not have a material assigned and it does not influence calculations. It only remembers the structural forces at the location of that "composed line". The curve of DIANA in fig. 4.25a looks much like a trendline for the Plaxis curve. This shows that the results are equal, as can been seen with the bending moment as well. The displacements in both programs can be found in appendix F.

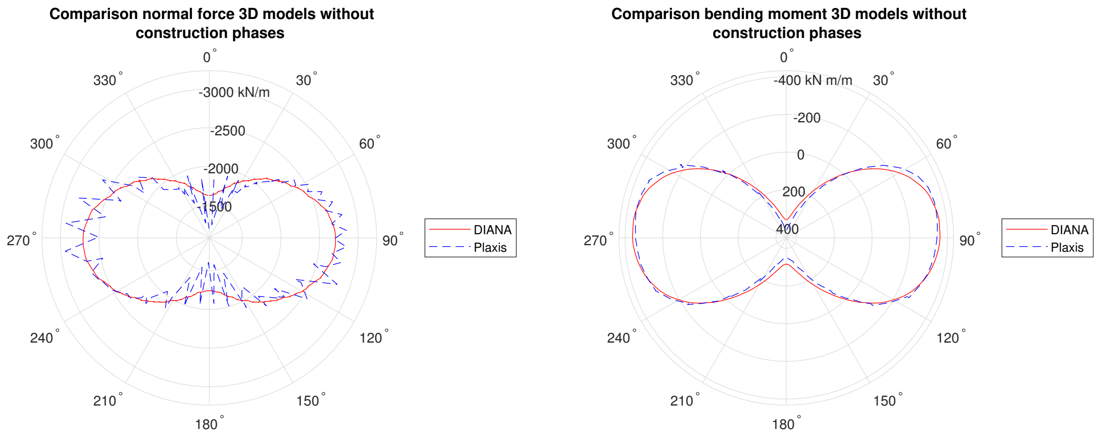

(a) (b)

Figure 4.25: The internal lining forces for the multiple ring models without construction phases

4.2.3. With construction phases

For the model with ten tunnel rings and the construction phases, the results shown in fig. 4.26 are acquired in comparison with the two-dimensional models. These results have been taken from the last ring. When considering a trendline for the Plaxis curve, it can be seen that the normal force is lower for 3D than for 2D. Because the difference is approximately the same over the entire lining. The bending moment is lower as well, this coincides with the decrease in bending moment in Plaxis for the model without construction phases as well (section 5.2.2). More will be discussed in section 5.2.3.

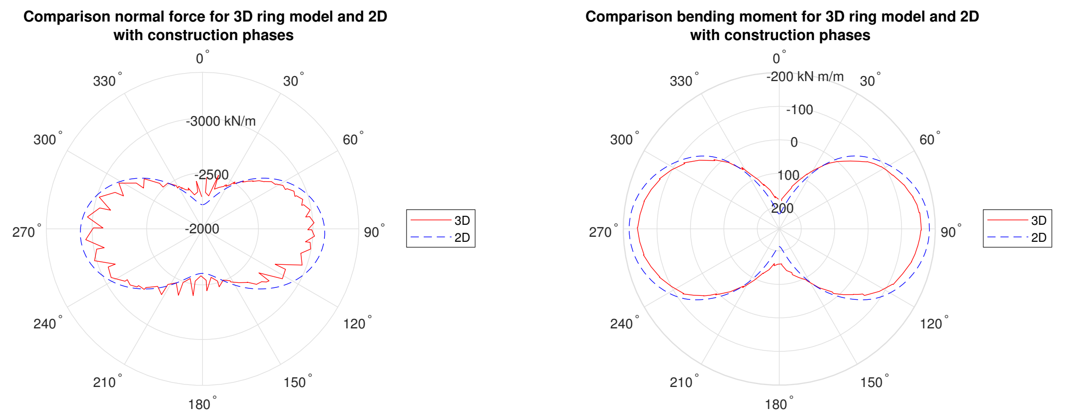

(a) (b)

Figure 4.26: The internal lining forces for the two and three dimensional models with the construction phases.

5

Discussion

In this chapter the results from chapter 4 will be discussed. The differences between the Plaxis and DIANA will be discussed and some sensitivity analyses as well.

5.1. 2-Dimensional

5.1.1. Model One

As seen in the results, there are very little differences between Plaxis and DIANA. However, the models have not be validated yet. In order to do so, a analytical approach is used to calculate the maximum normal force and bending moment in the lining. The calculations based on equations given by COB-L500 [18], Möller and Vermeer [66] can be found in appendix D. The results of these calculations are compared with the results from the models in table 5.1. Both analytical approaches show a good match with the finite elements models.

	Plaxis	DIANA	Möller and Vermeer [66]	COB-L500 [18]
Maximum normal force [kN/m]	2788	2800	2853	2858
Maximum bending moment [kN m/m]	538.4	562.7	557.2	556.3

Table 5.1: Validation of models with extreme values of analytical approach

5.1.2. Model Two

The small difference with the first model is caused by the different soil layers. The overal stiffness of the layers on top is slightly lower compared to model one. This causes larger displacements and therefore higher bending moments. This would be expected in reality as well.

5.1.3. Interface sensitivity

In Plaxis the interface strength, R_{inter}, is a rather arbitrary value. Therefore, its influence is assessed. Figure 5.1 shows the extreme values for the normal force and bending moment results for different values of this interface strength. The forces over the entire lining for every reduction factor in Plaxis are given in appendix E, the exact values of the extreme values are also given. Figure 5.1 shows that a decrease in interface strength leads to less extreme values of normal force in the lining. The maximum and minimum values get closer to each other with a lower strength.

For the bending moment, the extreme values become more extreme with decreasing strength of the interface and therefore the difference between these values increases.

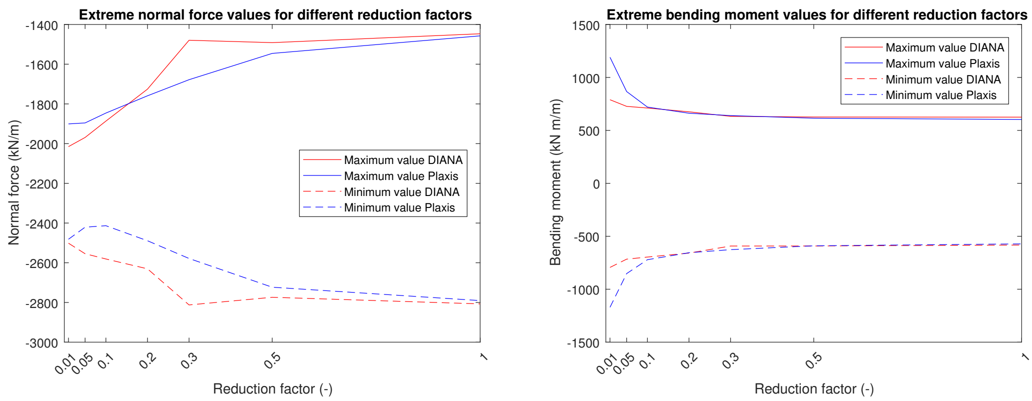

(a) Normal force (b) Bending moment

Figure 5.1: Lining forces for different reduction factors on interface strength in Plaxis and DIANA

As described in section 3.2.2, DIANA requires input parameters based on a reduction factor for the interface strength. To check the influence of this strength, the reduction value has been varied and the extreme values are also shown in fig. 5.1. The forces along the entire lining for every reduction factor are given in appendix E together with the extreme values.

There is very little difference between the results of the reduction values 1.0 to 0.3. Decreasing the reduction factor further towards zero, the extreme values for the normal force become less extreme. With decreasing strength, the difference between the maximum and minimum values for the normal force decreases. The bending moment for the different values of the reduction factor differ very little as well up to 0.1. When decreasing further, the bending moment becomes more extreme.

This is the case when a multiplication factor (f) of 100 for determination of the normal force in eq. (5.3) is used. The only influence of this multiplication factor is the normal interface strength. To assess the influence of this multiplication factor, the values for the normal interface strength are compared. The results for the two multiplication factors are compared in fig. 5.2. For a high value for the reduction factor, the results are equal, the same as seen in the results in fig. 5.1. For the lower values, they are almost the same as well. The only major difference that occurs is for a reduction factor of 0.01. For this reduction value, the minimum normal force is higher and this causes the bending moment to increase as well.

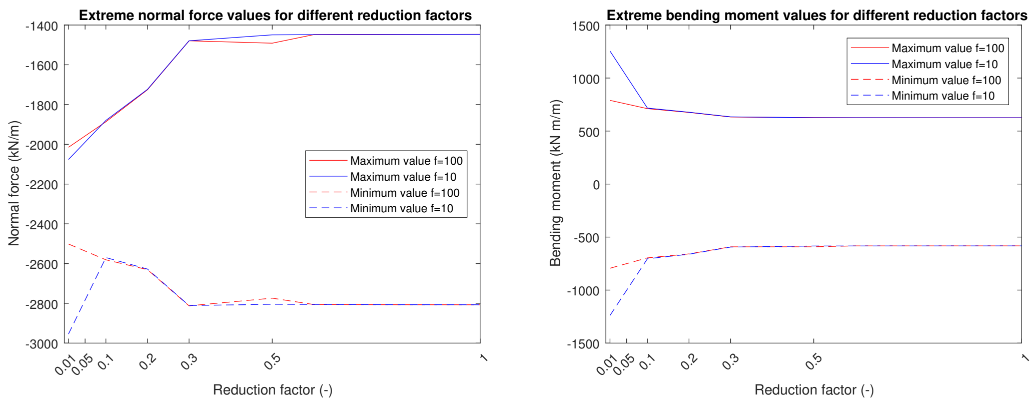

(a) Normal force (b) Bending moment

Figure 5.2: Lining forces for different reduction factors on interface strength for different multiplication factors in DIANA

Thus, the influence of the interface strength is the same for Plaxis as for DIANA. For the reduction values 1.0 - 0.3 has little influence on the internal force of the lining. The lower values of the reduction also show a resemblance. A decrease in interface strength leads to:

- Increase for maximum and decrease for minimum normal force, thus becoming less extreme;
- Increase for both maximum and minimum bending moment, thus becoming more extreme;

As discussed in section 2.2.4, a decrease in interface strength leads to less frictional resistance and shear stresses are decreased along the lining as well. This all leads to less support surrounding the tunnel. This causes the bending moment to increase. Which has also been discussed in this section. In reality, it is difficult to assess the actual slippage or loss of friction along the lining. Generally, the friction angle between a wall and the soil is 2/3 of the friction angle of the soil. Depending on the smoothness of the wall, this may be decreased. Figures 5.3 and 5.4 show the stresses in the interface for different values of the reduction factor in Plaxis and DIANA respectively. Decreasing the reduction factor leads to a decrease in interface stresses. This means that plastic displacements along the lining start to occur faster. For a reduction factor of 0.01 there is almost now shear stress any more. Both the normal stress and shear stress in the interface are alike for Plaxis and DIANA.

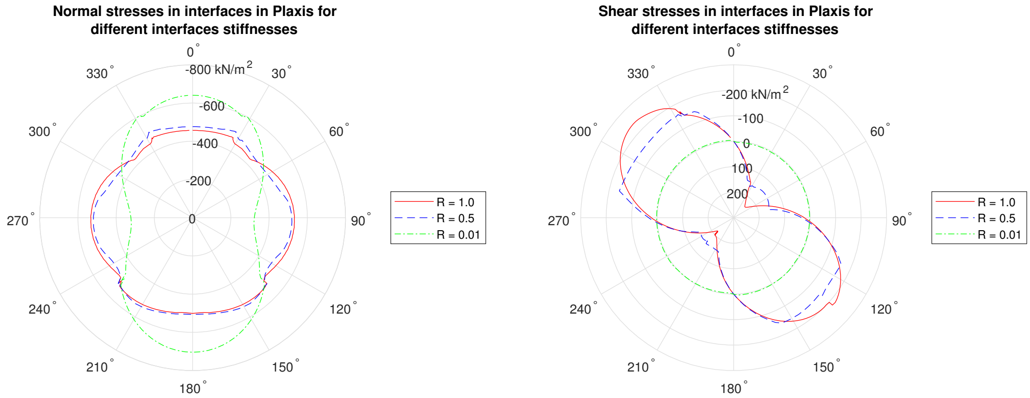

(a) Normal stress (b) Shear stress

Figure 5.3: Interface stresses for different values of the reduction factor in Plaxis

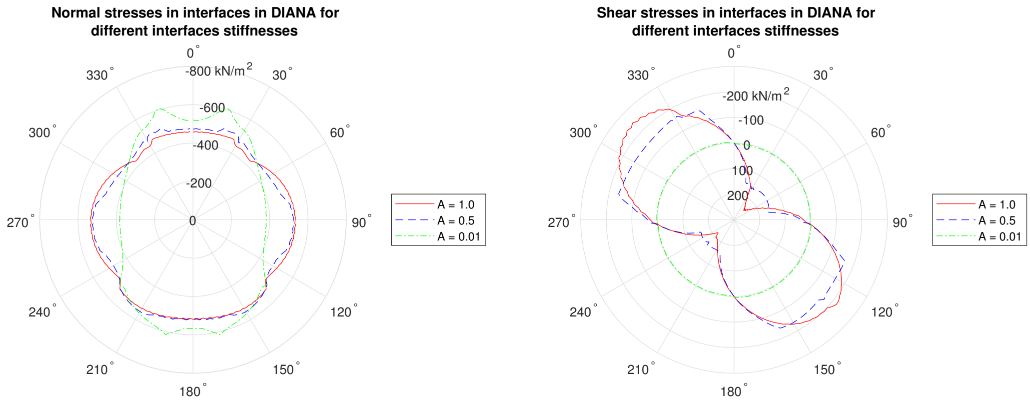

(a) Normal stress (b) Shear stress

Figure 5.4: Interface stresses for different values of the reduction factor in DIANA

5.1.4. Model Three

When modelling the interfaces and incorporating partial slip, differences may occur between Plaxis and DIANA especially for the lower reduction factors as discussed above. The cause of the difference between Plaxis and DIANA will be discussed in this section.

Figure 5.1 shows that the normal force values did not differ greatly between DIANA and Plaxis, which was also visible in fig. 4.5a. The same accounts for the bending moment except for a reduction factor of 0.01. In appendix E the forces over the entire lining of Plaxis and DIANA, of which the extreme values are shown in fig. 5.1, are combined.

While for DIANA different input parameters have to be given which can be determined with a reduction factor, the input in Plaxis is just a reduction factor. Following this reduction factor, Plaxis calculated the interface strength as follows [12]:

$$K_n = \frac{E_{oed,i}}{t_i} \tag{5.1}$$

$$K_s = \frac{G_i}{t_i} \tag{5.2}$$

with:

K_n	Normal stiffness of the interface;
K_s	Shear stiffness of the interface
t_i	Interface thickness;
$E_{oed,i}$	One-dimensional compression modulus of the interface, determined by eq. (5.3);
G_i	Shear modulus of the interface, determined by eq. (5.4)

$$E_{oed,i} = 2G_i \frac{1-\nu_i}{1-2\nu_i} \qquad ;\nu_i = 0.45 \tag{5.3}$$

$$G_i = R_{inter}^2 G_{soil} \tag{5.4}$$

A value for G_{soil} is chosen that corresponds with the stiffness parameters used as input in both Plaxis and DIANA. The thickness interface and reduction factor are the same as chosen for with the DIANA calculation: 0.01 m and 0.5 respectively. With G_{soil} is 14830 kN/m^2, the interface properties become:

		value	unit
Properties	Normal interface stiffness	4.08e+06	kN/m
	Shear interface stiffness	3.71e+05	kN/m^3
	Cohesion	3.2	kN/m^2
	Friction Angle	17.8	degrees
	Dilatancy angle	0	degrees

Table 5.2: Interface properties with the Plaxis calculation

The values shown in table 5.2 differ from the values given in table 3.2. This means there is already a difference in interface strength between Plaxis and DIANA for the same reduction factor. They are closer to the values for the interface strength with a multiplication factor of ten. Therefore a different value for the low reduction factor is expected. Figure 5.5 shows the difference between Plaxis and DIANA for the same interface strength (table 5.2). A combined figure of the forces in Plaxis and DIANA over the entire lining can be found in appendix E.

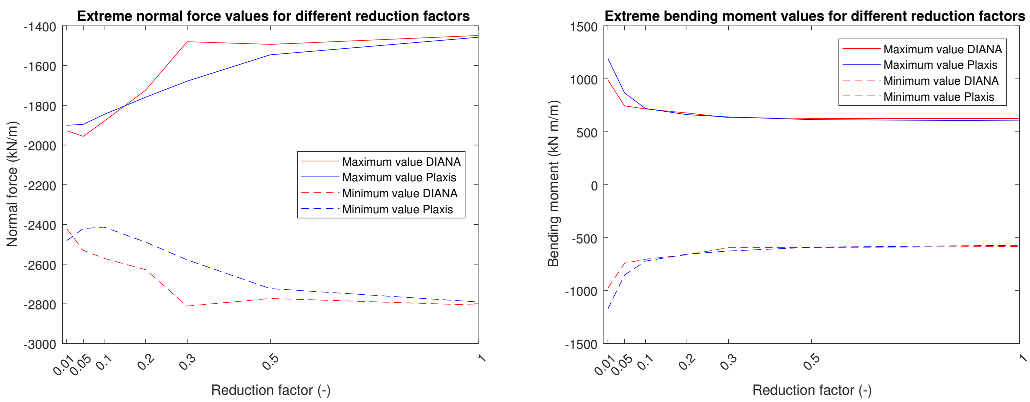

(a) Normal force (b) Bending moment

Figure 5.5: Lining forces for different reduction factors with the same input for the interface strength

With no difference in interface strength parameters, Plaxis and DIANA still show some differences. Again, the difference for the normal force and bending moment increases with a decreasing reduction factor. The difference for the lowest value of the reduction factor between Plaxis and DIANA is much less than in the previous case. This is especially visible for the bending moment. For the same input strength for the interfaces, the difference in extreme values between Plaxis and DIANA is approximately 200 kN m/m. While for the different interface strength parameters, the difference was approximately 400 kN m/m.

As for the results shown in section 4.1.3, they coincide with what has been discussed in section 5.1.3. Reducing the friction along the lining leads to a higher bending moment. In reality, there is no full friction either. With a conservative approach of reducing the friction along the lining by a half, the bending moments become slightly higher and therefore this value seems realistic.

5.1.5. Model Four

The change in soil material models mainly showed a reduction in bending moments. The soil behaves stiffer for unloading with this material models, causing less displacements. Something which is closer to reality than the Mohr-Coulomb material model, as already discussed in section 2.6.5.

The results presented in section 4.1.4 also include the difference between Plaxis and DIANA caused by the interface. The difference between the extreme values given in fig. 4.6 are different from the values given in fig. 4.5. That means there is a difference in the material model definition in Plaxis and DIANA on top of the interface difference. In order remove this little difference the interface is set to full bonding and the results from those models are shown in fig. 5.7. There is still a difference between Plaxis and DIANA and this is caused by the material models. In Plaxis, the material model is called "Hardening Soil" which is a material model Plaxis created themselves. DIANA has an equivalent of the "Hardening Soil" model called "Modified Mohr-Coulomb". The difference in the results shows that the two material models are not exactly the same. This can also be seen in the total displacements of this model (fig. 5.6), while there is no difference for the total displacements in model three appendix F. Figure 5.6 shows that there is less displacement of the surrounding soil in DIANA, thus with the Modified Mohr-Coulomb material model, the soil is stiffer than with the Hardening Soil material model in Plaxis. It is difficult to state which of the two is more realistic. Actual project data has to be used in order to validate both soil models.

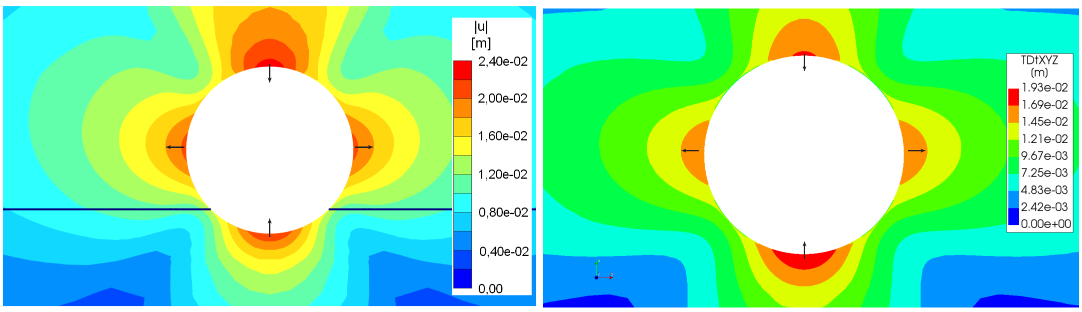

(a) Plaxis (b) DIANA

Figure 5.6: Total displacements for model four in Plaxis and DIANA

5.1.6. Mohr-Coulomb vs Hardening Soil

To illustrate the difference in internal lining forces for Mohr-Coulomb and Hardening Soil material models even better, figs. 5.8 and 5.9 have been created for Plaxis and DIANA respectively.

For the normal forces in Plaxis (fig. 5.8a), there is little difference between Mohr-Coulomb and Hardening Soil. The reduction factor of the interfaces is more influential. Which is already discussed in section 5.1.3. The reduction factor is also more influential for the bending moments (fig. 5.8b). However, the material models do have a significant influence. Figure 5.8a might be a bit misleading since it seems that the lines for a reduction factor of 0.5 are not that far apart which is caused by the high values on the axis. When looking at the difference in values between Mohr-Coulomb and Hardening Soil in figs. 5.8d and 5.8f, it can be seen that the differences are large. The results, however, for Hardening Soil are more realistic (section 2.6.5).

In DIANA, the material model change seems to have a larger influence on the internal forces of the lining compared to Plaxis. Similar results were found in section 4.1.4. Especially in fig. 5.9b it is clearly visible where

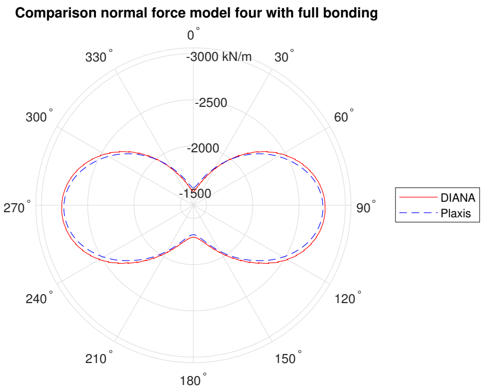

(a) Normal forces

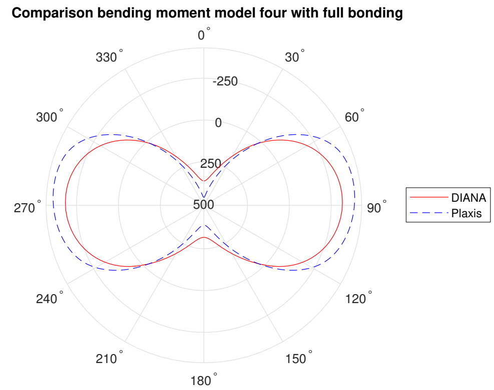

(b) Bending moments

	Max [kN/m]	Min [kN/m]
Plaxis	-1548	-2758
DIANA	-1509	-2783

(c) Extreme values for normal force

	Max [kN m/m]	Min [kN m/m]
Plaxis	463.8	-392.7
DIANA	365.0	-316.7

(d) Extreme values for bending moment

Figure 5.7: Results for the normal force and bending moment for model four with full bonding

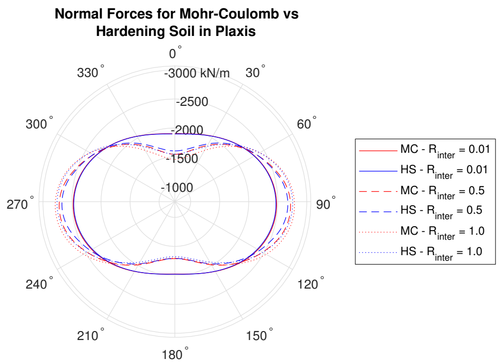

(a) Normal forces

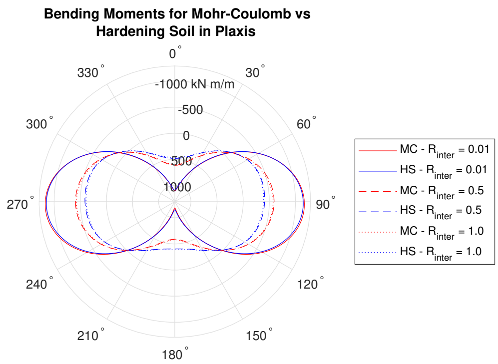

(b) Bending moments

R_{inter} [-]	Max [kN/m]	Min [kN/m]
0.01	-1901	-2482
0.5	-1546	-2723
1.0	-1457	-2791

(c) Extreme values for normal force with Mohr-Coulomb material model

R_{inter} [-]	Max [kN m/m]	Min [kN m/m]
0.01	1190	-1170
0.5	614.9	-589.9
1.0	603.3	-571.7

(d) Extreme values for bending moment with Mohr-Coulomb material model

R_{inter} [-]	Max [kN/m]	Min [kN/m]
0.01	-1896	-2471
0.5	-1604	-2674
1.0	-1548	-2758

(e) Extreme values for normal force with Hardening Soil material model

R_{inter} [-]	Max [kN m/m]	Min [kN m/m]
0.01	1155	-1149
0.5	482.1	-412.4
1.0	463.8	-392.7

(f) Extreme values for bending moment with Hardening Soil material model

Figure 5.8: Results for the normal force and bending moment for the Mohr-Coulomb and Hardening Soil material models in Plaxis

all the Mohr-Coulomb plots are close to each other and the Hardening Soil plots as well. The values for the bending moment for the Hardening Soil material model are almost half of the values for the Mohr-Coulomb material model figs. 5.9d and 5.9f. There is even a difference between Mohr-Coulomb and Hardening Soil for a reduction factor of 0.01 while this is not the case for Plaxis. Since the lining forces differ with the only difference between the models are the material models for the soil, the difference between Plaxis and DIANA is caused by these material models. The Modified Mohr-Coulomb/Hardening Soil material model in DIANA is not the same as the Hardening Soil model in Plaxis.

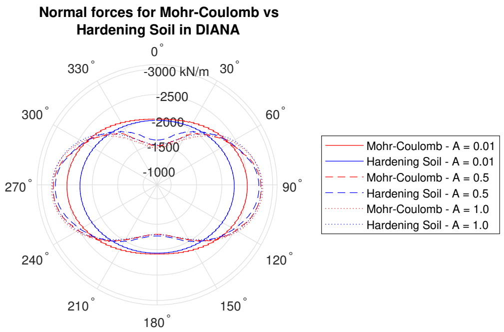

(a) Normal forces

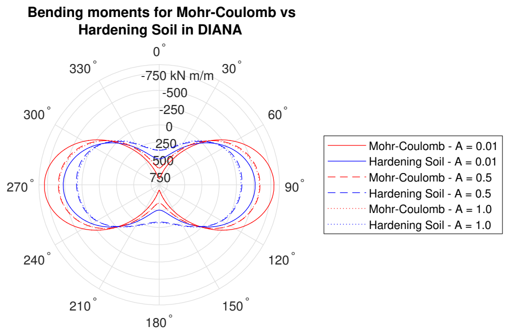

(b) Bending moments

A	Max	Min
[-]	[kN/m]	[kN/m]
0.01	-2015	-2502
0.5	-1491	-2774
1.0	-1447	-2807

(c) Extreme values for normal force with Mohr-Coulomb material model

A	Max	Min
[-]	[kN m/m]	[kN m/m]
0.01	789.5	-793.9
0.5	626.4	-591.6
1.0	625.0	-582.8

(d) Extreme values for bending moment with Mohr-Coulomb material model

A	Max	Min
[-]	[kN/m]	[kN/m]
0.01	-1990	-2246
0.5	-1603	-2731
1.0	-1509	-2783

(e) Extreme values for normal force with Hardening Soil material model

A	Max	Min
[-]	[kN m/m]	[kN m/m]
0.01	501.0	-521.3
0.5	368.1	-332.0
1.0	365.0	-316.7

(f) Extreme values for bending moment with Hardening Soil material model

Figure 5.9: Results for the normal force and bending moment for the Mohr-Coulomb and Hardening Soil material models in DIANA

5.1.7. Model Five

For this model, the interface stiffness had to be changed to a linear elastic interface with different input parameters in DIANA. This is caused by the hardened grout that is surrounding the lining and it has different stiffness parameters than the soil. For Plaxis, it automatically takes its interface parameters from the hardened grout. In this model a difference for the bending moment is still present. Figure 5.10 shows the phase displacements when of the phase in which the TBM is modelled. These displacements seem approximately the same in Plaxis and DIANA. The differences in bending moment still originate from the change in material models made in model four.

Including this phase does cause the bending moment to decrease while the normal force becomes more extreme. The more extreme normal forces are caused by the floating of the TBM. The weight of the TBM is lower than the excavated soil and it is non-porous. The pore pressure underneath the tunnel cause the TBM to start floating upwards, which can also be seen in fig. 5.10. It causes the normal force at the top and bottom to be decreased slightly. At the sides, the normal force is slightly increased due to the presence of the hardened grout. Since the hardened grout is also stiffer than the soil, it also slightly decreases the bending moment. In reality this hardened grout is stiffer than soil as well, how much stiffer is not always clear however. Therefore, its influence is discussed in section 5.1.8.

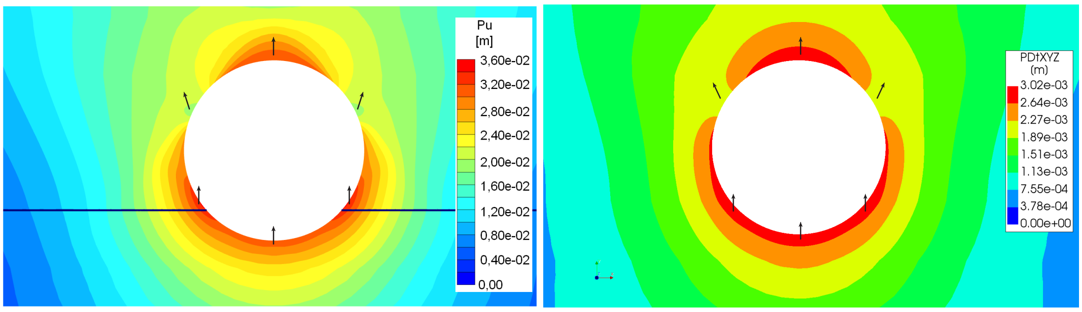

(a) Plaxis (b) DIANA

Figure 5.10: Phase displacement in phase with TBM

5.1.8. Hardened grout stiffness sensitivity

In model five, hardened grout is included. The influence of its stiffness is shown in fig. 5.11. The highest value taken for the stiffness of the grout is the stiffness of the weakest construction concrete that is used in the industry. The lowest value for the stiffness is that of the surrounding soil. It can be seen that for a higher hardened grout stiffness, the internal forces in the lining are reduced. This accounts both for Plaxis and for DIANA and it applies to the normal forces as well as the bending moments. The maximum values for the normal force are located at the top and bottom of the tunnel while the minimum value are found at the sides. The same accounts for the bending moments. Below a stiffness of 1e+06 kN/m^2, the values for the internal forces are approximately the same. When the stiffness becomes higher than 1e+06 kN/m^2, the hardened grout does not act as transfer medium for forces applied by the soil, but is taking on some of the forces itself and therefore reducing the forces in the lining. For a high hardened grout stiffness the forces in the lining even become positive, which means tension. This is all due to the fact that the surrounding grout starts to act as an extra lining. Regardless of the stiffness of the hardened grout, the difference between the bending moment in Plaxis and DIANA remains the same (fig. 5.11b). It is decided to take a value of 500e+03 kN/m^2 since it seems the most realistic value. This because it is stiffer than soil, as a mixture of soil and concrete would be, and it only has a slight influence on the lining forces for which most of it is transferred to the lining itself.

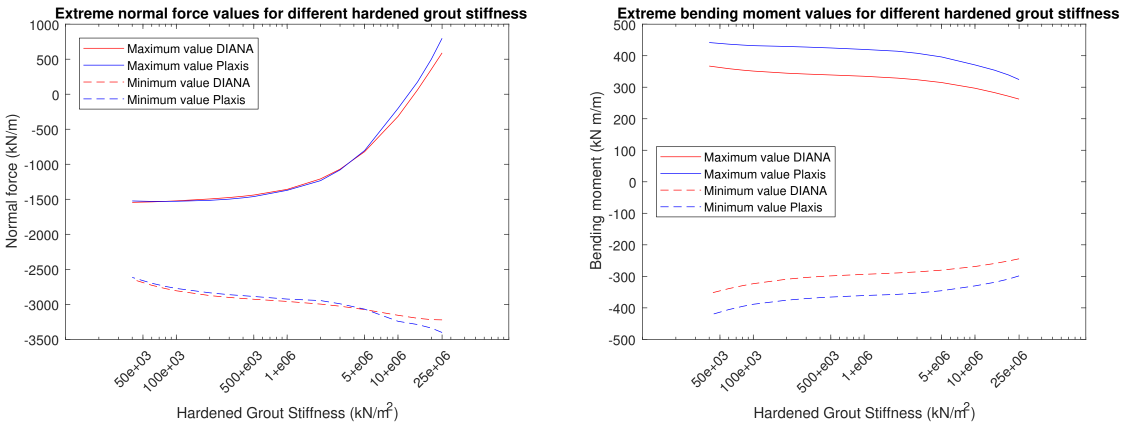

(a) Normal force (b) Bending moment

Figure 5.11: Lining forces for different values of the hardened grout stiffness

5.1.9. Model Six

In model six, the taper of the TBM is modelled. Realistically, taper leads to a stress release in the surrouding soil and thus resulting in a decrease in normal force. This is also seen in the results. The decrease in normal force in turn leads to a decrease in bending moment. However, in reality this amount of displacement, and therefore stress release, will probably not be acquired. Between the shield and the soil already flows liquid grout which comes from the back of the TBM. This already puts a pressure on the surrounding soil and therefore decreases the stress release of the soil.

This taper can be modelled in multiple ways as described in section 3.2. The results shown in section 4.1.6 are conducted with a stress release in DIANA and an applied contraction in Plaxis. A prescribed deformation can also be applied in DIANA. The advantage of prescribed deformation approach in DIANA and contraction approach in Plaxis is that the TBM remains active during modelling. This incorporates the weight of the TBM in the model. Therefore these two approaches will be assessed first. The phase displacements of the soil along the lining in which the taper is modelled are shown in fig. 5.12.

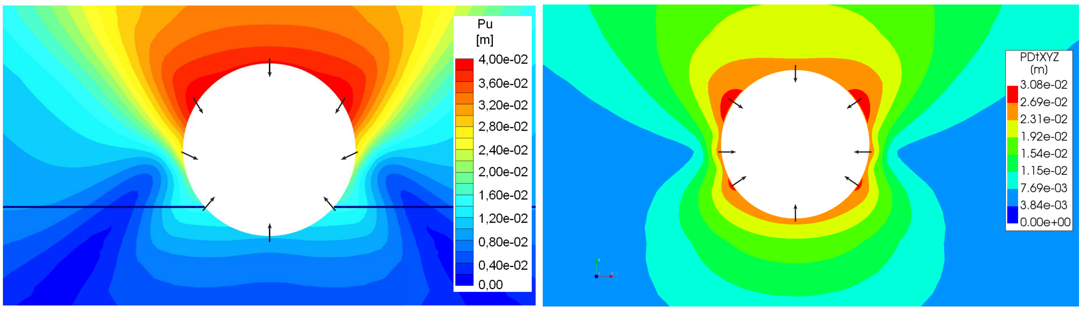

(a) Plaxis (b) DIANA

Figure 5.12: Phase displacement in the taper phase for contraction in Plaxis and prescribed deformation in DIANA

When modelling the taper in DIANA, the prescribed deformation ensure the TBM nodes on which the deformation is applied, move radially with the provided value. Therefore, the entire TBM moves inwards radially with a fixed axis. Within Plaxis, the contraction of the lining does not cause the soil around the TBM to move radially inward with a fixed axis. Plaxis ensures that the TBM diameter is decreasing, but it does not ensure that the axis is fixed. It is letting the TBM move while it is contracting. For DIANA, it can be seen that the soil moves towards the axis, it seems like the TBM is not allowed to move during the taper. With this approach, its advantage of an active TBM is also cancelled.

When applying a line contraction in Plaxis, it will decrease the element size, which in this case are plates. These plates will become smaller because of this line contraction. Be applying a specific value, as described in section 3.2, of this plate element contraction on all the TBM elements, the taper of the TBM is emulated.

The other approach of modelling the TBM taper, described in section 3.2, is investigated in order to see if those results are different. Figure 5.13 shows the results of stress release approach in Plaxis and DIANA. For these results, a stress release value is chosen for which the displacement in the borehole are equal to the taper amount of the TBM.

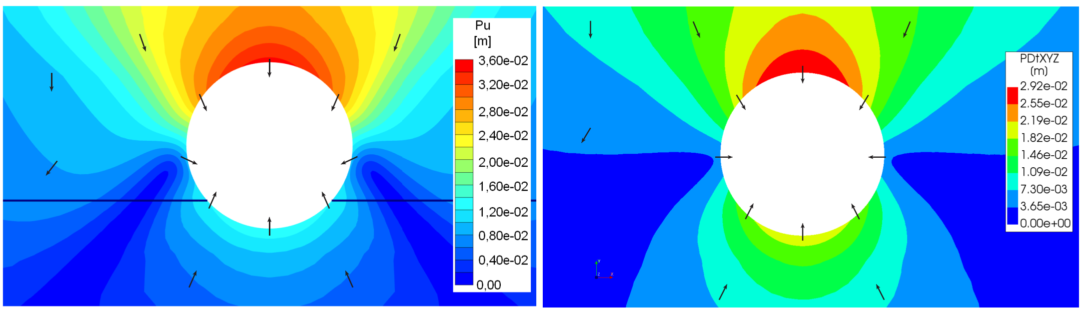

(a) Plaxis (b) DIANA

Figure 5.13: Phase displacement in the taper phase for stress release in Plaxis and DIANA

When assessing the influence of the stress release in both Plaxis and DIANA, fig. 5.15 is acquired. For an Mstage value of 0.15 in Plaxis the internal lining forces are the closest to the internal lining forces acquired with applying contraction. However, this is not the case with the displacement, the displacements at the top and bottom combined are only make up for half the displacement with contraction (2.8 cm against 5 cm). When Mstage is taken 0.28 approximately the displacement at top and bottom combined equal 5 cm. However, the division between top and bottom is different than when contraction is applied and the internal lining forces are slightly different as well. Figure 5.15 does show that the displacement at the bottom of the borehole is less than at the top, this accounts both for DIANA and Plaxis. This strengthens the contraction approach used by Plaxis in which the same phenomena was seen (fig. 5.12). For DIANA, the phase factor for modelling the stress should be taken 0.66. For this value the borehole has a combined radial inward displacement of 5 cm.

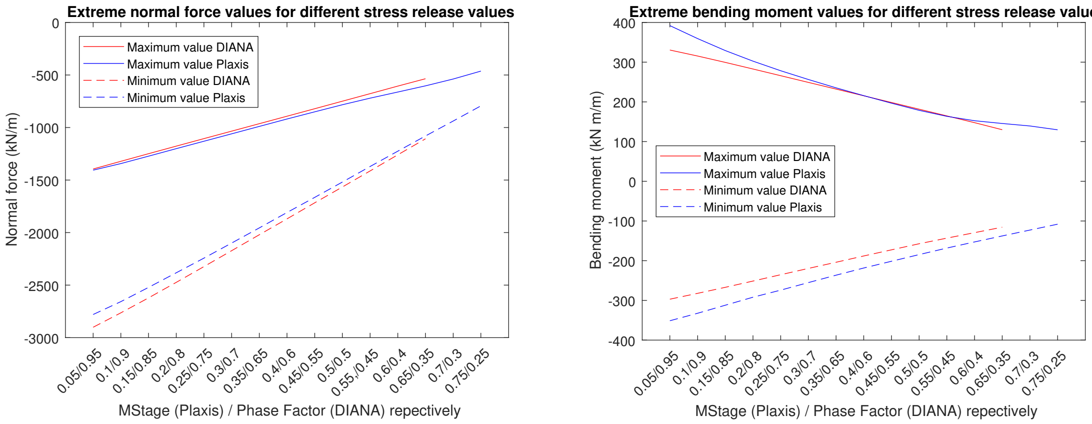

(a) Normal force (b) Bending moment

Figure 5.14: Lining forces for different values of the stress release

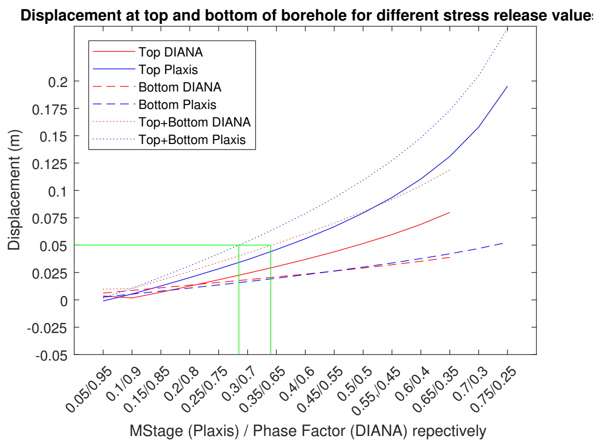

Figure 5.15: Displacement for top and bottom of the borehole for different stress releases

Which approach is more realistic depends on how the TBM is expected to behave in the soil. If assumed that the TBM axis is always equal to the tunnel axis, so the TBM is "floating" in the borehole (fig. 5.16a), the prescribed deformation approach in DIANA would be more realistic. If the TBM would behave by "lying" in the borehole (fig. 5.16b), the approach by contraction in Plaxis would be more realistic. For this case, the contraction approach in Plaxis and thus the stress release approach in DIANA have been chosen as suitable for modelling the taper of the TBM. The small difference in minimum normal force is caused by a difference in displacements on the sides of the tunnel. When comparing figs. 5.12a and 5.13b, it can be seen that the displacements on the side of the tunnel are different. Directly next to the tunnel lining they are of approximately equal values, but further way the difference becomes larger. For Plaxis the displacements increase slightly when moving away horizontally from the tunnel lining. For DIANA, the displacments stay approximately the same. In Plaxis the displacements reach a value of approximately one centimeter while DIANA stays at approximately three millimeters. In section 5.1.5 it was discussed that the soil behaves stiffer in the modified Mohr-Coulomb model than the Hardening Soil in Plaxis, this also causes the difference in displacements on the sides of the tunnel in this model. Which in turn leads to additional differences in lining forces.

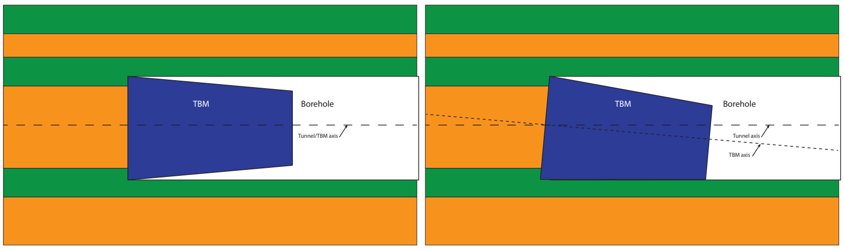

(a) "Floating" (b) "Lying"

Figure 5.16: Exaggeration of possible TBM behaviour in borehole

5.1.10. Model Seven

The almost equal normal forces and the close to zero bending moments are different from the previous models. This is caused by the type of analysis chosen for these models, namely: drained. Drained analysis is used for long term behaviour of the soil. In the construction process of a bored tunnel, the phases for the construction are relatively short. When loading a soil in a short period of time, excess pore pressures develop since there has not been enough time yet for the pore pressure to dissipate. When using a drained analysis, these excess pore pressure are not developed since it already assumed these will dissipate, this causes the soil skeleton to take on all the forces in order to reach an equilibrium. When modelling it with undrained behaviour, a consolidation phase has to be added in order for these pore pressure to dissipate. The comparison of the internal forces for drained and undrained behaviour in Plaxis is shown in fig. 5.17.

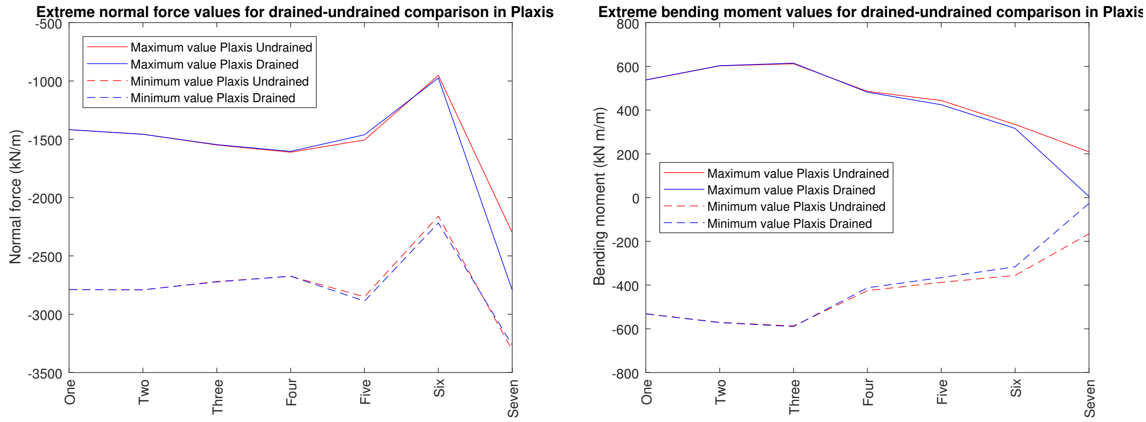

(a) Normal force (b) Bending moment

Figure 5.17: Lining forces for drained and undrained analysis in Plaxis for different models

Figure 5.17 shows that for the first six models, there is very little difference between drained or undrained modelling in Plaxis. In model seven the difference occurs between drained and undrained. In model seven, a grout pressure is applied. This grout pressure is the first load that causes a compression of the soil compared to all the other models where there is only relaxation of the soil. This load causes excess pore pressure in the soil surrounding the borehole, since it is undrained. These pore pressures take on a part of the grout load that is applied. When consolidation is allowed after, the excess pore pressure are allowed to dissipate and transfer the load it took on to the soil skeleton. This has to come in an equilibrium again. This leads to an increase in normal forces on the lining which in turn leads to higher bending moments.

These higher bending moments are of a more realistic value and therefore from this model onward, undrained analysis will be used instead of drained analysis. These values are also realistic when compared to the previous models. The grouting pressure puts a force on the borehole, which creates a displacement contrary to the taper phase. This reloaded soil wants to unload again after the grouting phase causing the increase in normal forces. The less stiff locations of the soil along the lining are displaced more, causing a more uniform unloading after the grouting phase. This leads to a decrease in bending moment. In reality, a grouting pressure is also put on the borehole. The exact pressure it puts on every location on the borehole remains unclear. As discussed in section 2.8.1, the behaviour of the grout is complex. The constant gradient applied in this research is not realistic. However, its influence on the model has been assessed in section 5.1.11.

As shown in fig. 5.17, there is no need in redoing the previous model undrained since there is little difference for those models between drained and undrained.

For DIANA, undrained analysis is also possible. However, consolidation for the excessive pore pressure to dissipate is not yet possible in the current version. Currently DIANA itself uses a workaround which includes use of a developers version. However, it is not proven yet that the workaround produces results which are trustworthy. As described above, modelling consolidation is important for the construction process of a bored tunnel. Since this is not possible in DIANA, further research in DIANA will not be possible.

5.1.11. Grout pressure increment sensitivity

The grout pressure applied on the borehole in model seven has an increment over depth. The exact behaviour of the grout is very complex (section 2.8.1). It has been assumed the grout has a constant vertical gradient over depth. In order to assess the influence of this gradient, different values have been taken from a very low value of 6 to 21 kN/m^2/m, with the latter equal to the specific weight of the grout.

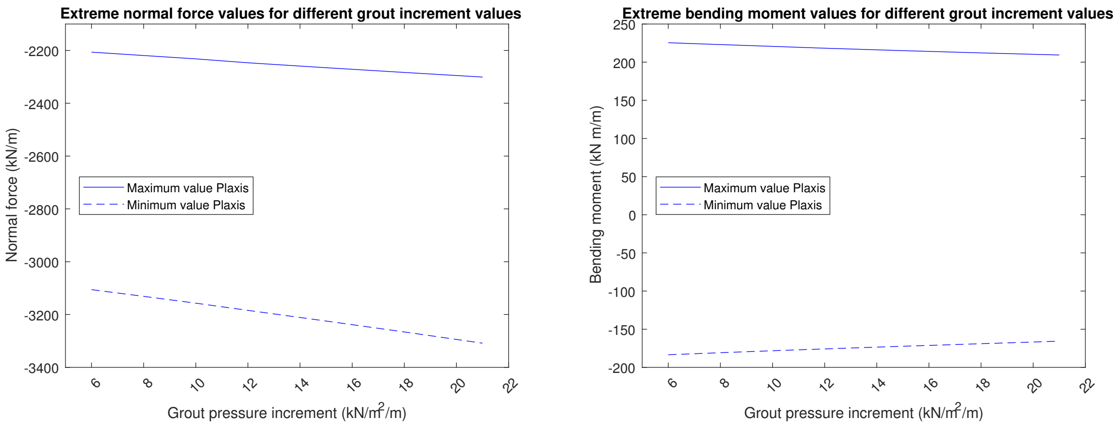

(a) Normal force (b) Bending moment

Figure 5.18: Lining forces for different values of the vertical grout pressure gradient

It can be seen that for an increase in grouting pressure increment, the normal forces in the lining will increase as well. The bending moment decreases with an increasing grout pressure gradient. The difference, however, between 6 and 21 kN/m^2/m is not that large for both the normal force and bending moment. Since the behaviour of grout is complex, the most conservative approach will be used from now on, so a value of 6 kN/m^2/m will be used as value for the increment of the grout pressure over depth.

5.1.12. Model Eight

There is little difference between model eight and seven. This is caused by the approach of the follow carts. In reality, they are only present for a short period of time and are therefore modelled undrained. After, the consolidation is applied again in which the follow cart load is not present. The follow cart load has little influence on the long term internal lining forces. During the passage of the follow carts, they do have quite an influence on the bending moment (fig. 5.19). However, the peak bending moment that is caused by the follow carts is much smaller than bending moments when consolidation has taken place. These peak bending moments are not realistic. While there will be a local increase in bending moment, the peak is too sharp. In reality the follow-carts are driving on a rails, which already distributes the load. The lining itself will also distributed some of the load over its thickness. The peak will therefore be more blunt in reality. For the forces of the lining in the follow-cart phase, DIANA has been added since this is still before a consolidation phase and therefore possible to model. However, the differences between Plaxis and DIANA are very small.

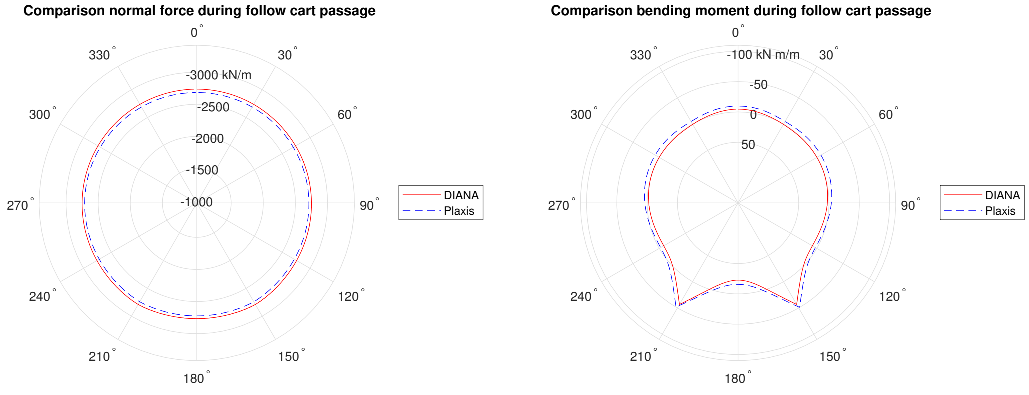

(a) Normal forces (b) Bending moments

Figure 5.19: Results for the normal force and bending moment for two follow cart modelling approaches

5.1.13. Model Nine

Since the inlay is already present during the consolidation phase, it might have an influence on the internal lining forces. The stiffness of this inlay is an arbitrary value again. It has a stiffness which is closer to soil than to concrete. Therefore the influence of this stiffness has been assessed (fig. 5.20). These figures show that the inlay would have an influence on the internal lining forces if it is larger than 2e+06 kN/m^2.

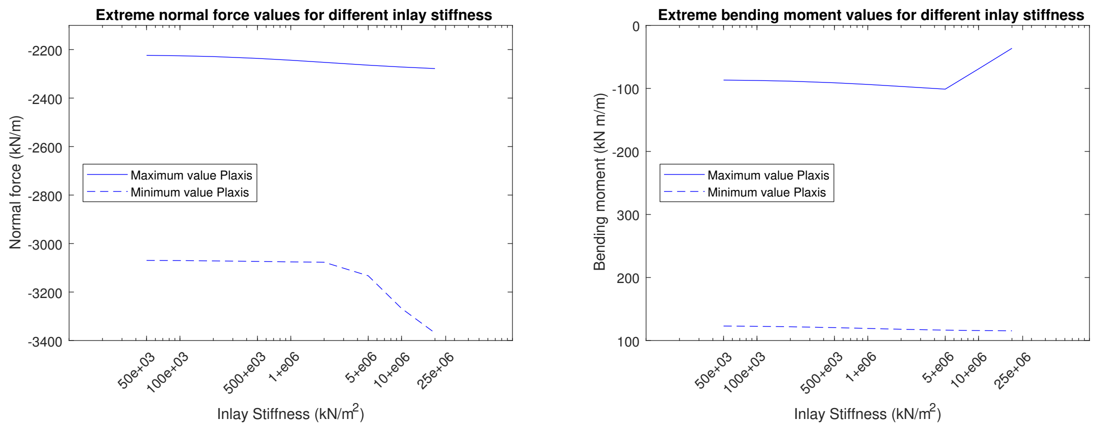

(a) Normal force (b) Bending moment

Figure 5.20: Extreme lining force values for different values of the inlay stiffness

However, these value are only the extreme values. When looking at the internal lining forces along the entire lining for the different stiffnesses, something else is showing (fig. 5.21). It can be seen that the inlay has an influence on the internal lining forces, regardless of its stiffness. With an increase in stiffness, both the normal force and bending moment increase as well. While this occurs for the bottom half of the tunnel, the largest influence is on the part of the lining that is supporting the inlay. It is decided to continue with a stiffness of 200e+05 kN/m^2. This values is chosen since it is a slightly higher stiffness than soil. When, in reality, it is installed before the consolidation takes place, it creates an extra load on the lining and therefore the soil below. Therefore the influence of the inlay should be included, which is the case with this value.

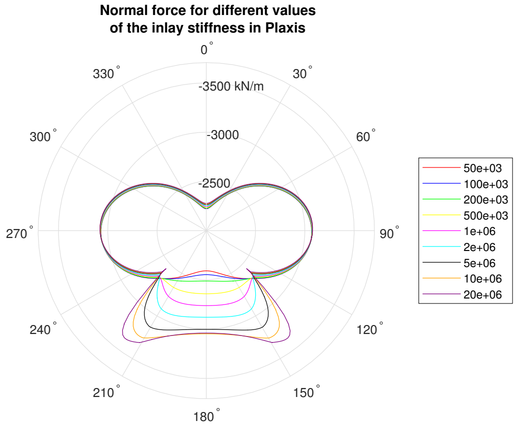

(a) Normal force

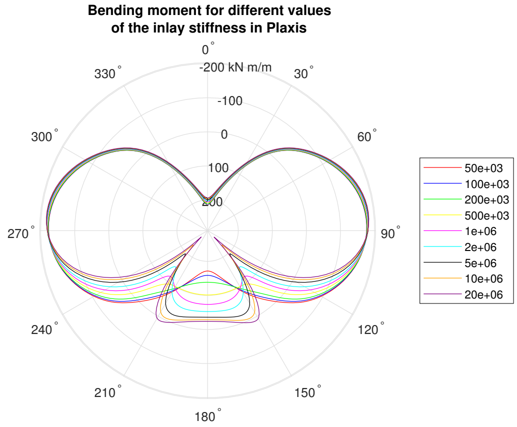

(b) Bending moment

Figure 5.21: Lining forces in the tunnel lining for different values of the inlay stiffness

So the difference with model nine and and the previous models is the inlay during the consolidation phase. What becomes clear is that the actual usage of the tunnel has very little influence on the internal lining forces. The passage of the metro train only works for a short period of time in which it is not exerting a significant force on the lining. Something for which a tunnel is designed in reality as well.

5.1.14. Model Ten

The largest difference between Mohr-Coulomb and Hardening Soil material models was seen in model six. This model included the taper of the TBM, which leads to stress release in the soil surrounding the borehole. More than other phases within the construction process of a bored tunnel. This is where the difference bewteen Mohr-Coulomb and Hardening Soil material models comes forward really well. In Mohr-Coulomb one value is given for different stiffnesses, so the primary loading stiffness is equal to the unloading stiffness and the reloading stiffness as well. With the Hardening Soil material models, however, different stiffness values are used, as described in section section 2.6 and the value for unloading stiffness is higher than the stiffness used in the Mohr-Coulomb material model. Therefore less loading of the soil on the lining takes place with the Hardening Soil material models than with the Mohr-Coulomb. In the grouting phase, the internal lining force become almost equal again for Mohr-Coulomb and Hardening Soil. This is also caused by the difference in defining the stiffness. The reloading stiffness in Hardening Soil is equal to the unloading stiffness and thus larger than the stiffness applied with the Mohr-Coulomb materials model. This can be seen in fig. 5.22 which shows the phase displacements for the grouting phase with Hardening Soil and Mohr-Coulomb material models. The displacements along the borehole are much larger for Mohr-Coulomb than for Hardenining Soil. The grout load in both cases is equal but due to the different reloading stiffness, the deformations differ. However, since the loading is the same for both cases, the soil exerts the same load on the lining when it is installed. This causes the difference between Hardening Soil and Mohr-Coulomb to be nullified. Again, the phases with the follow-cart and inlay load have little influence on the final internal lining forces.

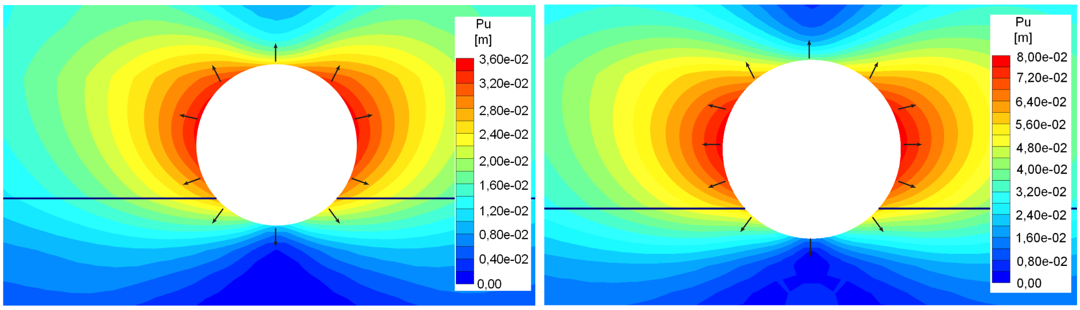

(a) Hardening Soil

(b) Mohr-Coulomb

Figure 5.22: Phase displacement in the grouting phase for Hardening Soil and Mohr-Coulomb material models in Plaxis

When the material models do not have an influence on the lining forces when the grouting is modelled as a load on the borehole, one can argue what would happen to the difference between Plaxis and DIANA that is caused by the difference in material models. If the soil actually does exert the same amount of force as has been placed on the borehole, the difference between Plaxis and DIANA will also be nullified. After which new differences may arise due to modelling of the joints or other causes. Unfortunately, it was not possible to include this in the research as previously explained.

5.1.15. Model Eleven

The small irregularities in the curves that are presented in section 4.1.12, are caused by the joints. These joints have some influence on the internal lining forces. The influence seems to be small since no peaks of low bending moments are found at the joint locations. However, the bending moment along the entire lining has been decreased due to these joints and it therefore does has some influence on the internal lining forces. This would also be the case in reality which was also discussed in section 2.5.

5.1.16. Model Twelve

The presence of buildings at the surface leads to a decrease in bending moment. The normal forces differ little compared to model eleven, but the difference in bending moment is larger. The joints cause the irregularities along the curves again.

5.1.17. Last models

When plotting the extreme values of models seven to twelve, fig. 5.23 is acquired. It shows that including more tunnel features in the model leads to a decrease in bending moments. In model ten all the phases were modelled with Mohr-Coulomb material models for the soil layers, this explains the inconsistency in the maximum normal force and minimum bending moment curves.

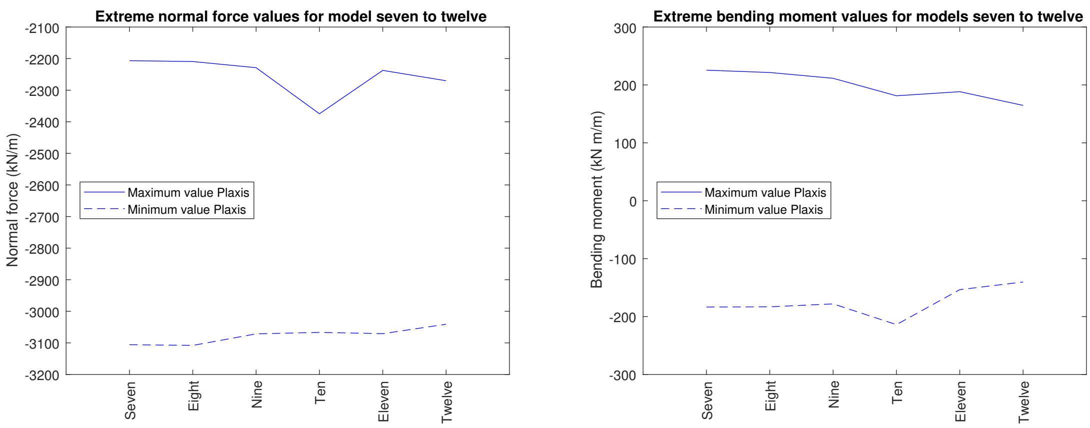

(a) Normal force

(b) Bending moment

Figure 5.23: Extreme lining force values for models seven to twelve

In order to assess whether the construction phases also have a positive influence on the combination of normal force and bending moment, moment-curvature relations have been investigated. The different NM-κ diagrams for all the models can be found in appendix H, in which a brief description of the graphs is given as well. An elaborate explanation and the calculations that form the base of this type of diagrams is given by Walraven [80]. The reinforcement is based on model four and is kept the same for all the models. In appendix H a brief explanation is given on how this is done. The reinforcement is kept the same since only the influence of the different construction phases is assessed.

With these moment-curvature relations, unity checks are also done. This is a ratio between the acting bending moment and the bending moment capacity of the lining. More on this is discussed in appendix H. When comparing the unity check for the different models, fig. 5.24 is acquired. It shows that the unity check is decreased when more construction features are included. Which means the difference between the capacity and acting moment becomes larger in favor of the capacity.

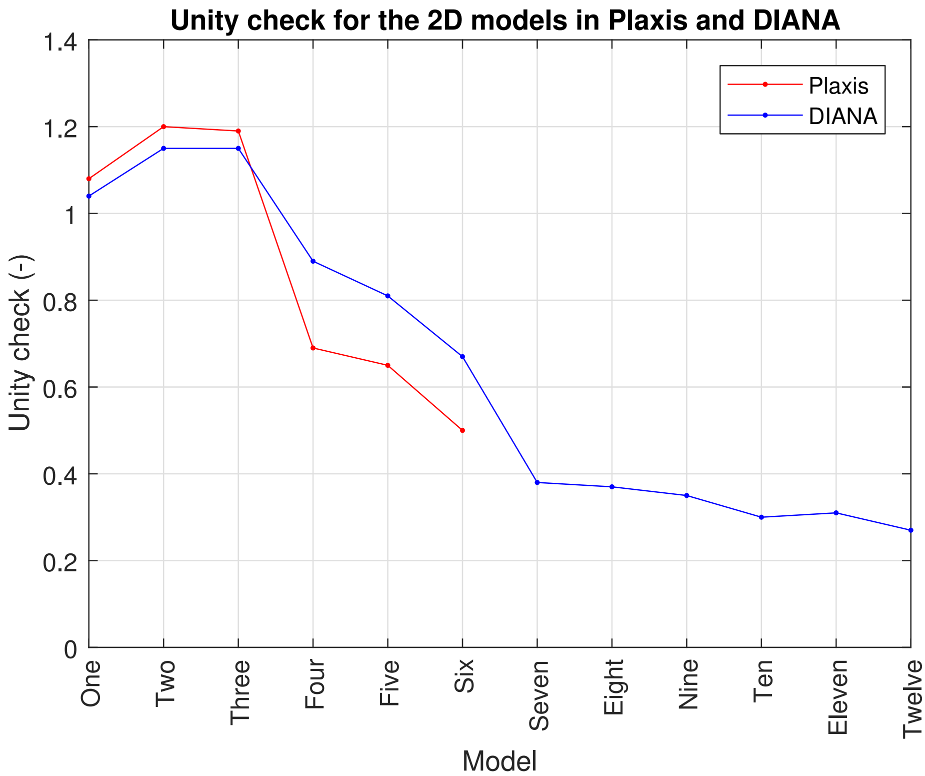

Figure 5.24: Unity check for all the models in 2D

5.2. 3-Dimensional

5.2.1. One-ring models

The one-ring models have only been created in Plaxis since it was possible to model all the different construction phases. This is not case in DIANA as explained in section 5.1.10 since consolidation is not yet applicable in the current version of DIANA.

The results in section 4.2.1 show little or no difference between the two dimensional models and the models with one ring. This was expected since the models are almost equal. What has been done with the three dimensional modelling is almost a plane strain approach which has been applied in the two dimensional models. Since it is only one ring and the model is not allowed to move in the direction of the tunnel axis, it tends to go towards a plane strain situation in which the model is supposedly of infinite length.

The phase with the follow-carts has been excluded due to meshing problems. As previously discussed in section 3.3.1 the very fine mesh which is needed for the analysis leads to a large computational time. When considering that the same results are acquired for these one-ring models as with 2D, it can be assumed that the follow carts will have the same influence in this model as in 3D, which is very little. Therefore it has been decided to no include this phase.

The same meshing problem occured when creating an inlay which is slightly smaller the clay soil cluster in the bottom of the tunnel. Due to the small difference between these two cluster, meshing was not possible for anything but the finest mesh. This also lead to a model with a large computational time. It was already concluded in the two dimensional models that the inlay does have some influence, but it is not very large. Therefore it has been decided to model the soil cluster as the inlay. It is assumed this increase in inlay volume is of little influence compared to the two dimensional models. The volume with this approach becomes one cubic meter larger per ring which is approximately an increase of seven percent.

5.2.2. Without construction phases

Described in section 3.3.1, the joints cannot be applied in the three dimensional version of Plaxis and are therefore not included in these models.

While it was expected that difference between Plaxis and DIANA would not be that large, this small was not expected either. Without the construction process both models have a monolithic tunnel and only two phases, therefore not a very realistic model. However, the difference between the two models is the material model for the soil. In Plaxis, the Hardening Hoil material model is applied and in DIANA Modified Mohr-Coulomb. In 2D, this caused the difference between Plaxis and DIANA. Figure 5.25 shows the curves for model four and the 3D model with multiple rings in DIANA. It shows that for the three dimensional model the bending moments are higher, this strokes with the results presented in sections 4.1.4 and 4.2.3. When looking at the difference between 2D and 3D in Plaxis (fig. 5.26), the opposite can be seen. The bending moment in 3D is slightly smaller than in 2D. Combine this and the increase in bending moment in DIANA from 2D to 3D and the difference in 2D between DIANA and Plaxis disappears. Where this differences come from has not been found, it does show that for 3D, Modified Mohr-Coulomb and Hardening Soil are more equal than in 2D. It seems the 2D Modified Mohr-Coulomb is an underestimation of the material model in 3D. For Plaxis the Hardening Soil 2D is an overestimated approach of the 3D Hardening Soil. Furthermore, it also seems the difference between DIANA 2D and 3D is less than with Plaxis. Not enough research has been conducted in order to conclude that for 3D the material models are equal and it might also be a coincidence there are coinciding like this.

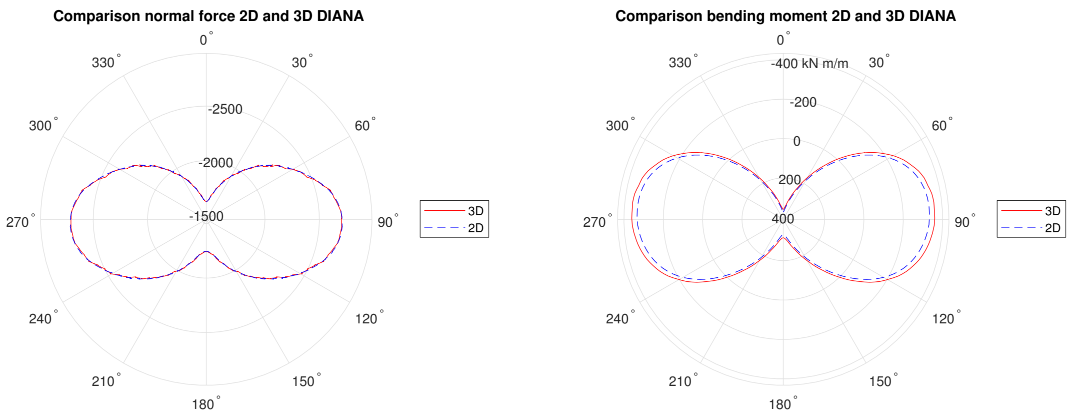

(a) (b)

Figure 5.25: The internal lining forces for model four and the 3D model in DIANA

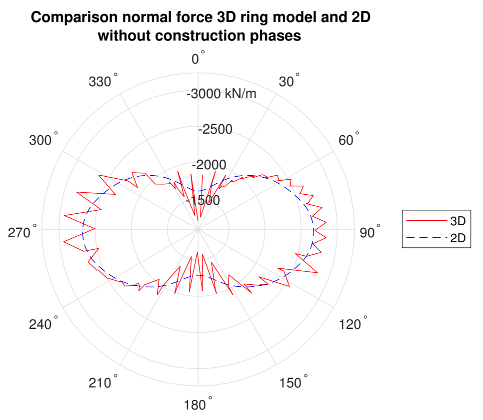

(a) (b)

Figure 5.26: The internal lining forces for model four and the 3D model in Plaxis

5.2.3. With construction phases

As described in section 3.3.1, it is not possible to apply a stiffness to the joints, the only options are free or fixed. Therefore the joints will not be applied in this model and the tunnel will be monolithic. As already described in section 5.1.10, the construction phases cannot be implemented in its entirety in DIANA and therefore will not be included. Thus this model is only created in Plaxis.

Figure 4.26 shows a difference for the normal force between 2D and 3D when modelling multiple rings and the construction process. As explained, the cross section is taken at the middle. Unlike the model in which the construction phases are not modelled, the normal force is not uniform over the ring along the tunnel axis. The front part of the ring, which gets attached to an already installed ring, has a lower normal force along the entire lining than the back part, this is shown in fig. 5.27. It is caused by the modelling sequence of the rings. When a new ring is installed, the front is attached to another ring. Since the first ring already had some deformation, one side of the new ring is deformed during installation in order to connect to the previous ring. This reduces the normal forces in that part of the ring. The back side, which is "free" does not have this deformation and therefore has more realistic values for the normal force. Figure 5.28a shows the bending moment in the longitudinal direction which shows that the front is deformed as well and the back is not and therefore creating the bending moments. This is the case when the front of the model (YMin) is only fixed in the normal direction, so in the direction of the tunnel. This means it can move vertically, what happens when modelling the first ring. With installation of the other rings, the entire tunnel becomes more stable and deformations of the lining start to decrease. This causes the normal forces for every new ring to slightly increase and the bending moment to decrease. When applying enough rings, these forces eventually will not change anymore for newly installed rings.

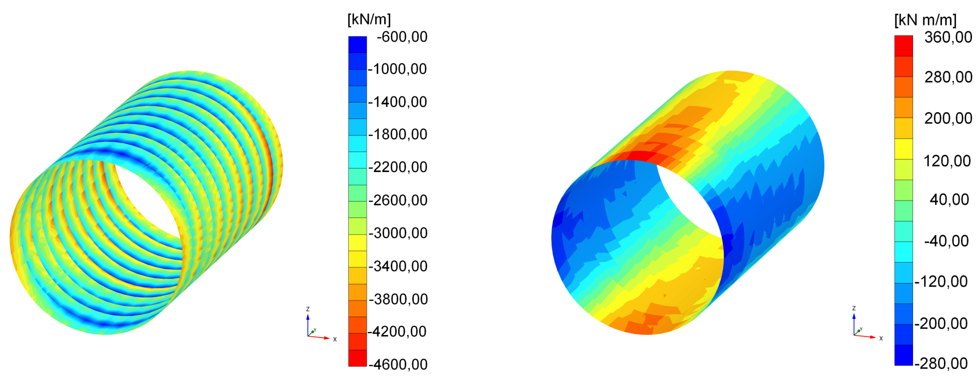

(a) Normal Force (b) Bending Moment

Figure 5.27: Internal lining force for the 10 ring model with construction phases in Plaxis

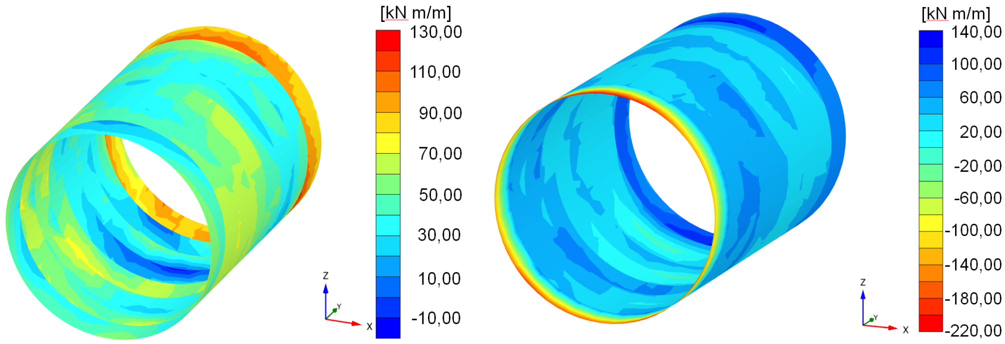

(a) Normally fixed

(b) Fully fixed

Figure 5.28: Bending moments in the longitudinal direction for newly installed rings with normally fixed (a) and fully fixed (b) front of the model

The front of the model (YMin) can also be fixed in all the directions, mimicking the first ring of a new tunnel. This first ring is attached to a ring in the jet grouting block and therefore cannot move, only rotate (section 2.3.3). The distribution of the normal forces and bending moment when applying this fixation are given in fig. 5.29. The same phenomena of different normal force over the longitudinal direction can be seen as in fig. 5.27. The bending moment in the longitudinal direction shows the same as well (fig. 5.28b). This time, however, the differences between front and back are smaller because of the fixation of the front of the first ring. This also causes the increase in bending moment for newly installed rings.

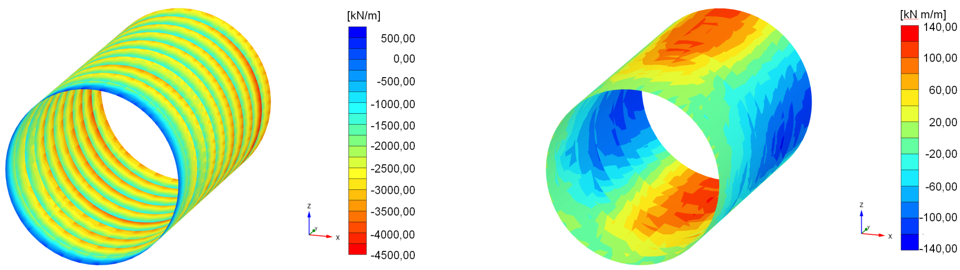

(a) Normal Force

(b) Bending Moment

Figure 5.29: Internal lining forces for the 10 ring model with construction phases in Plaxis with complete fixation at front of the model

When increasing the amount of rings for both approaches, the effect of the first rings should be minimized even further and both the approaches should acquire the same internal lining forces. In order to be sure, the number of rings and thus the size of the model has to be increased.

The front, back and middle of the ring have been plotted for the approach with the front of the model only normally fixed (fig. 5.30). It can be seen that taking the normal force at the middle gives the average normal force over the width of the entire ring. It can also be seen that the difference between the different curves is almost the same along the entire lining. The difference between the highest and lowest values remains the same as well. This causes the bending to differ very little over the width of the ring as shown in fig. 5.30b.

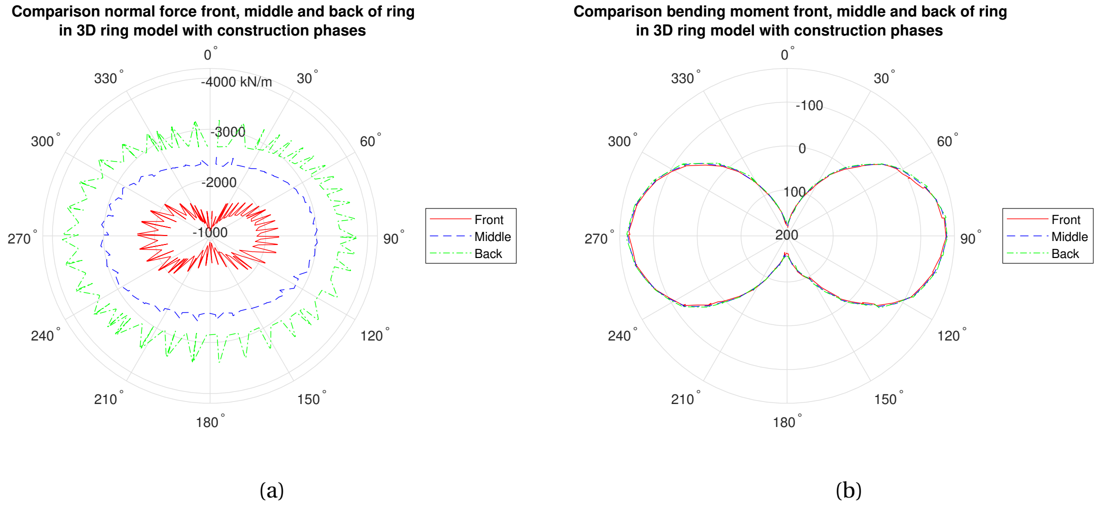

Figure 5.30: Lining forces for the front, middle and back of a ring in the 3D ring model with construction phases

This difference between the front and back of a ring, however, is not realistic. During tunnelling the rings are connected to eachother as soon as they are erected in the TBM. With the jacks the TBM provides a pressure on these rings, combined with the rings in the hardened grout, the rings in the liquid grout hardely move. Any deformation happening with the rings in the hardened grout would also lead to deformation in the rings for which the grout is still liquid. Which is not the case in these models.

6 Conclusion

The construction process of a bored tunnel is a process which includes many different aspects and different kind of loads. In order to answer the first subquestion, these loads have been discussed for each phase in the construction process in section 2.2. Because of the complexity, different methods have been created in order to assess the forces in the tunnel lining that may occur during and after construction. One of those methods is finite element modelling. This method is created since analytical methods were not sufficient or too complex. Nowadays, this method is available in the form of computer programs. The possibilities in these different programs (subquestion 2) have been discussed in section 2.4. By starting with simple models and increasing the complexity by including more and more aspects of the tunnelling process, it has been assessed what the possibilities are for modelling ground lining interaction of a bored tunnel in finite element programs. The aspects that are being modelled (subquestion 3) are discussed when the different models are discussed (section 3.1). In section 3.2 it is discussed how the joints are modelled (subquestion 4). Based on several criteria Plaxis and DIANA have been deemed most capable of modelling a bored tunnel during the literature study. Therefore, a comparison between the two has been made. What is deemed possible in both programs (subquestion 5 & 6) has been discussed in section 3.1. Chapter 5 discussed the modelling possibilities again whether or not they are actually applicable in the programs, something which also influences subquestion 3. Subquestion 7 is also discussed in chapter 5. The differences between each model, thus each step of the construction process (subquestion 8), have been discussed in chapters 4 and 5. Based on these results and the discussions, the following conclusions have been drawn regarding the possibilities of modelling the construction phases of a bored tunnel with regards to internal lining forces:

- DIANA 10.1 is not yet suitable for modelling consolidation. While it seemed a great program for modelling tunnels in the literature study, a consolidation phase in which the excessive pore pressures can dissipate cannot be modelled yet. As explained and shown, this is important for assessing the internal lining forces when modelling the construction phases of a bored tunnel.

- While predicted to be very capable of modelling joints in the tunnel lining, the two dimensional version of DIANA does not provide more options than Plaxis 2016.01. While they are constantly developing the program and adding features, the current 2D version does not allow yet for modelling the joints other than a rotational spring.

- For three dimensional modelling, Plaxis 2016 is not able to create joints except for connections which are either fixed or free while DIANA is able to have several connection types, including a connection with the Janssen theory. When not including the different phases of the construction process, this becomes the major difference between Plaxis and DIANA.

- The difference between the programs for 2D with the most impact is the different material models for the soil. The Hardening Soil material model differs from the Modified Mohr-Coulomb material model which leads to a significant difference in bending moment in the lining.

- Modelling the construction phases has a positive influence on the lining forces. The unity check decreases considerably when including these phases.

- When grouting pressures are applied on the borehole, the lining forces are independent of the material models for the soil. Unfortunately this has only been investigated in Plaxis for Hardening Soil and Mohr Coulomb. However, if this is true for other similar material models, one can argue that the difference between DIANA and Plaxis, caused by the material models, is nullified when construction phases are included.

- Interfaces can have a large influence on the model. As discussed, the reduction factor itself may only have a significant influence on the lining forces when it becomes very small. The preferred interface approach in Plaxis, however, deducts its strength parameters from the surrounding soil. In this case it was a linear elastic material with a relatively high stiffness compared to the surrounding soil. This leads to a different interface strength and thus different results in the internal lining forces.

- When creating a model with 10 rings, the first couple of rings that are modelled will have an influence on the lining forces when the construction phases are included. This accounts for a first ring that is attached to the jet grouting block ring or one that can move freely.

With finite element modelling, there will always be improvements that can be made. Due to time constraints it was decided to finish this current research but much more in this field could have been done. This will be discussed in the next chapter.

7
Recommendations

In this chapter, recommendations will be made for researchers that would like to continue on this research.

Extend 3D models
In section 2.3, the 3D phenomena of tunnel construction are discussed and not all of these have been included in the models. In 2D, many assumptions are made to account for these 3D phenomena and some phenomena are completely left out in the models in 2D. The three dimensional models that are created do not include all different phenomena either. In order to assess these 3D phenomena better, the current 3D models need to be extended. With extending, not only the length of the tunnel is taken into consideration, also the features present in the models. More features have to be applied to get a more complete image on the 3D phenomena and the modelling possibilities.

Program Experience
In order to thoroughly research the tunnelling construction process in these two programs, extensive knowledge about the program is recommended for several reasons:

- Creating proper, working models will take less time;
- Different options for modelling certain phenomena can be assessed;
- The program can be forced to step off the usual track for modelling certain phenomena;
- The impact of the modelling approach on the results can be understood well.

This accounts for both Plaxis and DIANA and for 2D as well as 3D.

Real Data
When modelling in finite element programs, a representation of the reality is created. Even when creating a model as close to reality as possible, it will not be reality. In order to create a benchmark for the models in Plaxis and DIANA, and potentially other programs, the internal lining forces in an actual tunnel ring during the construction of a tunnel should be assessed. Such a project has been done in the Second Heinenoord tunnel twenty years ago. However, the results of this project are not accepted by the entire tunnelling industry for several reasons. A similar investigation has to be done but it has to be done better in order to acquire proper results that will have the support of the tunnelling community. With this benchmark, the results acquired in different programs and from different models can be validated.

Other programs
In this research, Plaxis and DIANA have been compared, but many other programs state to be capable of modelling the tunnel construction process as well. Especially with something important as consolidation missing in DIANA, other programs may be more suitable. Taking into account these other programs and combining them with the benchmark discussed previously, it can be assessed which available program is the most accurate and where some programs lack the right tools. The ideal program for this research would have at least the following features:

- Hardening Soil or equivalent material model
- Line contraction for plates

- Material model for fluid form of grout
- Consolidation possibilities
- Janssen material models for interfaces in 2D & 3D

Other cases
This research has been conducted with a specific project as lead for its input properties. Unable to state whether the conclusions are directly project related, the outcome of this research may differ for a different project. Apart from the input parameters, the addition of some of the other loads that are acting on the tunnel lining, as presented in section 2.2, might give different results. Furthermore, some other engineering aspects for a tunnel have been left out e.g. creep, dynamic loading, adjacent tunnels and creating the cross passages. Some of these are complicated phenomena and may give completely different results.

Be careful with interfaces
The interface is an important difference between the two programs as described in chapter 6. DIANA provides a lot of freedom in modelling the interface, this, however, also makes it easier to be make errors. These interfaces have to be modelled with a lot of care. A better understanding of these interfaces would also improve their behaviour and can be used to assess its actual influence on ground-lining interaction.

Improve programs
In order to assess the actual difference of all the construction phases, DIANA needs to implement consolidation. There are still some interesting questions left on the differences between DIANA and Plaxis. Especially if the difference caused by the material models gets nullified by the grouting as seen in the Mohr-Coulomb and Hardening Soil comparison. The joints is another topic which requires improvement. The joints cannot be implemented in another way than rotational springs in 2D models. When a different joint setting is avaible for two dimensions in DIANA, preferably one with the Janssen theorem, it would be interesting to see the difference in the lining forces between this Janssen joint in DIANA and the rotational springs in Plaxis. It can then also be assessed whether the manual Janssen approach used in this research is valid. An implementation of new joint approaches in Plaxis for both two and three dimensions would also be interesting. Especially in 3D it would be interesting since it does not have an actual joint approach right now and the tunnelling phenomena are 3D. These programs need to improve or add these features in order to meet the ideal program, as discussed above, for modelling the construction process of bored tunnels.

Include construction phases in design process
It was concluded that the construction phases have a positive influence on the internal lining forces. While it is not stated in any of the tunnelling guidelines, the client requires the tunnel to be designed without any positive construction effects. When including these in the design process however, the tunnel can be designed more economically since not including them leads to a large overestimation of the lining forces. Convincing the client to include these will create a major advantage over other tunnel designers. However, before including these phases in the design process, the models used in this research need to be validated first, as discussed above. Preferably, the behaviour of grout is also better understood and it can even be modelled closer to reality than at the moment. With these two improvements, the design can be based on more realistic models and it will be easier to convince the client to include the construction phases.

Computational Time
If a recommendation for programs were to be made, computational time can be an important factor. Especially for the case were different programs provide the same results. Computational time also plays a part in choosing between 2D and 3D. With regards to the two programs, Plaxis tends to be faster than DIANA. For the largest model in both programs, the multiple rings without construction phases, Plaxis is approximately three times quicker. It has to be emphasized this is an approximation and that it depends on many different features. First, the computer itself is very important. A high performance computer will do the calculations quicker than a low performance one. Second, the size of the model, increasing the model size will increase the computational time. The created mesh in the model is of importance too. When a fine mesh is created, more elements and therefore nodes are in the model. These all have to be calculated by the program which leads to an increase in computational time. Therefore it is not surprising a 3D model has a larger computational time than 2D models. Based on computational time, a 2D model in Plaxis would therefore be the quickest. A recommendation on 2D versus 3D will be discussed below.

2D or 3D

The results show very little difference between the 2D and 3D, especially for the model without construction phases. Combine this with the larger computational time for 3D and it would be a better choice to model the tunnel in 2D when designing the tunnel. Especially since currently the construction phases are not included.

When, however, joints can be implemented, this recommendation may differ. The rings joints can only be implemented in 3D and creates multiple rings which interact instead of one long tunnel as in 2D. The 3D phenomena present during tunnelling will have an influence on the behaviour of these ring joints. In 3D, it is also possible to create segmental joints on different locations for each ring. In reality, the segmental joints do not continue along the tunnel axis over multiple rings. As shown in fig. 2.11 and discussed in section 2.3.4, the segments are constructed in a staggered configuration. This can only be modelled in 3D and might lead to significant other lining forces. The distribution of the bending moments will differ. This extra feature of joints together with the 3D phenomena needs to be assessed properly in order to give a recommendation on whether to use 3D or 2D models.

Bibliography

[1] O. Arnau and C. Molins. Experimental and analytical study of the structural response of segmental tunnel linings based on an in situ loading test. Part 2: Numerical simulation. *Tunnelling and Underground Space Technology*, 26(6):778–788, 2011.

[2] O. Arnau and C. Molins. Three dimensional structural response of segmental tunnel linings. *Engineering Structures*, 44:210–221, 2012.

[3] K.J. Bakker. Report K100-06 Second Heinenoord Tunnel Evaluation Report. Technical report, COB, Gouda, 2000.

[4] K.J. Bakker. Structural Design of Lining for Bored Tunnels in Soft Grond. *HERON*, 48(1):33–63, 2003.

[5] S. Bernat and B. Cambou. Soil-structure interaction in shield tunnelling in soft soil. *Computers and Geotechnics*, 22(3-4):221–242, 1998.

[6] A. Bezuijen, A.M. Talmon, F.J. Kaalberg, and R. Plugge. Field Measurements of Grout Pressures during Tunnelling of the Sophia Rail Tunnel. *Soils and Foundations*, 44(1):39–48, 2004.

[7] C.B.M. Blom. *Design philosophy of concrete linings for tunnels in soft soils.* PhD thesis, Delft University of Technology, 2002.

[8] C.B.M. Blom, E.J. Van der Horst, and P.S. Jovanovic. Three-dimensional Structural Analyses of the Shield-Driven "Green Heart" Tunnel of the High-Speed Line South. *Tunnelling and Underground Space Technology*, 14(2):217–224, 1999.

[9] P.J. Bogaards. *Liggerwerkig boortunnels.* Msc., Delft University of Technology, 1998.

[10] A.L. Bouma. *Mechanica van constructies.* Delftse Uitgevers Maatschappij b.v., Delft, 1993.

[11] R.B.J. Brinkgreve. Hypoplastic model, 2016.

[12] R.B.J. Brinkgreve, S. Kumarswamy, and W.M. Swolfs. *Plaxis 2016.* Plaxis bv, Delft, 2016.

[13] H. Chakeri and B. Ünver. A new equation for estimating the maximum surface settlement above tunnels excavated in soft ground. *Environmental Earth Sciences*, 71(7):3195–3210, 2014.

[14] COB-F220/230. 4D-Groutdrukmodel Plaxis. Technical report, COB, Gouda, 2005.

[15] COB-F220/230. Praktijkonderzoek Sophiaspoortunnel. Technical report, COB, Gouda, 2006.

[16] COB-K100. Bored railway tunnels in the Netherlands. Technical report, COB, Gouda, 1995.

[17] COB-K100. Praktijkonderzoek boortunnels K100, Cluster 9 Liggerwerking tunnelbuis. Technical report, COB, Gouda, 1996.

[18] COB-L500. Toetsingsrichtlijn voor het ontwerp van boortunnels voor weg en -railinfrastructuur. Technical report, COB, Gouda, 2000.

[19] COB-L520. 3D EEM-berekeningen. Technical report, COB, Gouda, 1997.

[20] COB-L520. Twee dimensionale belastingbepaling met Plaxis. Technical report, COB, Gouda, 1998.

[21] COB-L520. Validatie groutdrukmodel onderdeel belasting en ondersteuning.pdf. Technical report, COB, Gouda, 1999.

[22] COB-L520. Richtlijnen Groutdrukmodel. Technical report, COB, Gouda, 1999.

[23] COB-L520. Validatie groutdrukmodel aan de hand van metingen bij de Tweede Heinenoordtunnel. Technical report, COB, Gouda, 1999.

[24] COB-L530. Gesegmenteerde lining: Voeggedrag. Technical report, COB, Gouda, 1997.

[25] E.J. Cording. Control of groundmovements around tunnel in soil. In *Proceedings of the 9th Pan-American Conference on Soil Mechanics and Foundation Engineering, Valparaiso*, pages 2195–2244, 1991.

[26] CUR. CUR-Rapport 2003-7 Bepaling geotechnische parameters. Technical report, Stichting CUR, Gouda, 2003.

[27] DIANA FEA BV. DIANA Solutions for Tunnelling & Underground Structures, 2016.

[28] DIANA FEA BV. Guidelines to Set-up Material Parameters of Interface Elements, 2017. URL `https://dianafea.com/manuals/d101/GeoTech/node22.html`.

[29] DIANA FEA BV. Iterative procedures, 2017. URL `https://dianafea.com/manuals/d101/Analys/node513.html`.

[30] N.A. Do, D. Dias, P. Oreste, and I. Djeran-Maigre. 2D numerical investigation of segmental tunnel lining behavior. *Tunnelling and Underground Space Technology*, 37(August 2013):115–127, 2013.

[31] N.A. Do, D. Dias, P. Oreste, and I. Djeran-Maigre. Three-dimensional numerical simulation for mechanized tunnelling in soft ground: The influence of the joint pattern. *Acta Geotechnica*, 9(4):673–694, 2014.

[32] H. Duddeck and J. Erdmann. Structural design models for tunnels in soft soils. In *Tunnelling 1982 , Proceedings of the 3rd International Sumposium*, pages 83–91, London, 1982. Insitution of Mining and Metallurgy.

[33] R.J. Finno and G.W. Clough. Evaluation of Soil Response to EPB Shield Tunneling. *Journal of Geotechnical Engineering*, 111(2):155–173, 1985.

[34] A. Fioranelli Jr, A. Cavalcante, T. Pessoa, and A. Ferreira. Plugin for Tunneling and Geotechnical Analysis in Abaqus. In *SIMULIA Customer Conference*, Providence, 2012.

[35] J.N. Franzius. *Behaviour of buildings due to tunnel induced subsidence*. Phd., University of London, 2003.

[36] G Galli, A Grimaldi, and A Leonardi. Three-dimensional modelling of tunnel excavation and lining. *Computers and Geotechnics*, 31(3):171–183, 2004.

[37] G.M.L. Gladwell. *Contact problems in the classical theory of elasticity*. Springer Science & Business Media, Alphen aan de Rijn, 1980.

[38] N.J.S. Gorst, S.J. Williamson, P.F. Pallett, and L.A. Clark. Friction in temporary works. Technical report, The Univeristy of Birmingham, Birmingham, 2003.

[39] J. Greenhalgh. 20 years of fibre concrete linings in the UK, 2010.

[40] Y. Hejazi, D. Dias, and R. Kastner. Impact of constitutive models on the numerical analysis of underground constructions. *Acta Geotechnica*, 3(4):251–258, 2008.

[41] F.J.M. Hoefsloot and A. Verweij. 4D grouting pressure model PLAXIS. In *5th International Symposium on Geotechnical Aspects of Underground Construction in Soft Ground*, pages 529–534, Amsterdam, 2006.

[42] I.T.A. Guidelines for the design of shield tunnel lining. *Tunnelling and Underground Space Technology*, 15(3):303–331, 2000.

[43] Itech. Cesar-LCPC, 2016.

[44] Itech. Constitutive models for materials, 2016.

[45] P. Janssen. *Tragverhalten von tunnelausbauten mit gelenktubbings*. PhD thesis, University of Braunschweig, 1983.

[46] M. Kalhor and M. Azadi. Assessment of changes in elasticity module and soil Poisson ' s Ratio on applied forces to tunnel lining during seismic loading. *International Research Journal of Applied and Basic Sciences*, 4(9):2756–2761, 2013.

[47] M Karakus. Appraising the methods accounting for 3D tunnelling effects in 2D plane strain FE analysis. *Tunnelling and Underground Space Technology*, 22(1):47–56, 2007.

[48] T. Kasper and G. Meschke. A 3D finite element simulation model for TBM tunnelling in soft ground. *International Journal for Numerical and Analytical Methods in Geomechanics*, 28(14):1441–1460, 2004.

[49] T. Kasper and G. Meschke. On the influence of face pressure, grouting pressure and TBM design in soft ground tunnelling. *Tunnelling and Underground Space Technology*, 21(2):160–171, 2006.

[50] T. Kasper and G. Meschke. A numerical study of the effect of soil and grout material properties and cover depth in shield tunnelling. *Computers and Geotechnics*, 33(4-5):234–247, 2006.

[51] H. Katebi, A. H. Rezaei, M. Hajialilue-Bonab, and A. Tarifard. Assessment the influence of ground stratification, tunnel and surface buildings specifications on shield tunnel lining loads (by FEM). *Tunnelling and Underground Space Technology*, 49(June):67–78, 2015.

[52] C. Klappers, F. Grübl, and B. Ostermeier. Structural analyses of segmental lining – coupled beam and spring analyses versus 3D-FEM calculations with shell elements. *Tunnelling and Underground Space Technology*, 21(3-4):254–255, 2006.

[53] A.J. Koek. Axial pre-stresses in the lining of a bored tunnel. In *Geotechnical Aspects of Underground Construction in Soft Ground*, pages 559–564, 2006.

[54] K.M. Lee and X.W. Ge. The equivalence of a jointed shield-driven tunnel lining to a continuous ring structure. *Canadian Geotechnical Journal*, 38(3):461–483, 2001.

[55] K.M. Lee, X.Y. Hou, X.W. Ge, and Y. Tang. An analytical solution for a jointed shield-driven tunnel lining. *International Journal for Numerical and Analytical Methods in Geomechanics*, 25(4):365–390, 2001.

[56] H.J. Lengkeek. *Analyse grond-tunnelinteractie: Analytische en numerieke bepaling van veerstijfheid van de grond voor toepassing in ring- en liggermodel*. Msc., Delft University of Technology, 1997.

[57] H. Y. Liu, J. C. Small, and J. P. Carter. Full 3D modelling for effects of tunnelling on existing support systems in the Sydney region. *Tunnelling and Underground Space Technology*, 23(4):399–420, 2008.

[58] A. Luttikholt. *Ultimate limit state analysis of a segmented tunnel lining: Results of full-scale tests compared to finite element analysis*. PhD thesis, Delft University of Technology, 2007.

[59] B. Maidl, L. Schmid, W. Ritz, and M. Herrenknecht. Joint Detailing. In *Hardrock Tunnel Boring Machines*, pages 282–288. Ernst, Berlin, 2008.

[60] R.J. Mair and R.N. Taylor. Theme lecture: Bored tunnelling in the urban environment. In *Proceedings of the 14th International Conference on Soil Mechanics and Foundation Engineering (Hamburg, 1997)*, pages 2353–2385. Balkema, 1999.

[61] P.M. Mayer, A. Libreros-Bertini, and H.M. Hilber. Numerical modelling of cam-pocket coupling systems for concrete lining. In *Advances in Construction Materials*, pages 57–65. Springer Berlin Heidelberg, Berlin, Heidelberg, 2007.

[62] MIDAS Information Technology. Tunnels, 2016. URL `http://midasgtsnx.com/solutions/tunnels.asp`.

[63] MIDAS Information Technology. *Analysis Reference*. 2016.

[64] MIDAS Information Technology. Printing out the analysis, 2016. URL `http://midasgtsnx.com/`.

[65] S.C. Möller. *Tunnel induced settlements and structural forces in linings*. Phd, Universität Stuttgart, 2006.

[66] S.C. Möller and P.A. Vermeer. Prediction of settlements and structural forces in linings due to tunnelling. In *Proceedings of the 5th International Symposium on Geotechnical Aspects of Underground Construction in Soft Ground, Amsterdam, The Netherlands*, pages 621–627, 2005.

[67] S.C. Möller and P.A. Vermeer. On numerical simulation of tunnel installation. *Tunnelling and Underground Space Technology*, 23(4):461–475, 2008.

[68] C.W.W. Ng and G.T.K. Lee. Three-dimensional ground settlements and stress- transfer mechanisms due to open-face tunnelling. *Geotech. J*, 42:1015–1029, 2005.

[69] M. Nikkhah, S.S. Mousavi, and O. Khademhosseini. Evaluation of structural analysis of tunnel segmental lining using beam- spring method and force-method (Case study: Chamshir water conveyance tunnel). *Journal of Minning & Environment*, 8(1):1–21, 2016.

[70] M. Palassi and M.M. Mohebbi. Design of lining of tunnels excavated in soil and soft rock. *Electronic Journal of Geotechnical Engineering*, 13(E), 2008.

[71] H. Schulze and H. Duddeck. Statische Berechnung Schieldvorgetriebener Tunnel (Structural analysis of tunnels excavated with shield support). In *Beton- und Monierbau AG 1889-1964*, pages 87–114. 1964.

[72] C. Surarak. *Geotechnical Aspects of the Bangkok MRT Blue Line Project*. Phd, Griffith University, 2010.

[73] C. Surarak, S. Likitlersuang, D. Wanatowski, A. Balasubramaniam, E. Oh, and H. Guan. Stiffness and strength parameters for hardening soil model of soft and stiff Bangkok clays. *Soils and Foundations*, 52 (4):682–697, 2012.

[74] A.M. Talmon and A. Bezuijen. Grouting the tail void of bored tunnels : the role of hardening and consolidation of grouts. In *Proceedings of the 5th International Symposium on Geotechnical Aspects of Underground Construction in Soft Ground*, Amsterdam, The Netherlands, 2005.

[75] A.M. Talmon, L. Aanen, and W.H. Van der Zon. Stromingsgedrag Groutinjectie Delft Cluster. Technical Report February, WL | Delft Hydraulics, Delft, 2002.

[76] A.M. Talmon, C.A. Schoofs, and A. Bezuijen. Evaluatie grouting staartspleet Botlekspoortunnel, F300-W050. Technical report, COB, Gouda, 2003.

[77] A.M. Talmon, A. Bezuijen, and F.J.M. Hoefsloot. Evaluatie tweede fase Groene Hart Tunnel: Ontwerpparameters bij krachtswerking, groutdruk en invloed beweging tunnelbuis. Technical report, COB, Gouda, 2007.

[78] S. Teachavorasinskun and T. Chub-uppakarn. Influence of segmental joints on tunnel lining. *Tunnelling and Underground Space Technology*, 25(4):490–494, 2010.

[79] P.A. Vermeer, P.G. Bonnier, and S.C. Möller. On a smart use of 3D-FEM in tunnelling. *Numerical Models in Geomechanics*, pages 361–366, 2002.

[80] J.C. Walraven. *Gewapend beton: college CTco3050: dictaat behorende bij college CT3050*. TU Delft, Delft, 4 edition, 1997.

[81] O.C. Zienkiewicz, R.L. Taylor, and J.Z. Zhu. The standard discrete system and origins of the finite element method. In *The Finite Element Method Set*, volume 1, pages 1–18. Elsevier, 2005.

A

Schematic overview modelling

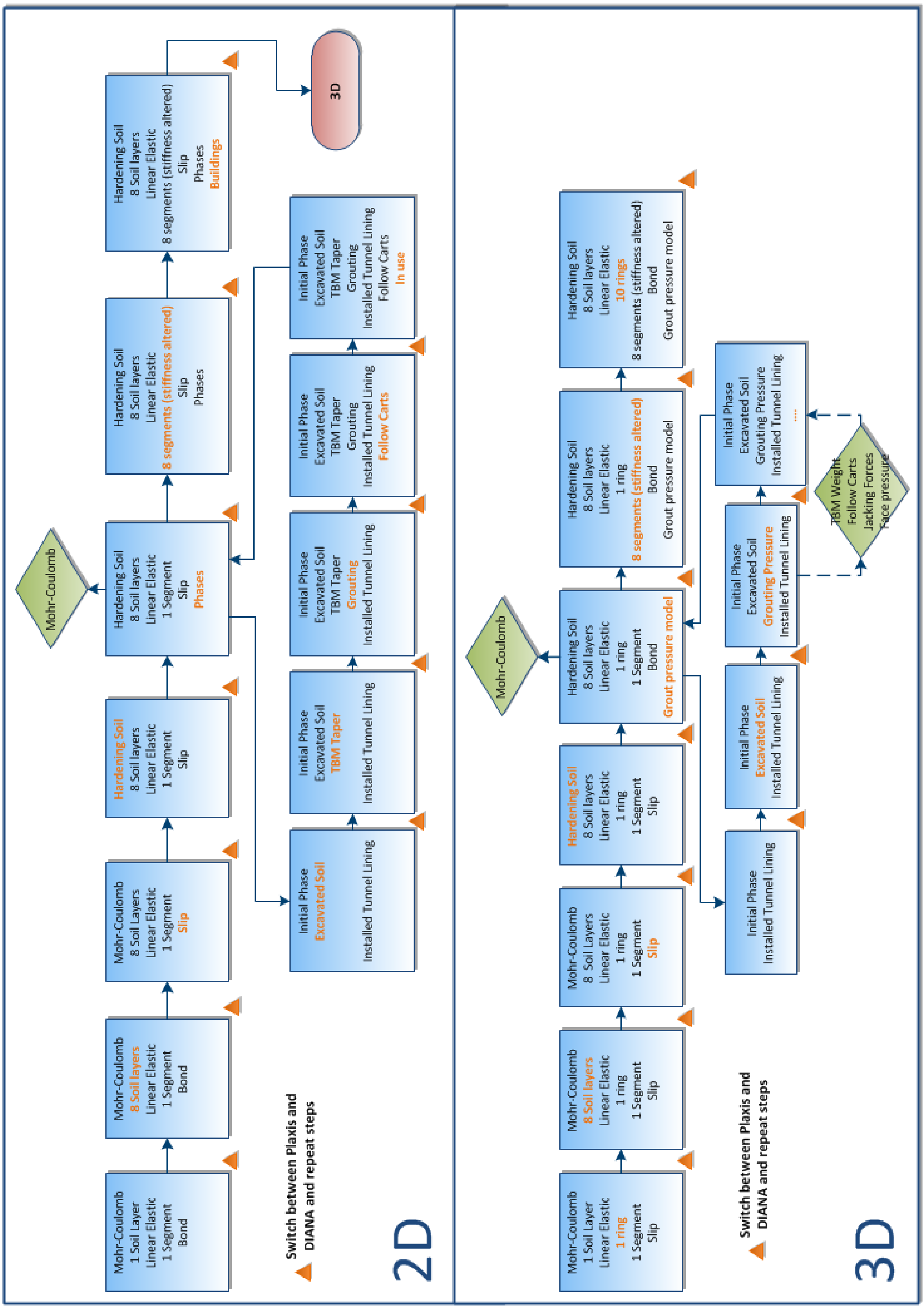

Mohr-Coulomb
1 Soil Layer
Linear Elastic
1 Segment
Bond
Mohr-Coulomb
8 Soil layers
Linear Elastic
1 Segment
Bond
Mohr-Coulomb
8 Soil Layers
Linear Elastic
1 Segment
Slip
Hardening Soil
8 Soil layers
Linear Elastic
1 Segment
Slip
Hardening Soil
8 Soil layers
Linear Elastic
1 Segment
Slip
Phases
Mohr-Coulomb
Hardening Soil
8 Soil layers
Linear Elastic
8 segments (stiffness altered)
Slip
Phases
Hardening Soil
8 Soil layers
Linear Elastic
8 segments (stiffness altered)
Slip
Phases
Buildings
3D
Initial Phase
Excavated Soil
Installed Tunnel Lining
Initial Phase
Excavated Soil
TBM Taper
Installed Tunnel Lining
Initial Phase
Excavated Soil
TBM Taper
Grouting
Installed Tunnel Lining
Initial Phase
Excavated Soil
TBM Taper
Grouting
Installed Tunnel Lining
Follow Carts
Initial Phase
Excavated Soil
TBM Taper
Grouting
Installed Tunnel Lining
Follow Carts
In use
Switch between Plaxis and DIANA and repeat steps
2D
Mohr-Coulomb
1 Soil Layer
Linear Elastic
1 ring
1 Segment
Slip
Mohr-Coulomb
8 Soil layers
Linear Elastic
1 ring
1 Segment
Slip
Mohr-Coulomb
8 Soil layers
Linear Elastic
1 ring
1 Segment
Slip
Hardening Soil
8 Soil layers
Linear Elastic
1 ring
1 Segment
Slip
Hardening Soil
8 Soil layers
Linear Elastic
1 ring
1 Segment
Bond
Grout pressure model
Mohr-Coulomb
Hardening Soil
8 Soil layers
Linear Elastic
1 ring
8 segments (stiffness altered)
Bond
Grout pressure model
Hardening Soil
8 Soil layers
Linear Elastic
10 rings
8 segments (stiffness altered)
Bond
Grout pressure model
Initial Phase
Installed Tunnel Lining
Initial Phase
Excavated Soil
Installed Tunnel Lining
Initial Phase
Excavated Soil
Grouting Pressure
Installed Tunnel Lining
Initial Phase
Excavated Soil
Grouting Pressure
Installed Tunnel Lining
....
TBM Weight
Follow Carts
Jacking Forces
Face pressure
Switch between Plaxis and DIANA and repeat steps
3D

B

Model overview

Model One

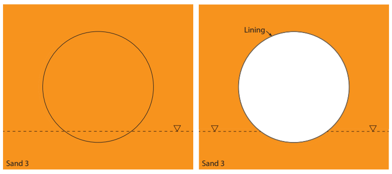

Figure B.1: Phases in model one

Model Two/Three/Four

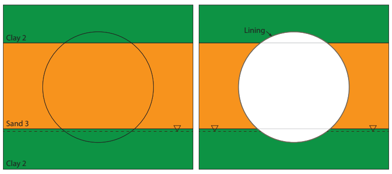

Figure B.2: Phases in model two

Model Five

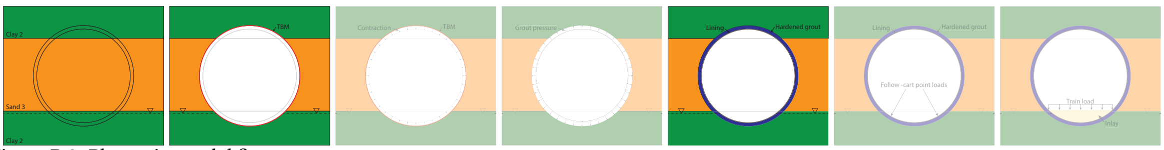

Figure B.3: Phases in model five

Model Six

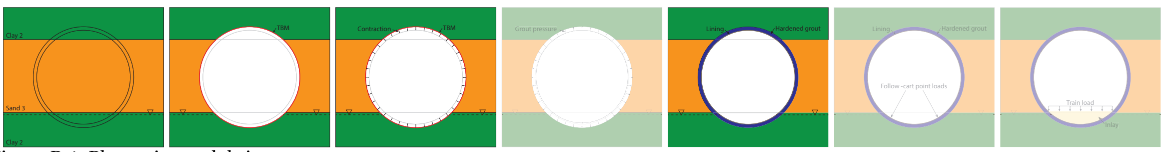

Figure B.4: Phases in model six

Model Seven

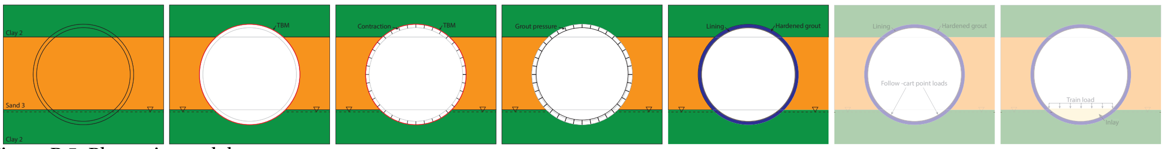

Figure B.5: Phases in model seven

Model Eight

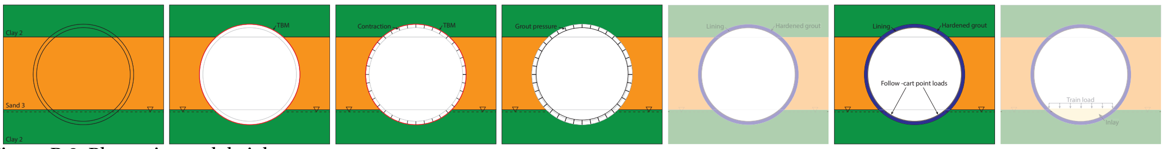

Figure B.6: Phases in model eight

Model Nine

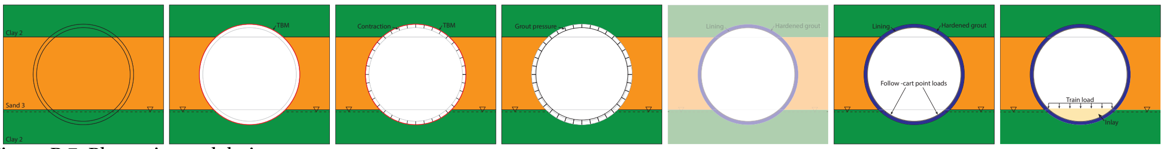

Figure B.7: Phases in model nine

One-ring model

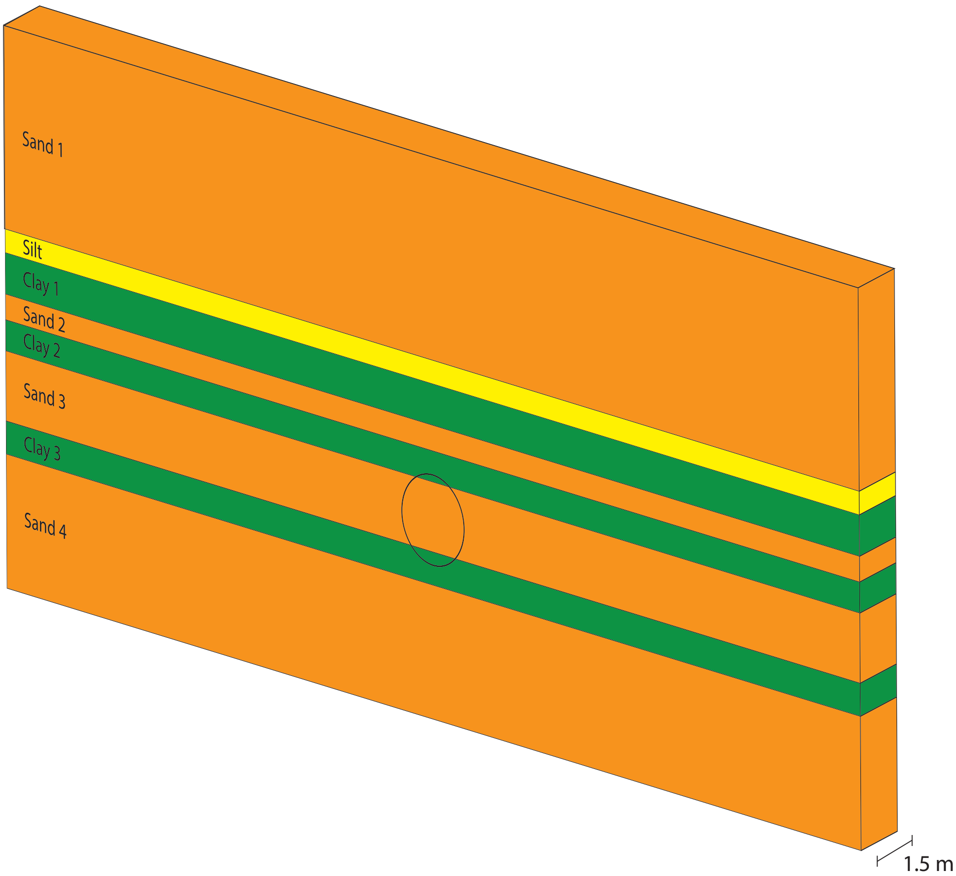

Figure B.8: One-ring 3D model

C

Finite element models

In this chapter, more information on the models is given. The given model properties for 2D apply to all 2D models with exception of the different loads. For the 3D models, it will be explained per property.

C.1. General information

Normative section
For the 3D models in DIANA, the fourth out of six rings is normative for the models without construction phases and the sixth out of ten rings for Plaxis. For the models with construction phases, the normative cross section is discussed in section 5.2.3.

Programs
The version of the programs used:

- Plaxis 2D 2016.01
- Plaxis 3D 2016
- DIANA 10.1

Calculation dates
February - July

Sensitivity analyses
Sensitivity analyses have been done in chapter 5.

Element attachment deviations
With regards to the elementmodel in 3D, rings are attached for the model without construction phases while in reality, they are not.

C.2. Input

This section will discuss the input used in the program and motivate the choices that have been made regarding this input.

Data origin
As previously discussed, the input of the models has been acquired from a project by Arthe CS in Masshad, Iran. The soil parameters have been acquired by the soil investigation that has been done.

Schematic overview models
Schematised representations of the models and its different phases are shown in section 3.1, in which they are also explained.

Axes
With regards to the axes in the models, the following will be used:

- **2D:**
  - x-axis horizontal
  - y-axis vertical
- **3D:**
  - x-axis horizontal
  - z-axis vertical
  - y-axis horizontal 3rd dimension

Units
For the units in Plaxis, the default units have been used. These default units ensure convenient input values:

- Length: m
- Force: kN
- Time: day

For DIANA, the input units are changed. This is done to ensure convenience regarding the values itself and also to have the same input as Plaxis. This reduces the possibility of making input errors. The unit for time is different than in Plaxis, this unit however is not used and if changed to days, the other units are changed as well. Therefore the unit for time is kept at the seconds. The units will be as follows:

- Lenght: m
- Mass: T
- Force: kN
- Time: seconds
- Angle: Degree

Elements
In Plaxis 2D, the default elements have been used. When compared with the elements with less nodes and of a different order, the results are almost equal as well. The following elements are used:

- Soil: 15 noded triangular elements
- Lining/TBM: 5 noded plate elements
- Interface: 5+5 noded interface elements

The size of the plate elements is 0.4 meters. Within Plaxis it is not directly possible to set the element size. For input, it can only be given which parts of the geometry require a fine mesh. The automatic mesh generator in Plaxis creates the elements with a size Plaxis itself finds convenient.

In DIANA 2D, the element types can be set, but the specific element choice is made by DIANA itself when meshing. As a size, 0.4 m is taken for the lining elements. The following elements have been used in this research:

- Soil: 6 noded triangular elements of type CT12E
- Lining/TBM: 3 noded infinite curved shell elements of type CL9PE
- Interface: 3+3 noded interface elements of type CL12I

In Plaxis, there is only one option for the elements in 3D. The size of the plates is set onto 1.5 meters. The following elements are used:

- Soil: 10 noded tetrahedral elements
- Lining/TBM: 6 noded triangular plate elements
- Interface: 6+6 noded interface elements

For DIANA, the same element types are used as with Plaxis but there is also a composed line in order to assess the lining forces in the fourth ring. The size of the plates in DIANA is set to 0.75 meters. The elements used in DIANA are the following:

- Soil: 10 noded tetrahedral elements of type CTE30
- Lining/TBM: 6 noded triangular curved shell elements of type CT30S
- Interface: 6+6 noded interface elements of type CT36I
- Composed line: 3 noded composed line elements of type CL3CM

Mesh

In Plaxis 2D, it is set that for the lining and TBM a fine mesh is required. When the mesh is created by the automatic mesh creator in Plaxis, it creates the convenient mesh based on the refinements given prior the meshing. When the lining is not meshed fine enough, an extra refinement should be applied to the lining prior the meshing. When meshing, automatically the element size will increase gradually outwards.

To ensure gradual increase in size of the soil elements outwards in DIANA, the boundaries between different soil layers are given a gradation. For the boundaries next to lining a non-symmetrical gradation is given while for the other soil boundaries a symmetrical gradation is given. Figure C.1 shows the size given for the gradation of the soil boundaries.

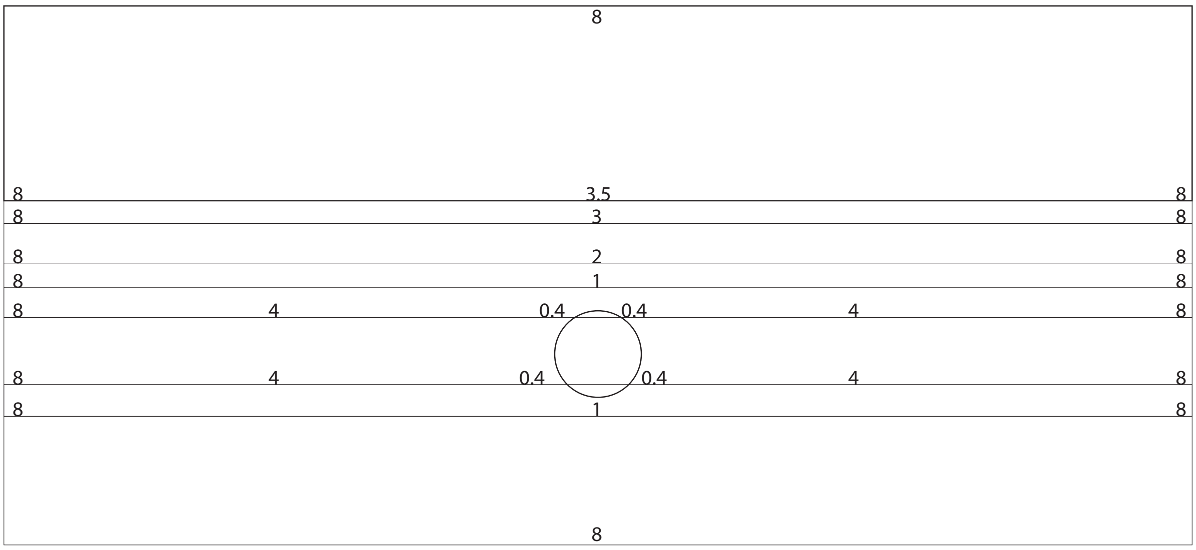

Figure C.1: Gradation of soil layer boundaries in meters in DIANA.

For Plaxis 3D, the same approach is used as with 2D only with a different size for the lining elements. In DIANA, the same approach is used as well as in 3D, but the gradations are slightly different. The gradation for the soil layer boundaries next to the lining do not start with 0.4 but with 0.75.

The meshes for 2D in Plaxis and DIANA are shown in figs. C.2 and C.3 respectively with the following number of nodes and soil elements:

	Plaxis	DIANA
Number of soil elements	2587	5343
Number of nodes	21830	9367

Table C.1: Number of nodes and soil elements in the 2D models

The mesh of the 3D models are shown in figs. C.4 and C.5 for Plaxis and DIANA respectively with the following number of nodes and soil elements:

	Plaxis	DIANA
Number of soil elements	20225	18654
Number of nodes	35953	30537

Table C.2: Number of nodes and soil elements in the 3D models

Istropic or orthotropic
All the models are modelled with isotropic behaviour. It is assumed the soil behaves the same in all directions.

Calculated stiffnesses
For the input in Plaxis, the axial stiffness and flexural rigidity of the lining have to be calculated, this is done in section 3.2.1.

Supports
The supports modelled in 2D will be the following. They are shown for Plaxis and DIANA in figs. C.2 and C.3 repectively.

- Sides (Xmin & Xmax) These are translationally fixed in the x-direction.
- Bottom (Ymin) This is fixed in every direction (fully fixed).
- Top (Ymax) This is free.

For 3D the following support wil be modelled, also shown in figs. C.6 and C.7 for Plaxis and DIANA respectively:

- Sides (Xmin & Xmax) These are translationally fixed in the x-direction (normally fixed).
- Bottom (Zmin) This is fixed in every direction (fully fixed).
- Front & back (Ymin & Ymax) These are translationally fixed in the y-direction (normally fixed)
- Top (Zmax) This is free.

Used calculation model
For Plaxis 2D the 15 noded soil elements that have been used are fourth order elements. There is, however, little difference in the lining results between this fourth order elements and the quadratic 6 noded elements.

The lining, TBM and hardened grout are modelled linear elastic. The soil is modelled linear elastic prefectly plastic in the first models before it is changed to an isotropic hardening material model. More about these material models is discussed in section 2.6.

In DIANA, the elements are quadratic. For the lining, TBM, hardened grout and the soil, the same applies as with Plaxis.

For 3D, both the progams have quadratic elements. The lining, TBM, hardened grout and soil are modelled as previously discussed.

For the analysis, different approaches have been used in the programs. In Plaxis, everything is set to default. For every phase, an elastic-plastic deformation analysis is done and followed by a consolidation analysis when modelled undrained.

DIANA requires more input for doing the calculations than Plaxis. "Structural nonlinear" is the analysis module that will be used in DIANA for every phase. This module allows for activating and deactivating element sets. The iteration method to acquire an equilibrium has been set to Secant (Quasi-Newton) with the BFGS (Broyden, Fletcher, Goldfarb and Shanno) type. This method works better for geotechnical issues than the default method "Regular Newton-Raphson". More information on these iterative procedures is explained by DIANA FEA BV [29]. For the convergence norms, both the displacement and force have to be satisfied with a convergence norm of 0.001.

Loading Assumptions
Different loading assumptions have been made in this research. These loads have been schematised when discussing the models in section 3.1. With these loads, the selfweight is always present. For recap puposes, these are the loading combination used in Plaxis 2D:

- Self weight & hydraulic head
- Self weight & hydraulic head & Contraction
- Self weight & hydraulic head & Grouting pressure (line load)

- Self weight & hydraulic head & Follow-cart load (point load)
- Self weight & hydraulic head & Metro load (line load)

For 3D, only the first three load combinations have been used.

In DIANA, for both 2D and 3D, the first load combination has been applied. The second load combination has also been used for DIANA 2D. Explanation on why not all load combinations have been used, is given in chapter 5.

Material Properties

The properties of the different soil layers, lining, TBM and hardened grout have all been discussed in section 2.9.

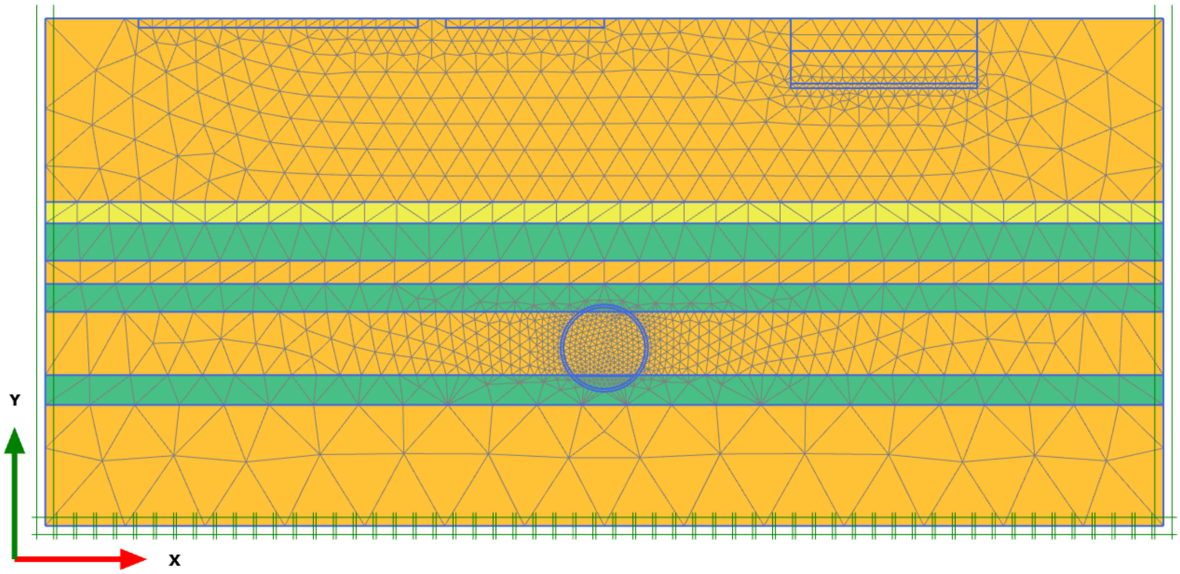

Figure C.2: Mesh and supports of 2D Plaxis model

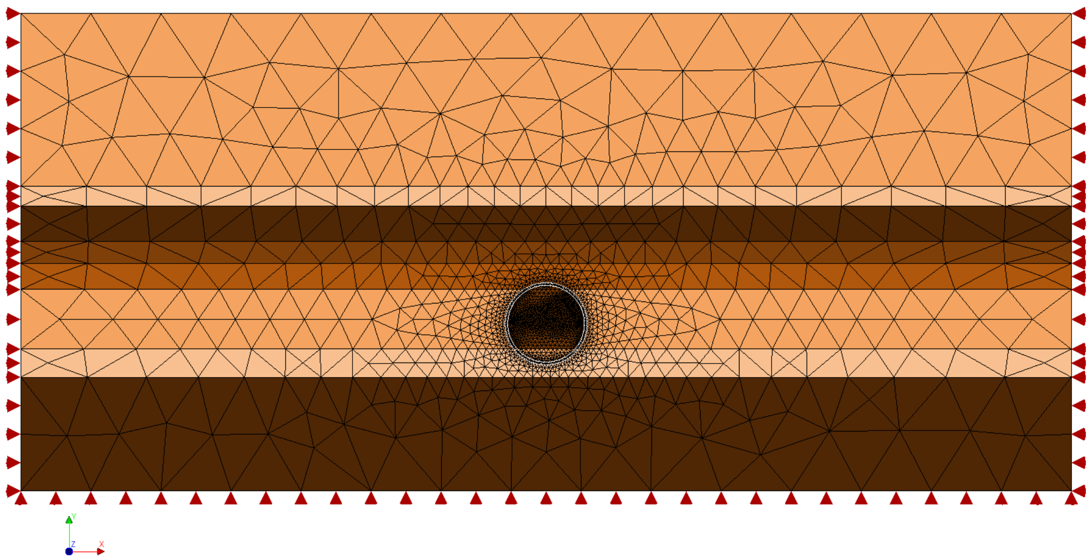

Figure C.3: Mesh and supports of 2D DIANA model

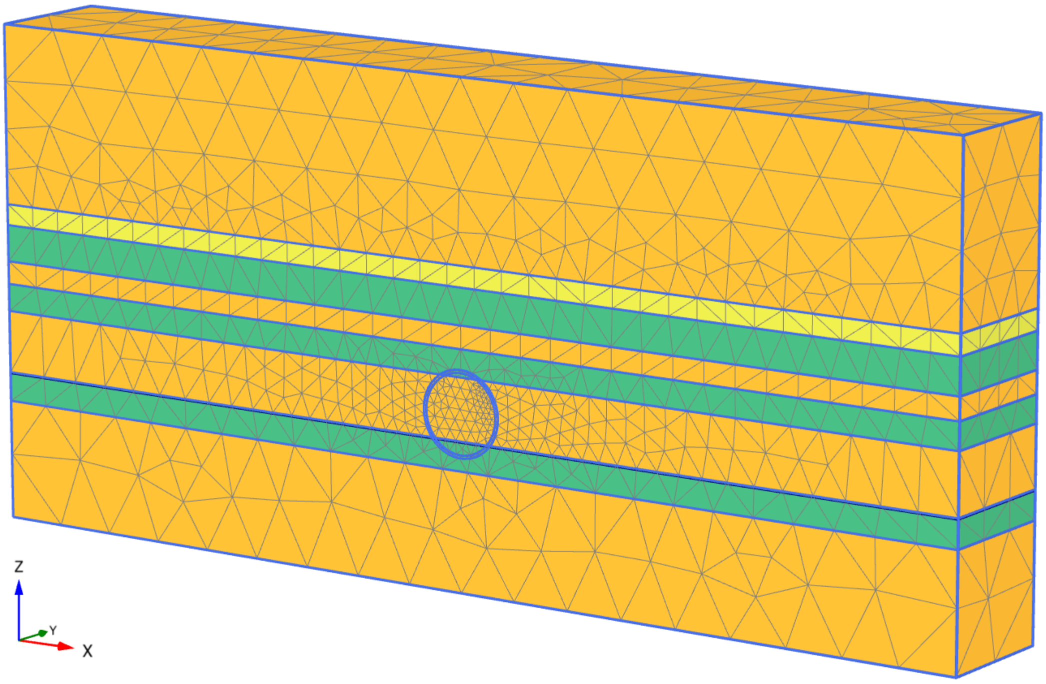

Figure C.4: Mesh of 3D Plaxis model

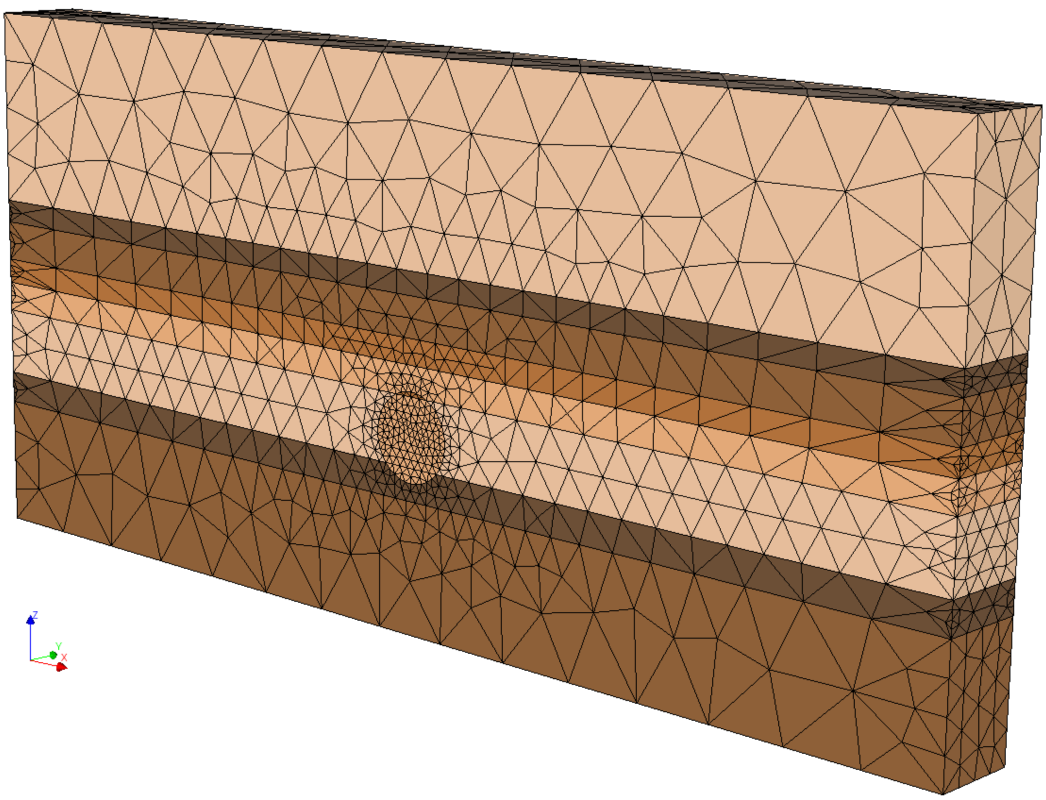

Figure C.5: Mesh 3D DIANA model

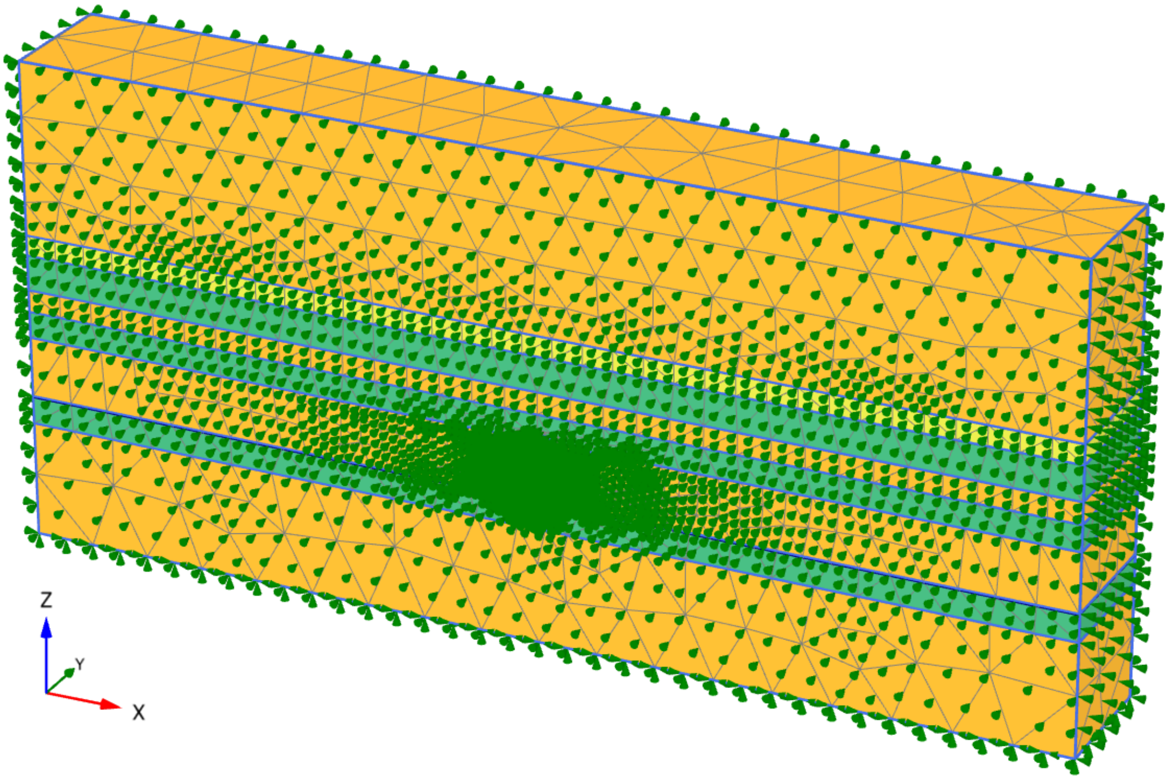

Figure C.6: Supports of 3D Plaxis model

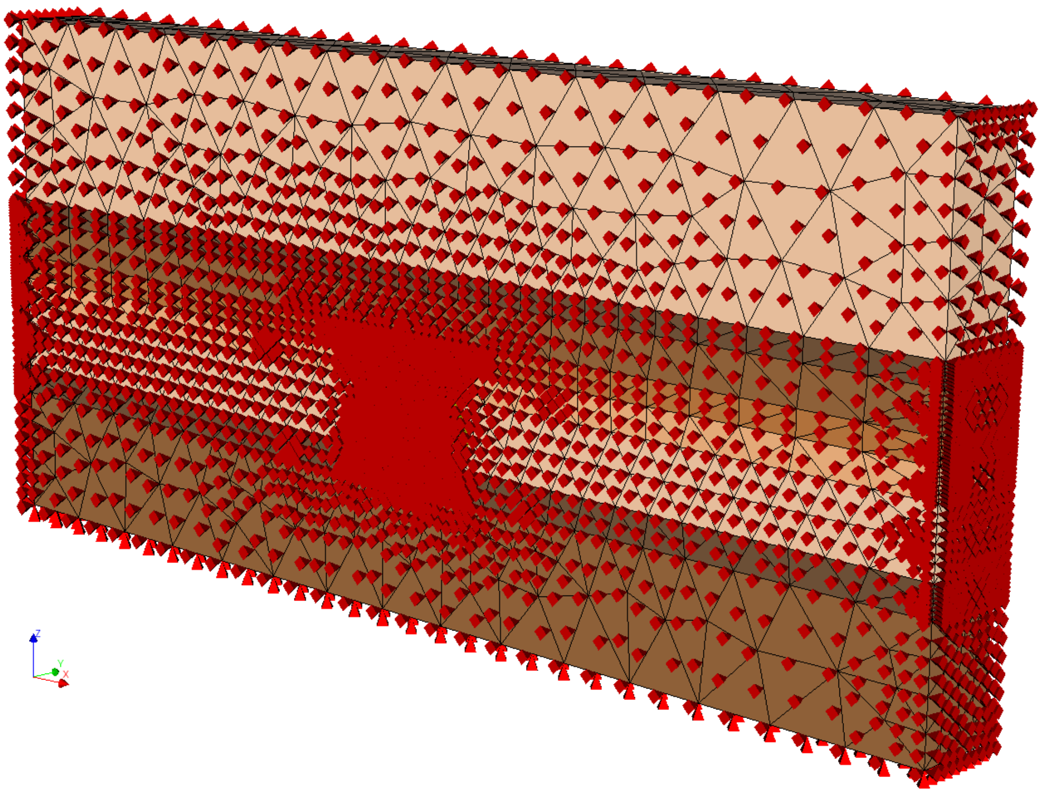

Figure C.7: Supports of 3D DIANA model

D

Analytical validation

Möller and Vermeer [66]

$$N = N_1 + N_2 \tag{D.1}$$

$$N_1 = \gamma H \frac{1+K_0}{2} \frac{R}{1 + \frac{1}{1+v}\beta + \frac{\beta}{\alpha}} \tag{D.2}$$

$$N_2 = \frac{\gamma H \frac{1-K_0}{2} R (1 + \frac{1}{12(1+v)}\alpha + \frac{1}{4(1+v)}\beta)}{1 + \frac{3-2v}{12(3-4v)(1+v)}\alpha + \frac{5-6v}{4(3-4v)(1+v)}\beta + \frac{1}{12(3-4v)(1+v)^2}\alpha\beta} \tag{D.3}$$

$$M = \frac{\gamma H \frac{1-K_0}{2} R^2 (1 + \frac{1}{2(1+v)}\beta)}{2 + \frac{3-2v}{6(3-4v)(1+v)}\alpha + \frac{5-6v}{4(3-4v)(1+v)}\beta + \frac{1}{6(3-4v)(1+v)^2}\alpha\beta} \tag{D.4}$$

with:

N	Maximum Normal Force
M	Maximum Bending Moment
γ	Unit weight of soil
H	Depth of tunnel axis
K_0	Coefficient of lateral Earth Pressure
R	Radius of "hartlijn" tunnel
v	Poisson ratio of soil
α, β	Coefficients given by eqs. (D.5) and (D.6)

$$\alpha = \frac{ER^3}{(EI)_l} \tag{D.5}$$

$$\beta = \frac{ER}{(EA)l} \tag{D.6}$$

with:

E	Young's modulus of soil
$(EI)_l$	Flexural rigidity of lining
$(EA)_l$	Normal stiffness of lining

$$\alpha = \frac{38750 \cdot 4.375^3}{1.25e+05} = 25.828 \tag{D.7}$$

$$\beta = \frac{38570 \cdot 4.375}{1.225e+07} = 1.378e^{-02} \tag{D.8}$$

		value	unit
Properties	Unit weight of soil	19.5	kN/m^3
	Depth of tunnel axis	35.4	m
	Coefficient of lateral earth pressure	0.4598	-
	Radius of "hartlijn" tunnel	4.375	m
	Poisson ratio of soil	0.3	-
	Young's modulus of soil	38570	kN/m^2
	Flexural rigidity of lining	1.25e+05	kN m^2/m
	Axial stiffness of lining	1.225e+07	kN/m

$$N_1 = 19.5 \cdot 35.4 \frac{1+0.4598}{2} \frac{4.375}{1+\frac{1}{1+0.3}1.378e^{-02}+\frac{1.378e^{-02}}{25.828}} = 2180.08kN/m \tag{D.9}$$

$$\begin{aligned} N_2 = &\frac{19.5 \cdot 35.4 \cdot \frac{1-0.4598}{2} \cdot (1+\frac{1}{12(1+0.3)} \cdot 25.828 + \frac{1}{4(1+0.3)} \cdot 1.378e^{-02})}{1+\frac{3-2\cdot 0.3}{12(3-4\cdot 0.3)(1+0.3)}25.828+\frac{5-6\cdot 0.3}{4(3-4\cdot 0.3)(1+0.3)}1.378e^{-02}+\frac{1}{12(3-4\cdot 0.3)(1+0.3)^2}25.828 \cdot 1.378e^{-02}} \\ &= 673.01kN/m \end{aligned} \tag{D.10}$$

$$N = 2180.08 + 673.01 = 2853.09kN/m \tag{D.11}$$

$$\begin{aligned} M = &\frac{19.5 \cdot 35.4 \frac{1-0.4598}{2} 4.375^2 (1+\frac{1}{2(1+0.3)}1.378e^{-02})}{2+\frac{3-2\cdot 0.3}{6(3-4\cdot 0.3)(1+0.3)}25.828+\frac{5-6\cdot 0.3}{4(3-4\cdot 0.3)(1+0.3)}1.378e^{-02}+\frac{1}{6(3-4\cdot 0.3)(1+0.3)^2}25.828 \cdot 1.378e^{-02}} \\ &= 557.16kNm/m \end{aligned} \tag{D.12}$$

COB-L500 [18]

$$N = n_0(\sigma_v + \sigma_h)R + n_2(\sigma_v - \sigma_h)R \tag{D.13}$$

$$M = m_2(\sigma_v - \sigma_h)R^2 \tag{D.14}$$

with:

N	Maximum Normal Force
M	Maximum Bending Moment
σ_v	Total vertical stress
σ_h	Total horizontal stress ($= \sigma_v \cdot K_0$)
R	Radius of "hartlijn" tunnel
n_0, n_2, m_2	Coefficients given in eqs. (D.15) to (D.17)

$$\frac{1}{n_0} = 2 + (1+K_0)\frac{2(1-\nu)}{(1-2\nu)(1+\nu)}\beta \tag{D.15}$$

$$\frac{1}{n_2} = 2 + \frac{4\nu\alpha}{(3-4\nu)(12(1+\nu)+\alpha)} \tag{D.16}$$

$$\frac{1}{m_2} = 4 + \frac{3-2\nu}{3(1+\nu)(3-4\nu)}\alpha \tag{D.17}$$

with:

K_0	Coefficient of lateral earth pressure
ν	Poisson ratio of soil

α, β Coefficients given in eqs. (D.15) to (D.17)

$$\alpha = \frac{12 E_g R^3}{E_b d^3} \tag{D.18}$$

$$\beta = \frac{E_g R}{E_b d} \tag{D.19}$$

with:

E_g Young's modulus of soil
E_b Young's modulus of concrete
d Thickness of lining

		value	unit
Properties	Total vertical stress	690.3	kN/m
	Total horizontal stress	317.4	kN/m
	Radius of "hartlijn"tunnel	4.375	m
	Coefficient of lateral earth pressure	0.4598	-
	Poisson ratio of soil	0.3	-
	Young's modulus of soil	38570	kN/m^2
	Young's modulus of concrete	3.5e+07	kN/m^2
	Thickness of lining	0.35	m

$$\alpha = \frac{12 \cdot 38570 \cdot 4.375^3}{3.5e^{+07} \cdot 0.35^3} = 25.828 \tag{D.20}$$

$$\beta = \frac{38570 \cdot 4.375}{3.5e^{+07} \cdot 0.35} = 1.378e^{-0.2} \tag{D.21}$$

$$\begin{aligned} \frac{1}{n_0} &= 2 + (1 + 0.4598)\frac{2(1-0.3)}{(1-2\cdot 0.3)(1+0.3)} 1.378e^{-0.2} \\ n_0 &= 0.495 \end{aligned} \tag{D.22}$$

$$\begin{aligned} \frac{1}{n_2} &= 2 + \frac{4 \cdot 0.3 \cdot 25.828}{(3-4\cdot 0.3)(12(1+0.3)+25.828)} \\ n_2 &= 0.414 \end{aligned} \tag{D.23}$$

$$\begin{aligned} \frac{1}{m_2} &= 4 + \frac{3 - 2\cdot 0.3}{3(1+0.3)(3-4\cdot 0.3)} 25.828 \\ m_2 &= 0.0779 \end{aligned} \tag{D.24}$$

$$N = 0.495 \cdot (690.3 + 317.4) \cdot 4.375 + 0.414 \cdot (690.3 - 317.4) \cdot 4.375 = 2857.85 kN/m \tag{D.25}$$

$$M = 0.0779 \cdot (690.3 - 317.4) \cdot 4.375^2 = 556.31 kNm/m \tag{D.26}$$

E

Interface sensitivity graphs

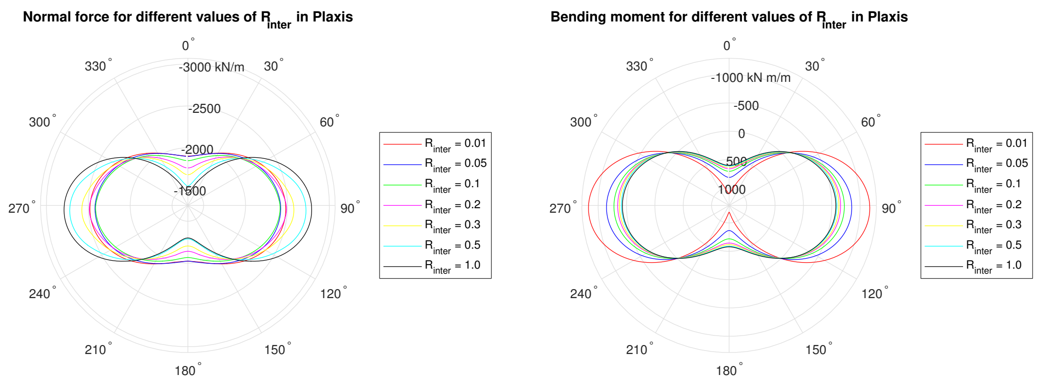

(a) Normal forces

(b) Bending moments

R_{inter} [-]	Max [kN/m]	Min [kN/m]
0.01	-1901	-2482
0.05	-1896	-2421
0.1	-1846	-2413
0.2	-1759	-2489
0.3	-1678	-2579
0.5	-1546	-2723
1.0	-1457	-2791

(c) Extreme values for normal force

R_{inter} [-]	Max [kN m/m]	Min [kN m/m]
0.01	1190	-1170
0.05	866.9	-852.3
0.1	720.1	-721.2
0.2	661.9	-655.2
0.3	639.6	-626.2
0.5	614.9	-589.9
1.0	603.3	-571.7

(d) Extreme values for bending moment

Figure E.1: Internal lining force results regarding the influence of the interface in Plaxis

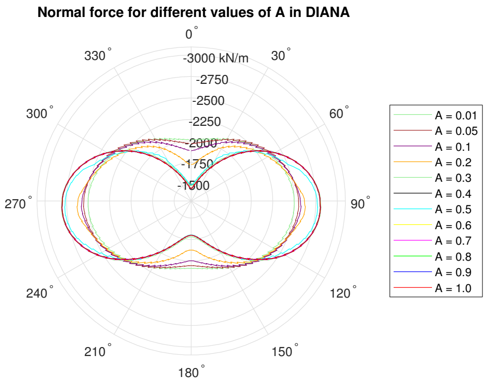

(a) Normal forces

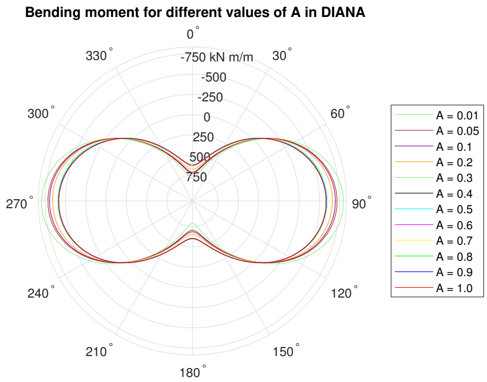

(b) Bending moments

A	Max	Min
[-]	[kN/m]	[kN/m]
0.01	-2015	-2502
0.05	-1969	-2555
0.1	-1887	-2581
0.2	-1726	-2631
0.3	-1479	-2812
0.4	-1451	-2804
0.5	-1491	-2774
0.6	-1448	-2806
0.7	-1448	-2806
0.8	-1447	-2807
0.9	-1447	-2807
1.0	-1447	-2807

(c) Extreme values for normal force

A	Max	Min
[-]	[kN m/m]	[kN m/m]
0.01	789.5	-793.9
0.05	726.8	-716.0
0.1	711.2	-696.1
0.2	675.5	-658.7
0.3	632.5	-592.0
0.4	625.3	-583.7
0.5	626.4	-591.6
0.6	625.1	-583.1
0.7	625.1	-583.0
0.8	625.0	-582.9
0.9	625.0	-582.9
1.0	625.0	-582.8

(d) Extreme values for bending moment

Figure E.2: Internal lining force results regarding the influence of the interface in DIANA

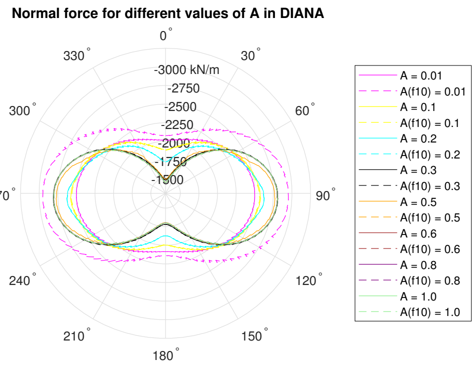

(a) Normal forces

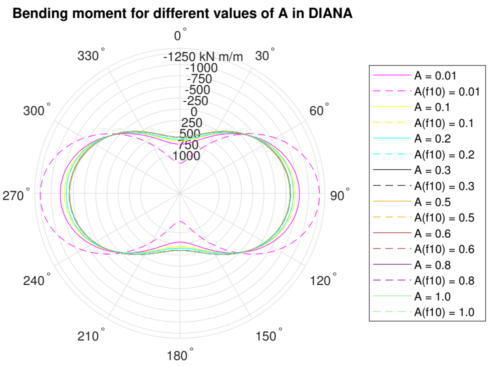

(b) Bending moments

A	Max	Min
[-]	[kN/m]	[kN/m]
0.01	-2015	-2502
0.1	-1887	-2581
0.2	-1726	-2631
0.3	-1479	-2812
0.5	-1491	-2774
0.6	-1448	-2806
0.8	-1447	-2807
1.0	-1447	-2807

(c) Extreme values for normal force for f=100

A	Max	Min
[-]	[kN m/m]	[kN m/m]
0.01	789.5	-793.9
0.1	711.2	-696.1
0.2	675.5	-658.7
0.3	632.5	-592.0
0.5	626.4	-591.6
0.6	625.1	-583.1
0.8	625.0	-582.9
1.0	625.0	-582.8

(d) Extreme values for bending moment for f=100

A	Max	Min
[-]	[kN/m]	[kN/m]
0.01	-2077	-2954
0.1	-1880	-2570
0.2	-1724	-2628
0.3	-1479	-2811
0.5	-1449	-2806
0.6	-1448	-2806
0.8	-1447	-2807
1.0	-1448	-2807

(e) Extreme values for normal force for f=10

A	Max	Min
[-]	[kN m/m]	[kN m/m]
0.01	1254	-1239
0.1	716.7	-704.4
0.2	677.5	-661.5
0.3	634.0	-594.2
0.5	625.8	-584.2
0.6	625.6	-583.7
0.8	625.3	-583.3
1.0	625.1	-583.0

(f) Extreme values for bending moment for f=10

Figure E.3: Internal lining force results regarding the influence of multiplication factor for the interface strength in DIANA

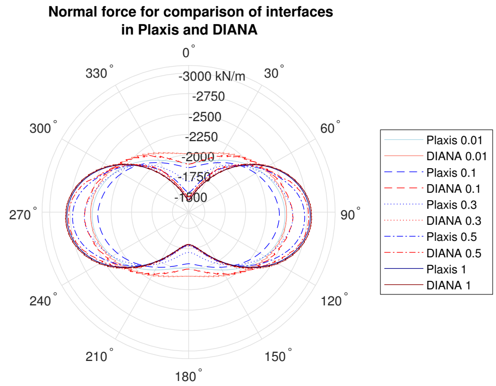

(a) Normal forces

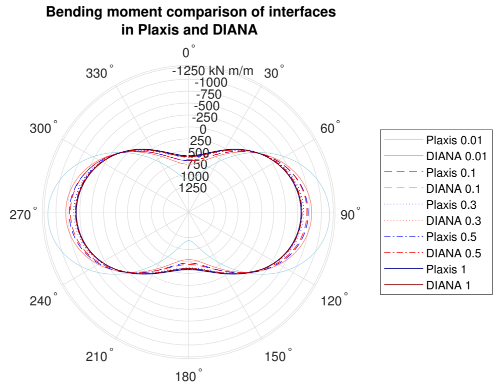

(b) Bending moments

R_{inter} [-]	Max [kN/m]	Min [kN/m]
0.01	-1900	-2482
0.1	-1842	-2418
0.3	-1674	-2583
0.5	-1542	-2728
1.0	-1454	-2794

(c) Extreme values for normal force in Plaxis

R_{inter} [-]	Max [kN m/m]	Min [kN m/m]
0.01	1194	1174
0.1	741.0	-741.6
0.3	658.2	-645.9
0.5	632.7	-608.8
1.0	620.8	-590.2

(d) Extreme values for bending moment in Plaxis

A [-]	Max [kN/m]	Min [kN/m]
0.01	-2015	-2502
0.1	-1887	-2581
0.3	-1479	-2812
0.5	-1491	-2774
1.0	-1447	-2807

(e) Extreme values for normal force in DIANA

A [-]	Max [kN m/m]	Min [kN m/m]
0.01	789.5	-793.9
0.1	711.2	-696.1
0.3	632.5	-592.0
0.5	626.4	-591.6
1.0	625.0	-582.8

(f) Extreme values for bending moment in DIANA

Figure E.4: Internal lining force results regarding the influence of the interface in Plaxis and DIANA

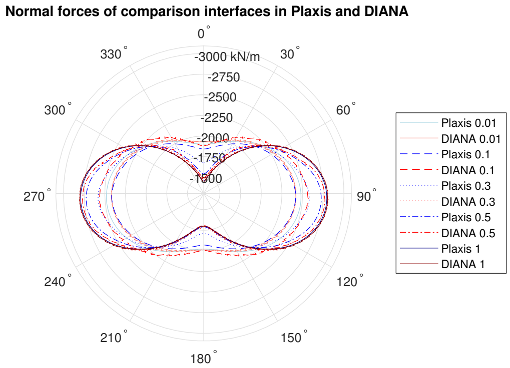

(a) Normal forces

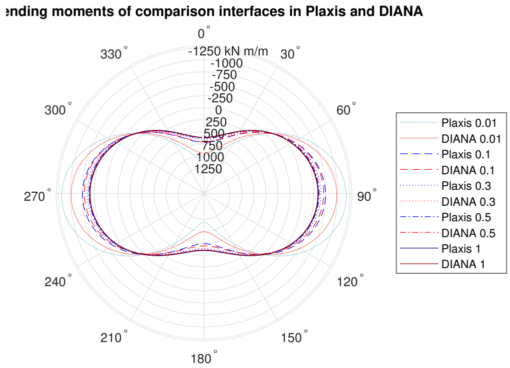

(b) Bending moments

R_{inter} [-]	Max [kN/m]	Min [kN/m]
0.01	-1900	-2482
0.1	-1842	-2418
0.3	-1674	-2583
0.5	-1542	-2728
1.0	-1454	-2794

(c) Extreme values for normal force in Plaxis

R_{inter} [-]	Max [kN m/m]	Min [kN m/m]
0.01	1194	-1174
0.1	741.0	-741.6
0.3	658.2	-645.9
0.5	632.7	-608.8
1.0	620.8	-590.2

(d) Extreme values for bending moment in Plaxis

A [-]	Max [kN/m]	Min [kN/m]
0.01	-1928	-2421
0.1	-1881	-2571
0.3	-1480	-2811
0.5	-1493	-2773
1.0	-1449	-2806

(e) Extreme values for normal force in DIANA

A [-]	Max [kN m/m]	Min [kN m/m]
0.01	987.4	-975.9
0.1	716.2	-703.6
0.3	633.9	-594.1
0.5	626.5	-592.7
1.0	625.5	-583.1

(f) Extreme values for bending moment in DIANA

Figure E.5: Results for the normal force and bending moment regarding the influence of the interface with the same strength input parameters

F

Total displacements around tunnel

Model Three

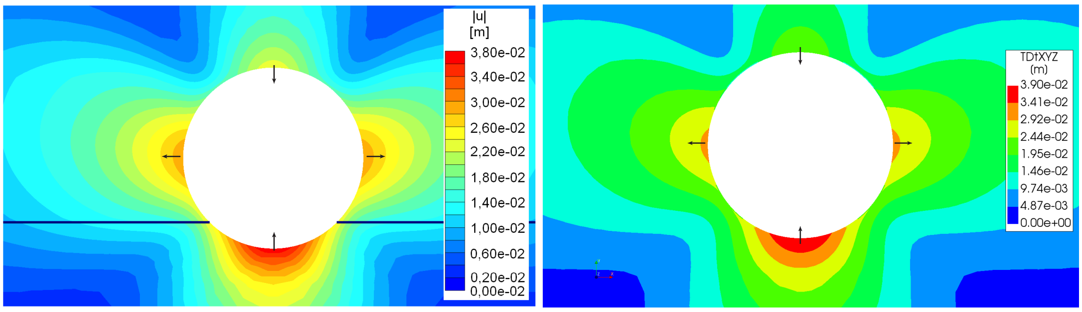

(a) Plaxis

(b) DIANA

Figure F.1: Total displacements for model three in Plaxis and DIANA

Model Four

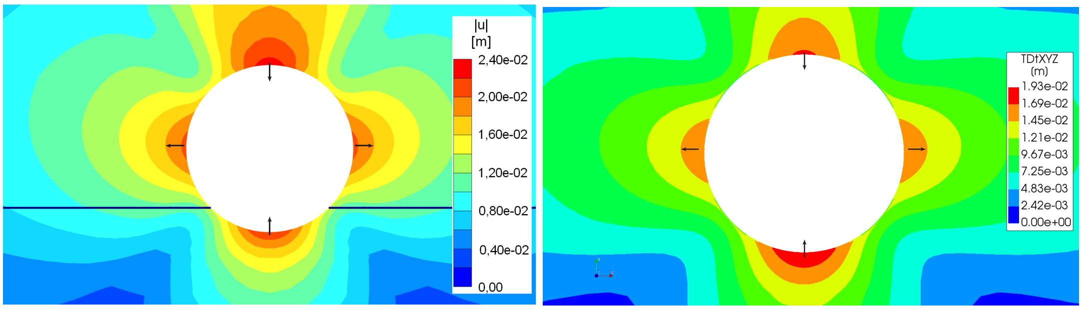

(a) Plaxis

(b) DIANA

Figure F.2: Total displacements for model four in Plaxis and DIANA

Model Five

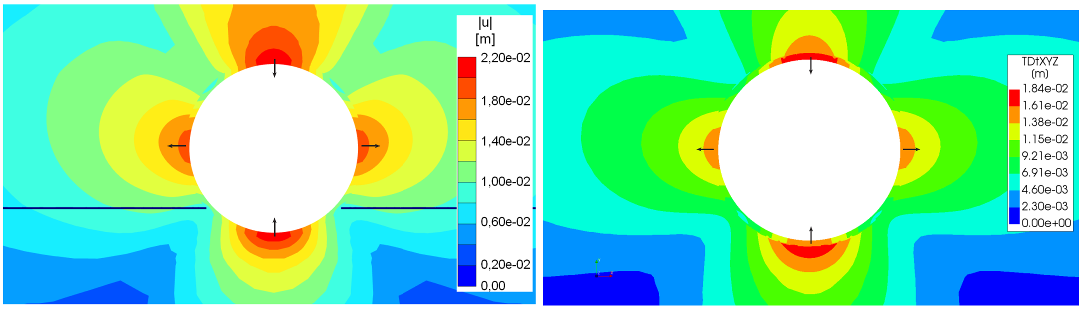

(a) Plaxis (b) DIANA

Figure F.3: Total displacements for model five in Plaxis and DIANA

Model Six

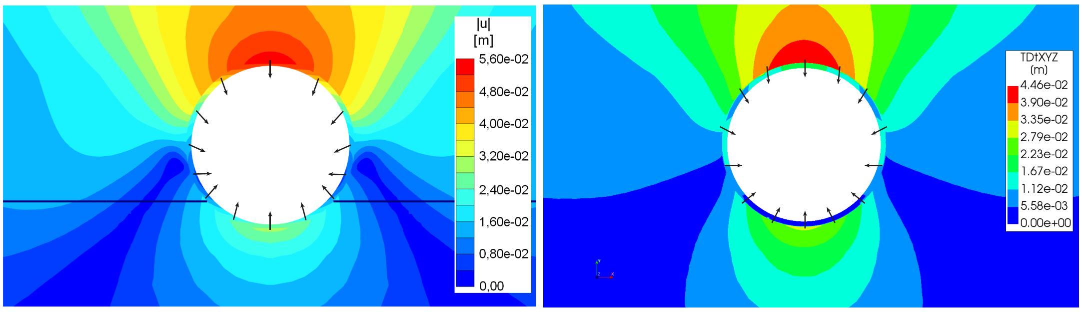

(a) Plaxis (b) DIANA

Figure F.4: Total displacements for model six in Plaxis and DIANA

Model Seven

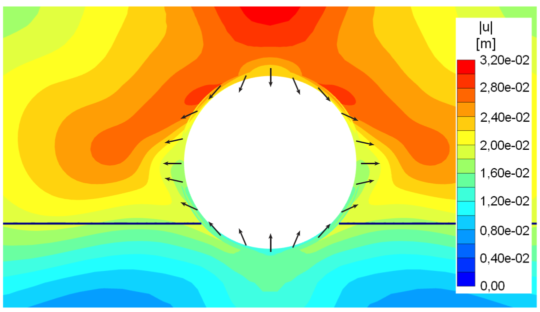

Figure F.5: Total displacements for model seven in Plaxis

Model Nine

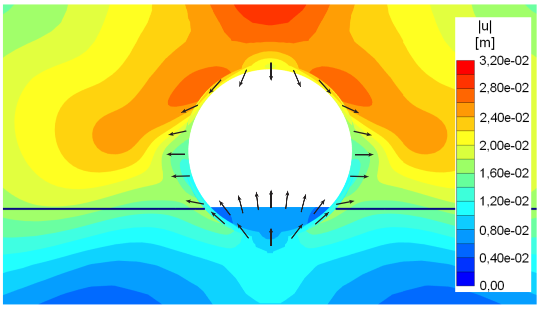

Figure F.6: Total displacements for model nine in Plaxis

3D model without construction phases

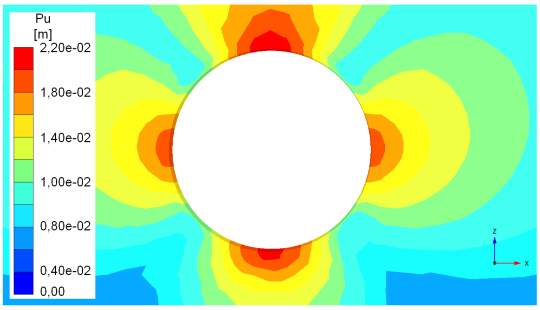

(a) Plaxis

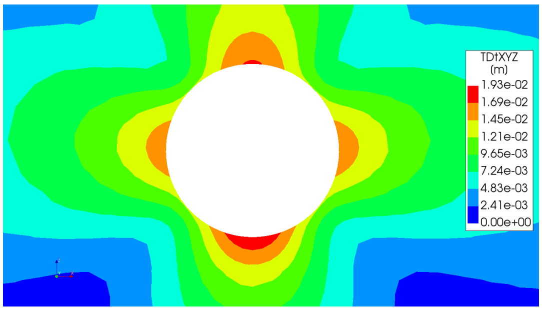

(b) DIANA

Figure F.7: Total displacements for front of 3D model without construction phases

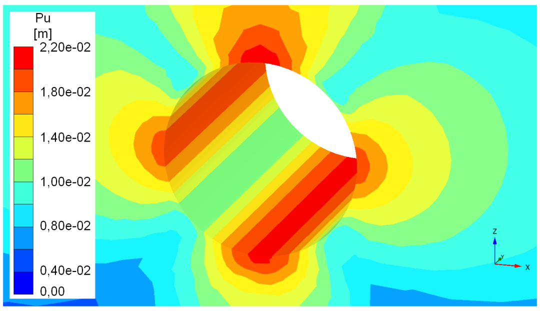

(a) Plaxis

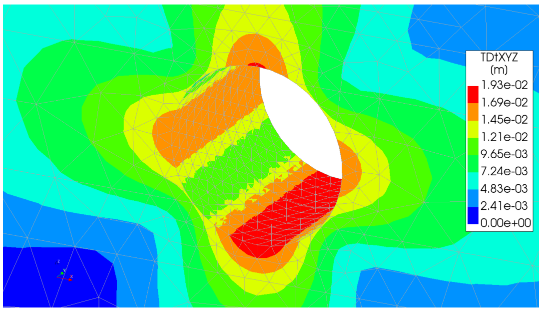

(b) DIANA

Figure F.8: Total displacements of 3D model without construction phases

G
Hardened grout stiffness sensitivity

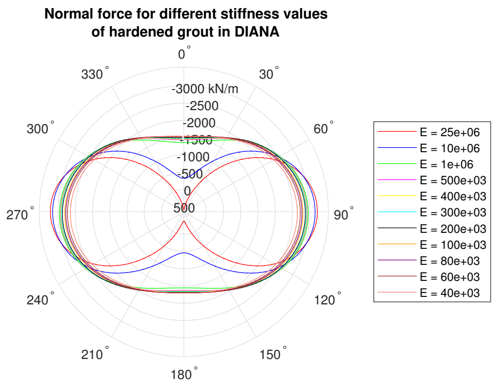

(a) Normal forces

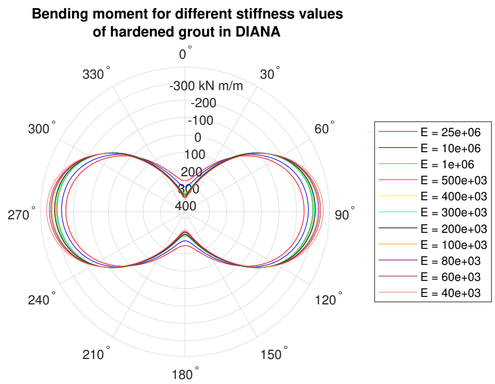

(b) Bending moments

E [kN/m^2]	Max [kN/m]	Min [kN/m]
25e+06	590.3	-3222
10e+06	-317.6	-3156
1e+06	–1358	-2958
500e+03	-1439	-2927
400e+03	-1457	-2917
300e+03	-1475	-2901
200e+03	-1495	-2875
100e+03	-1522	-2806
80e+03	-1529	-2775
60e+03	-1537	-2727
40e+03	-1544	-2642

(c) Extreme values for normal force

E [kN/m^2]	Max [kN m/m]	Min [kN m/m]
25e+06	262.3	-244.3
10e+06	296.8	-268.9
1e+06	334.8	-293.7
500e+03	338.9	-298.6
400e+03	340.1	-300.5
300e+03	341.8	-303.5
200e+03	344.5	-309.1
100e+03	351.2	-323.3
80e+03	354.2	-329.6
60e+03	358.9	-339.0
40e+03	367.1	-354.6

(d) Extreme values for bending moment

Figure G.1: Results for the normal force and bending moment for different hardened grout stiffnesses in DIANA

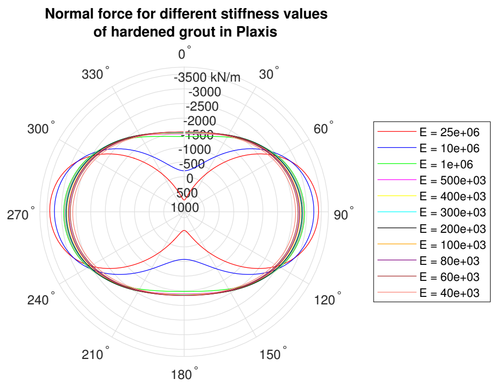

(a) Normal forces

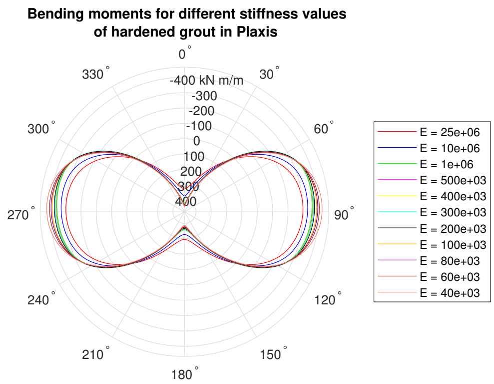

(b) Bending moments

E [kN/m^2]	Max [kN/m]	Min [kN/m]
25e+06	798.8	-3402
10e+06	-203.3	-3242
1e+06	-1372	-2925
500e+03	-1461	-2888
400e+03	-1491	-2876
300e+03	-1498	-2862
200e+03	-1515	-2835
100e+03	-1529	-2773
80e+03	-1530	-2744
60e+03	-1530	-2699
40e+03	-1524	-2616

(c) Extreme values for normal force

E [kN/m^2]	Max [kN m/m]	Min [kN m/m]
25e+06	324.3	-298.5
10e+06	370.7	-330.3
1e+06	419.9	-360.9
500e+03	424.6	-360.9
400e+03	425.8	-367.5
300e+03	427.4	-370.5
200e+03	429.3	-375.6
100e+03	431.9	-388.6
80e+03	433.8	-395.2
60e+03	436.6	-405.6
40e+03	441.7	-423.5

(d) Extreme values for bending moment

Figure G.2: Results for the normal force and bending moment for different hardened grout stiffnesses in Plaxis

H

MN-kappa diagrams 2D

MN-κ diagrams are created to calculate deformations in concrete beams. κ is the curvature of the beam and is directly related to the stiffness of the beam through:

$$\kappa = \frac{M}{EI} \tag{H.1}$$

EI is not a constant since it is influenced by cracking and plastic behaviour. Therefore κ is used to assess the deformations.

The most important features of the MN-κ diagrams will be discussed briefly. Based on the internal lining forces and the properties of the lining and the reinforcement, points for the graph are determined. Walraven [80] provides the explanation and equations for the calculation of these points:

- **Mr**: For the moment given at this point, cracks start to form in the concrete of the lining. This point has been assessed for un-reinforced concrete;
- **Mb;pl**: At this point, the concrete starts to behave plastically and irreversible deformations are occuring;
- **Ms;pl**: At this point, steel becomes in the plastic zone and irreversible deformations start occuring;
- **Current state**: The current state of the internal lining forces (red point);

From the last point onwards, either Mb;pl or Ms;pl, the curvatures in the lining are plastic until the failure point is reached. The plastic behaviour is already considered undesirable and therefore the failure point is not plotted. In reality, the internal lining forces start changing when cracking starts to occur. Therefore failure of the lining cannot be assessed with this approach.

In order to acquire the three points, a reinforcement has to be estimated. This reinforcement is estimated for model four. In order to assess which reinforcement is suitable, a unity check is done. This unity check is the ratio between the acting moment in the lining and the moment capacity of the lining. This moment capacity is calculated from the lining properties, normal force and reinforcement properties. A ratio below 1.0 is required since it means the bending moment capacity of the lining is higher than the acting bending moment. A ratio above 1.0 means failure of the reinforcement. The reinforcement properties in the lining are changed until an unity check of 0.9 is acquired.

This reinforcement is not changed throughout the different models. The purpose of this part of the research is to see what the influence of these construction phases is. Therefore, the amount of reinforcement is kept equal for all models.

The lowest normal force and the bending moment at the same location in servicability limit state are taken for determination of these relations. In reality, the reinforcement is determined based on the ultimate limit state instead of the serviceability limit state. Again, the purpose is not to acquire the right reinforcement but to assess the influence of the different construction phases and therefore serviceability limit state will suffice. In reality, the lowest normal force and the matching bending moment might not be the normative lining forces. Therefore in reality, many points along the lining are assessed to calculate the reinforcement. As mentioned earlier, the influence of the construction phases is being assessed, not the reinforcement. Therefore the current approach is sufficient.

H.1. Plaxis

Model One

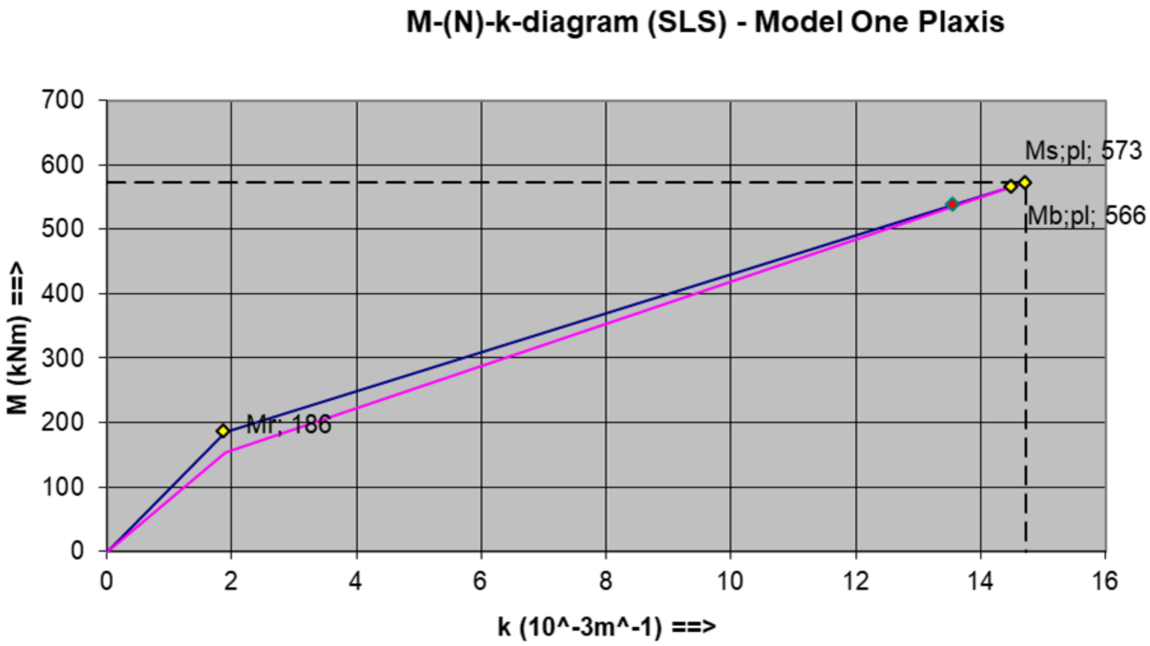

Figure H.1: MN-kappa diagram Model One in Plaxis

Model Two

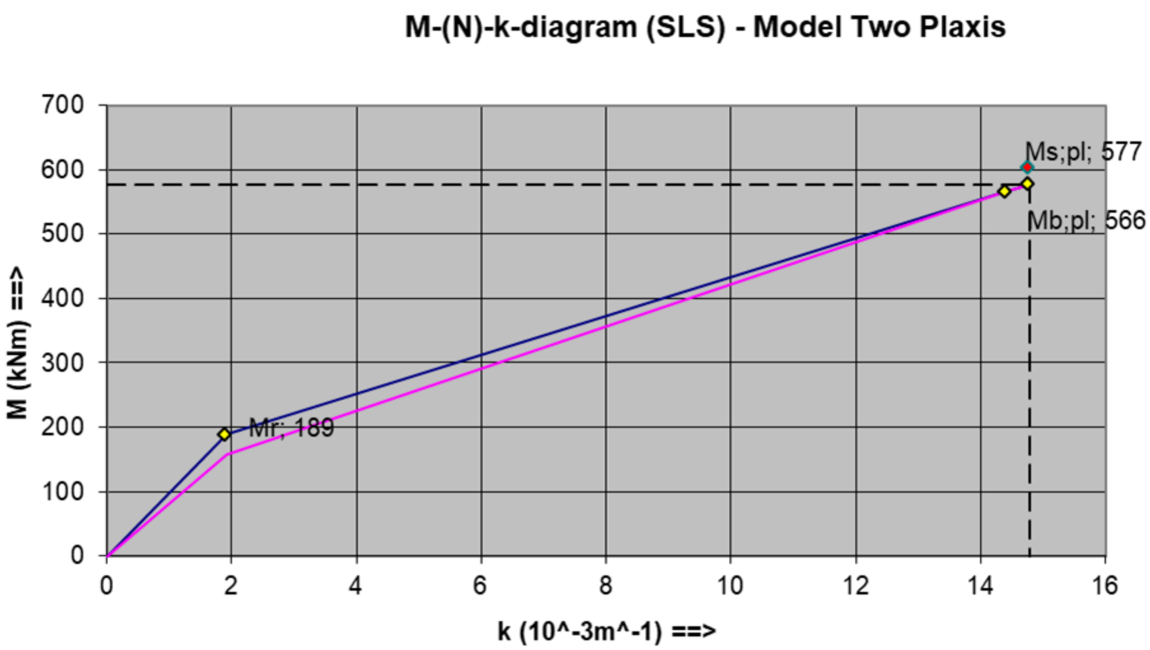

Figure H.2: MN-kappa diagram Model Two in Plaxis

Model Three

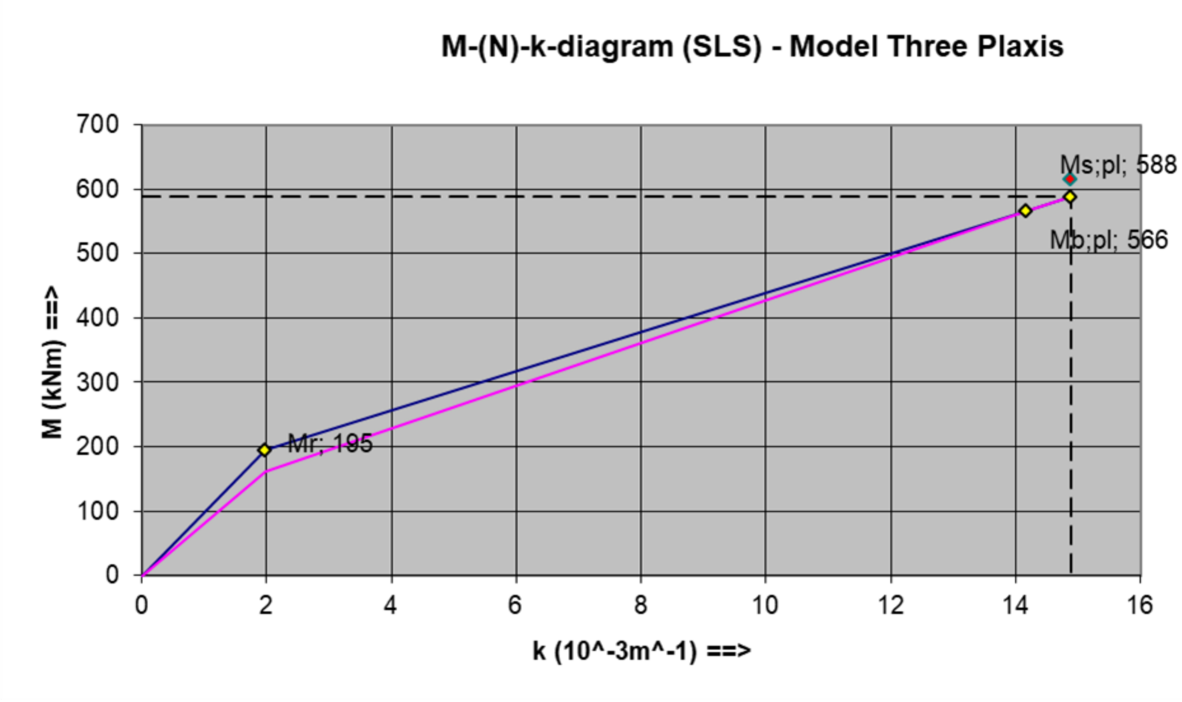

Figure H.3: MN-kappa diagram Model Three in Plaxis

Model Four

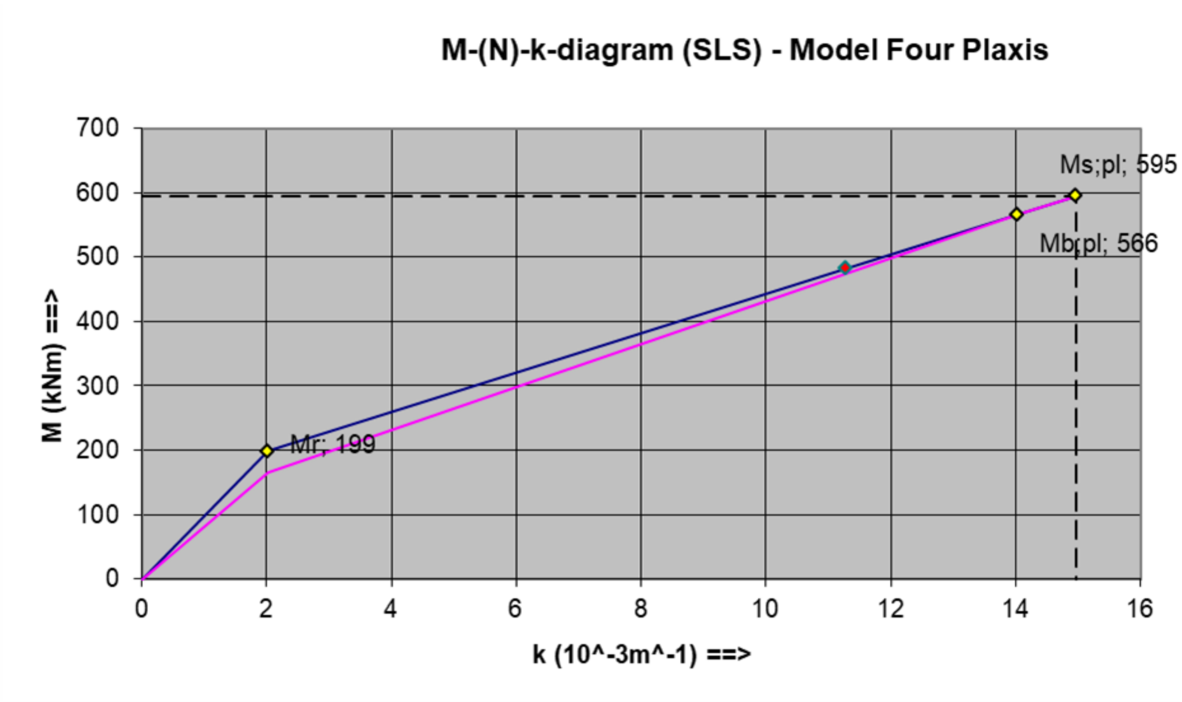

Figure H.4: MN-kappa diagram Model Four in Plaxis

Model Five

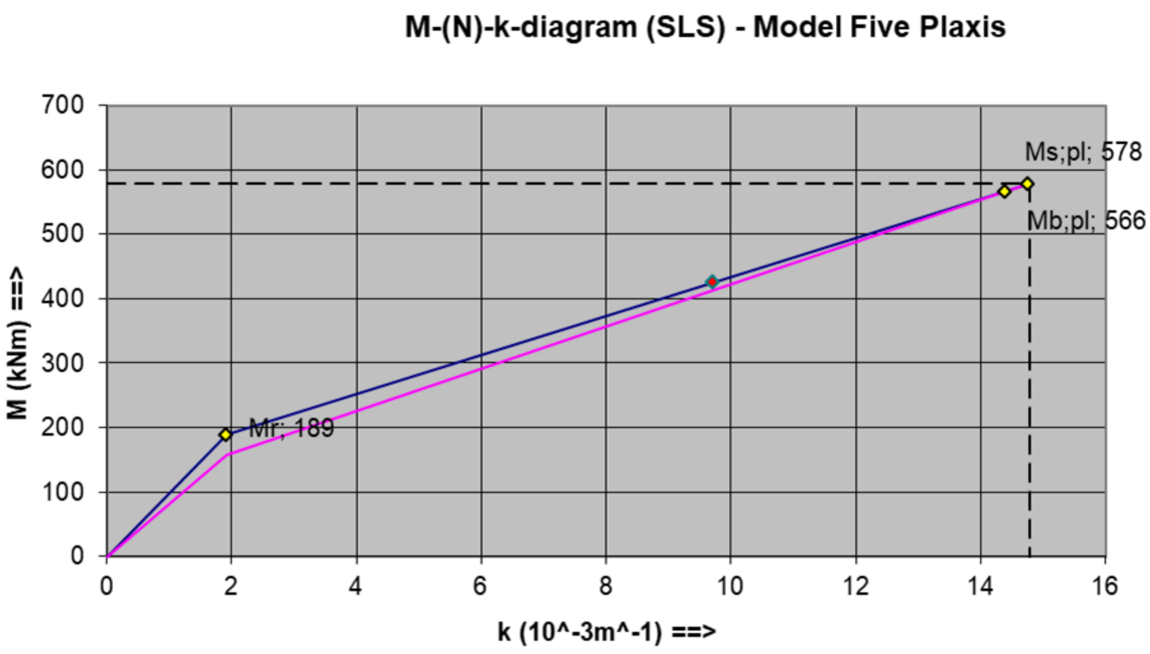

Figure H.5: MN-kappa diagram Model Five in Plaxis

Model Six

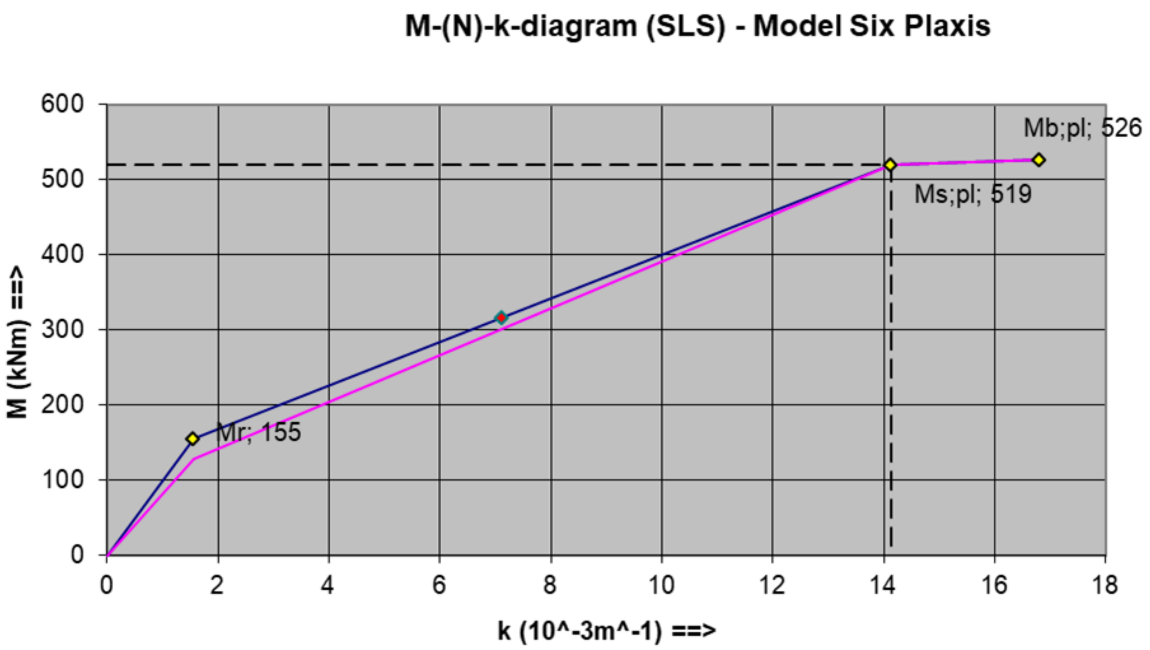

Figure H.6: MN-kappa diagram Model Six in Plaxis

Model Seven

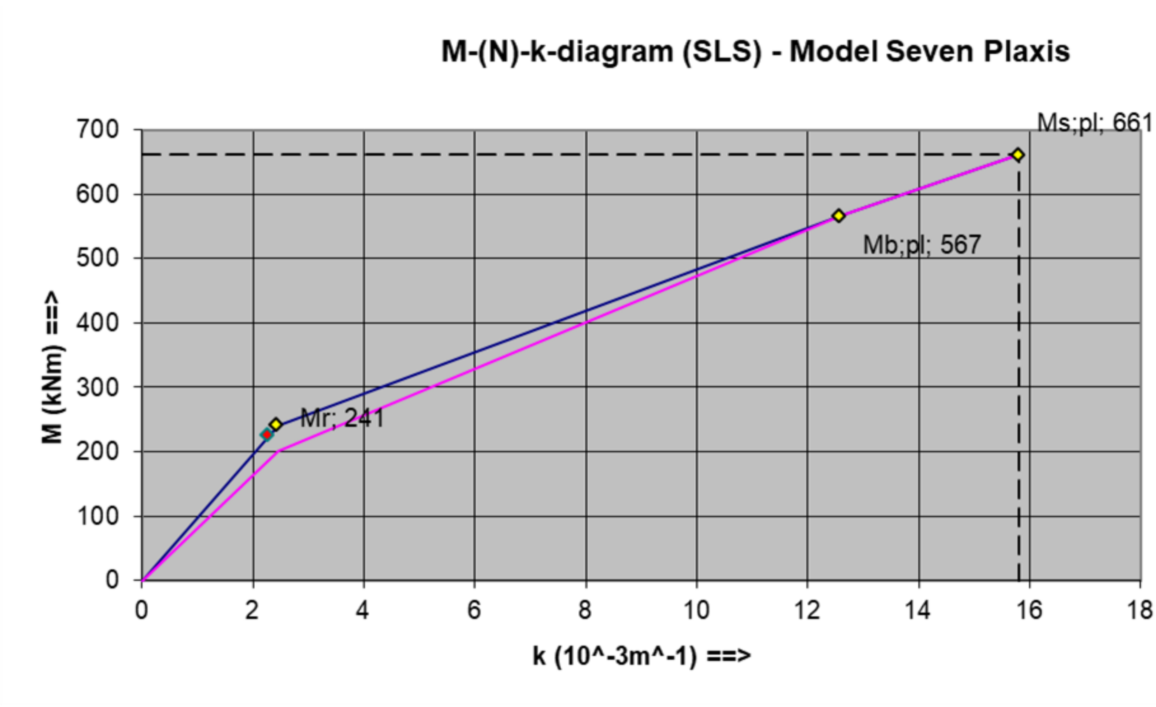

Figure H.7: MN-kappa diagram Model Seven in Plaxis

Model Eight

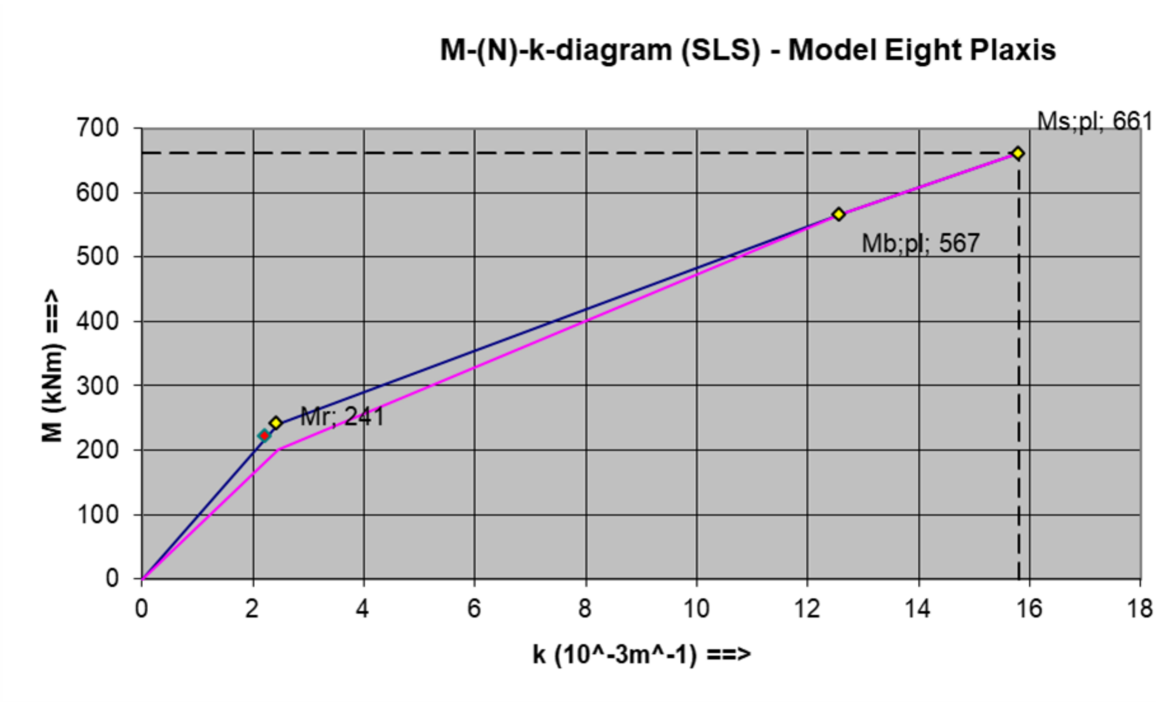

Figure H.8: MN-kappa diagram Model Eight in Plaxis

Model Nine

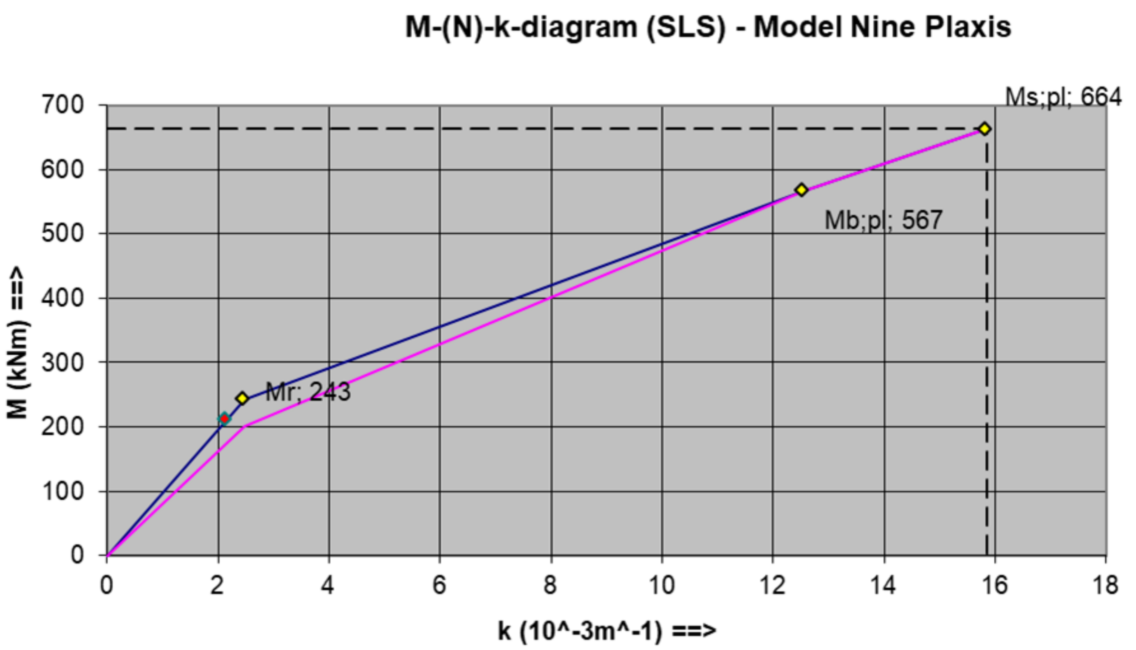

Figure H.9: MN-kappa diagram Model Nine in Plaxis

Model Ten

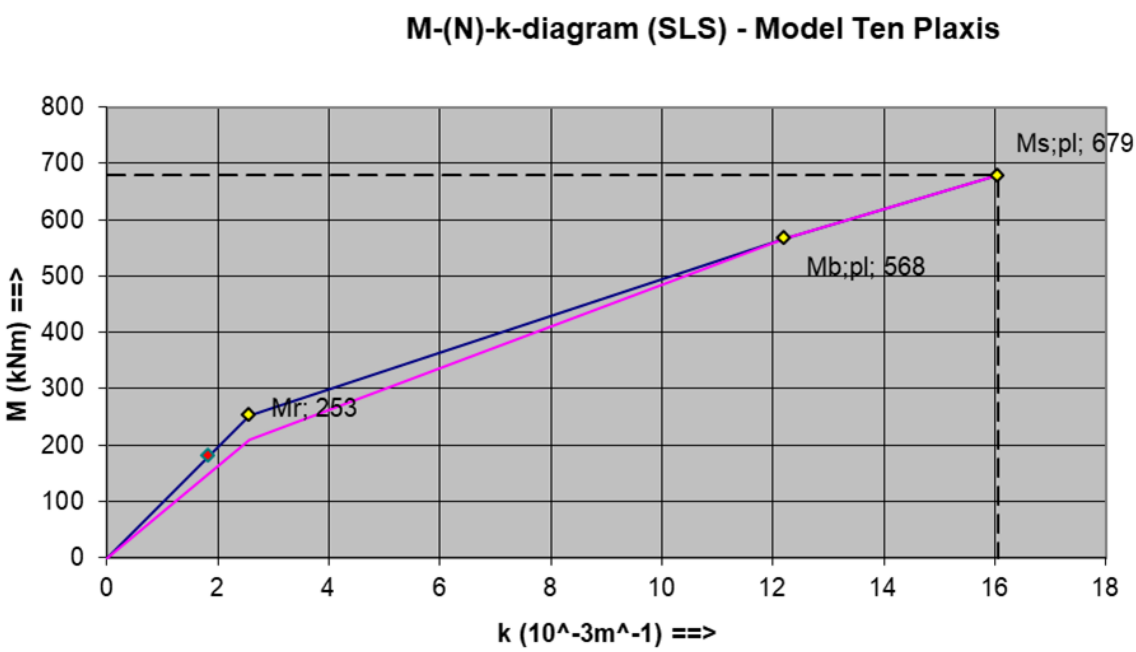

Figure H.10: MN-kappa diagram Model Ten in Plaxis

Model Eleven

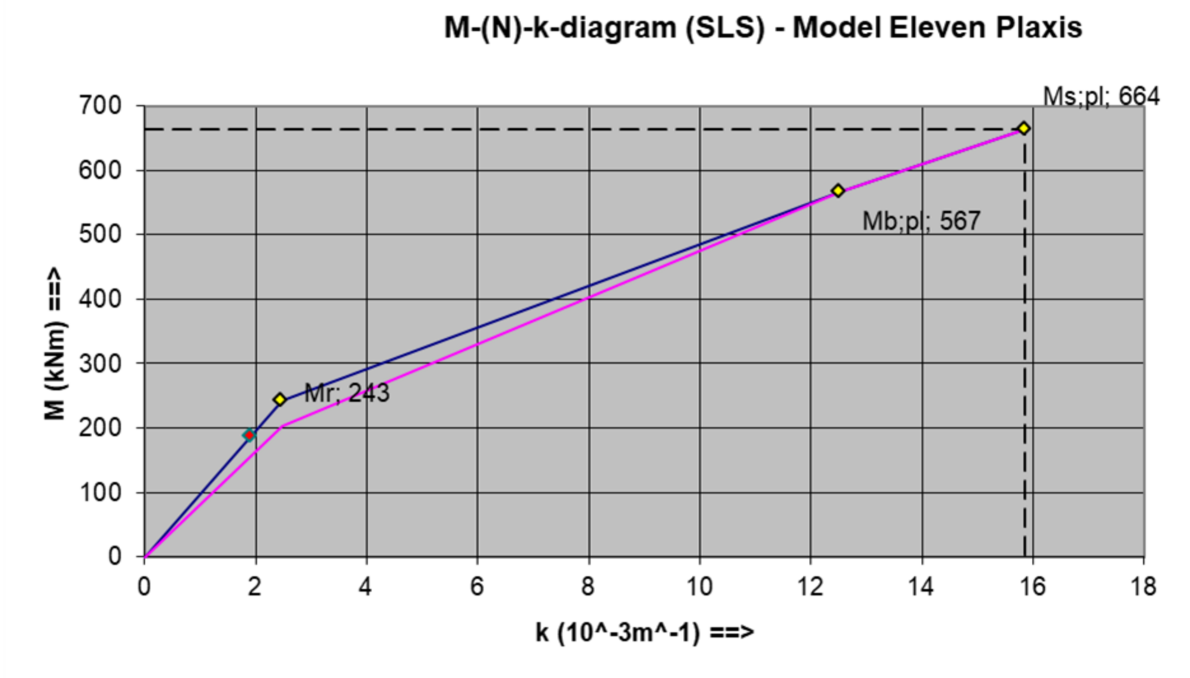

Figure H.11: MN-kappa diagram Model Eleven in Plaxis

Model Twelve

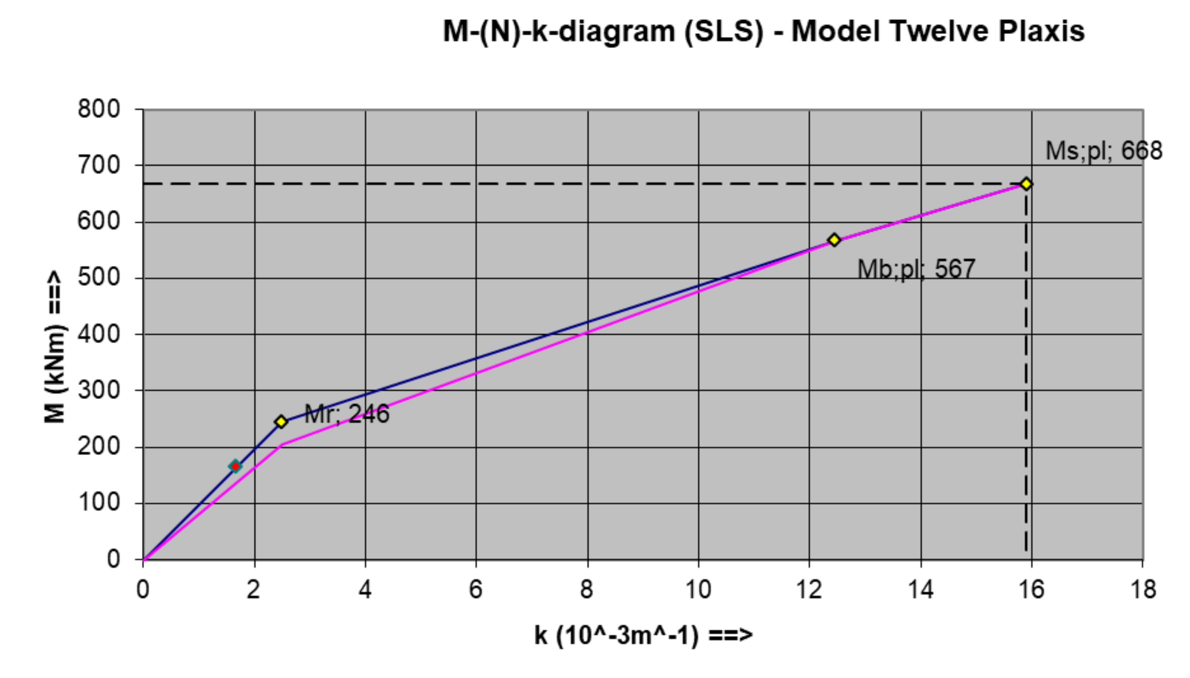

Figure H.12: MN-kappa diagram Model Twelve in Plaxis

H.2. DIANA

Model One

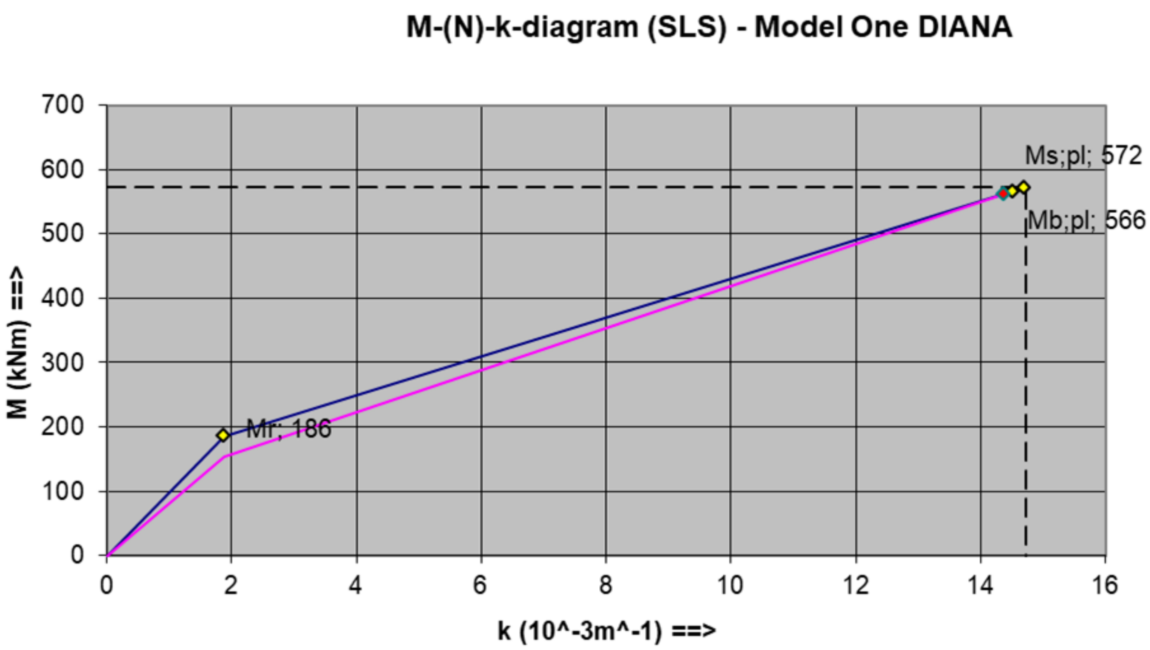

Figure H.13: MN-kappa diagram Model One in DIANA

Model Two

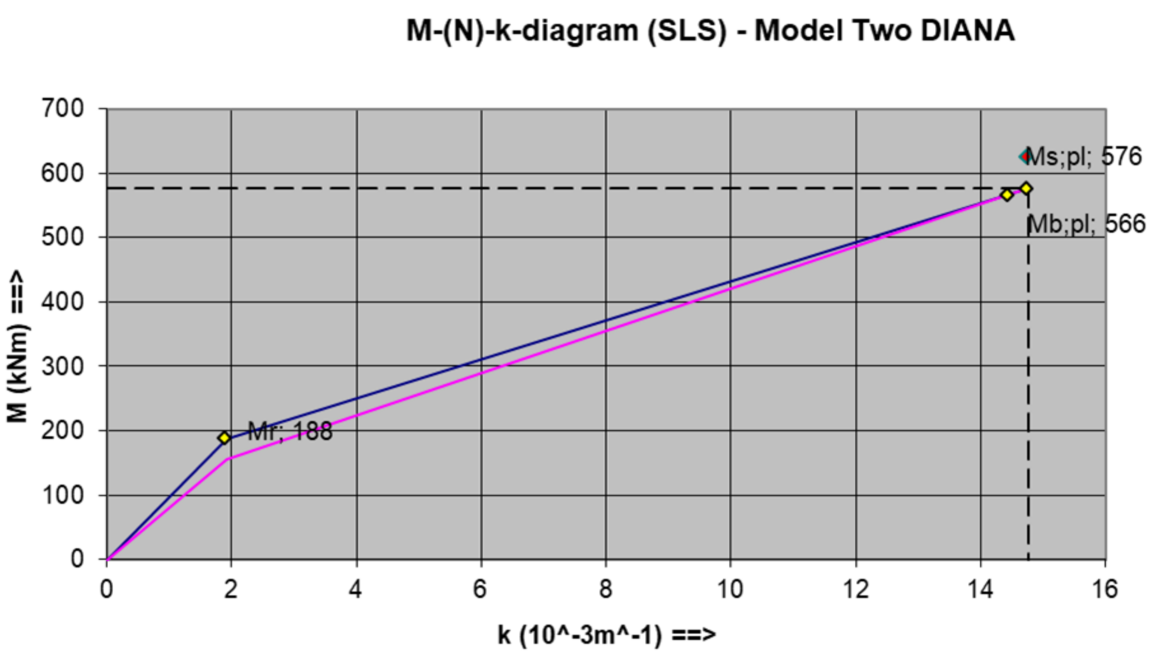

Figure H.14: MN-kappa diagram Model Two in DIANA

Model Three

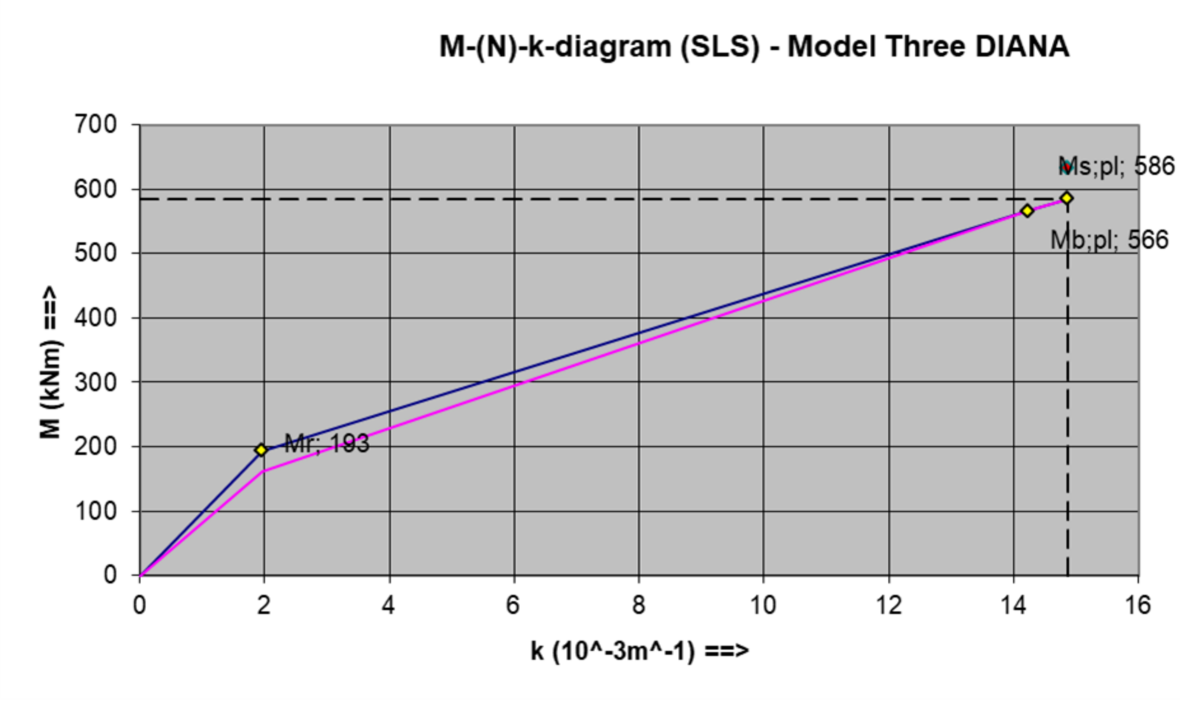

Figure H.15: MN-kappa diagram Model Three in DIANA

Model Four

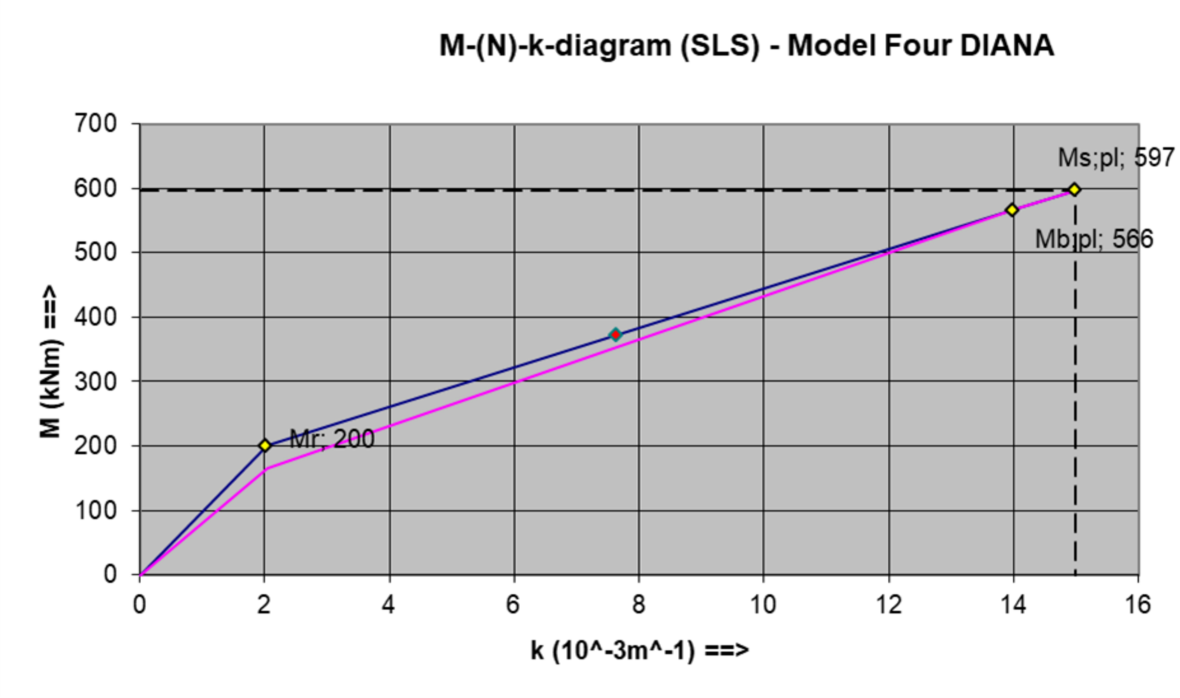

Figure H.16: MN-kappa diagram Model Four in DIANA

Model Five

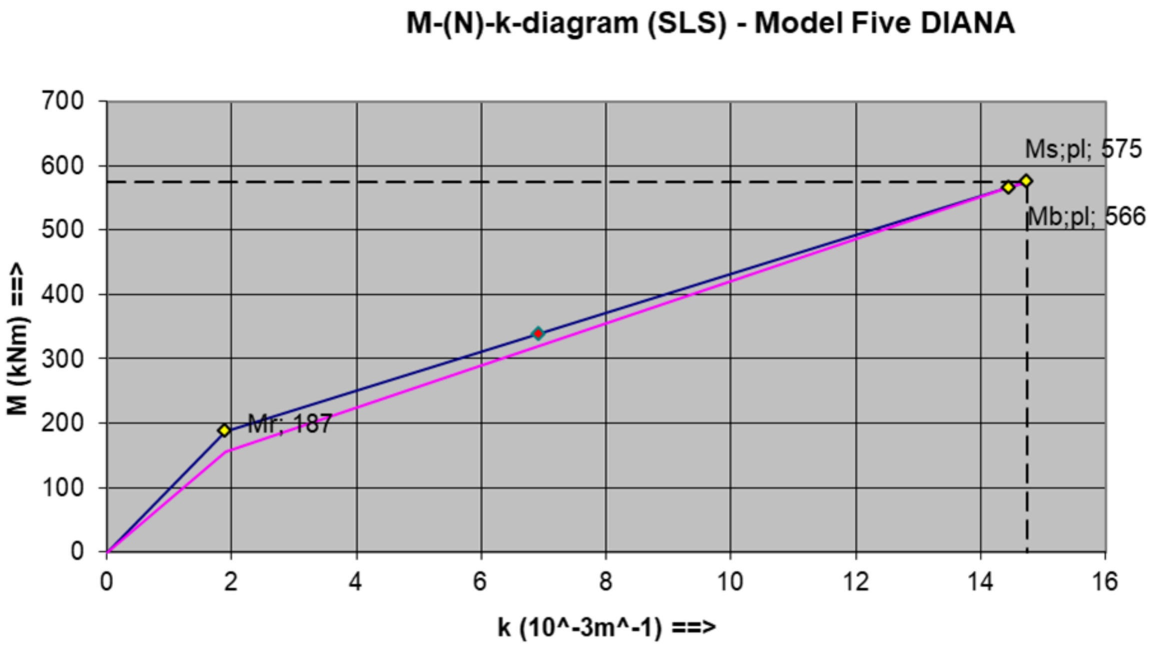

Figure H.17: MN-kappa diagram Model Five in DIANA

Model Six

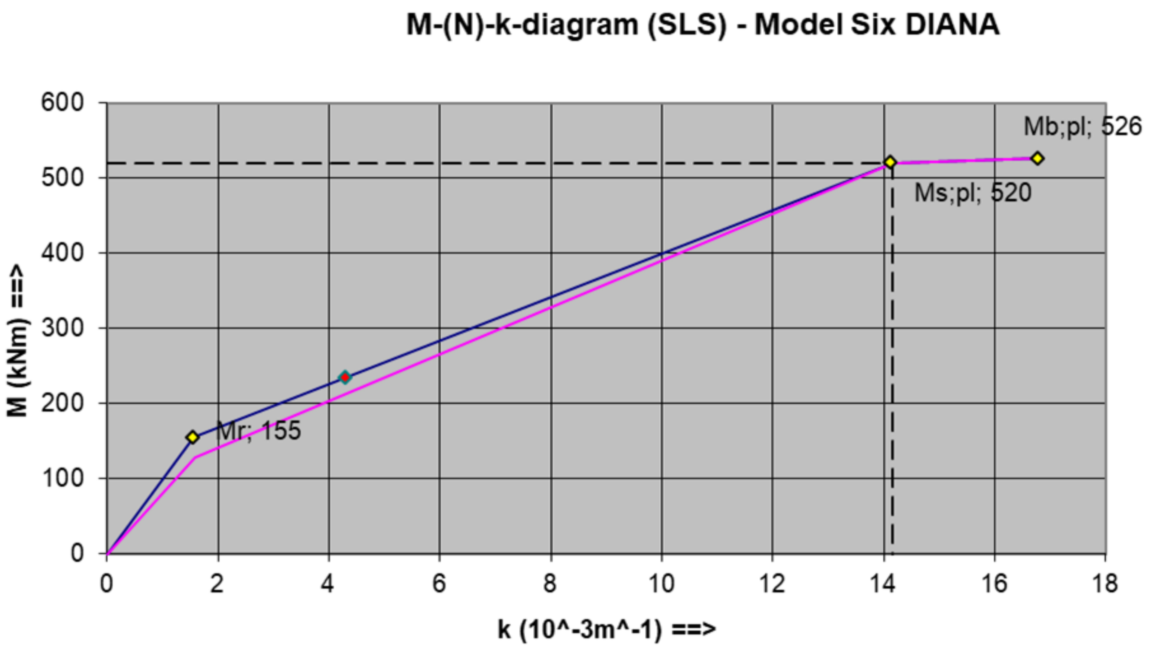

Figure H.18: MN-kappa diagram Model Six in DIANA

I

One-ring models comparison

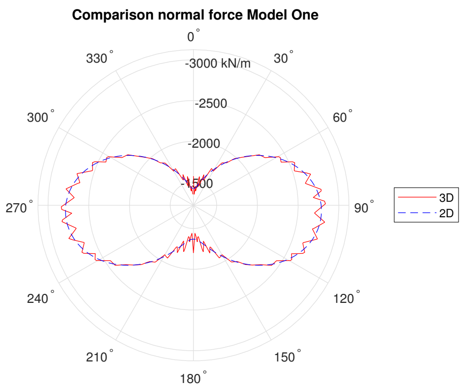

(a) Normal forces

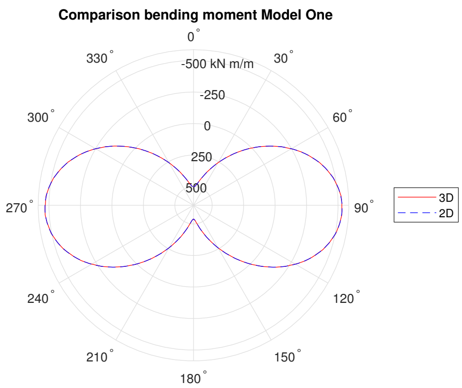

(b) Bending moments

Figure I.1: Results for the normal force and bending moment for model one in 2D and 3D

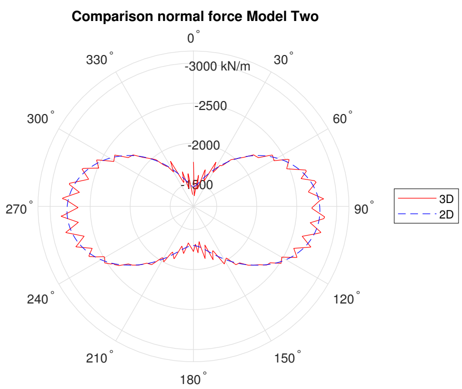

(a) Normal forces

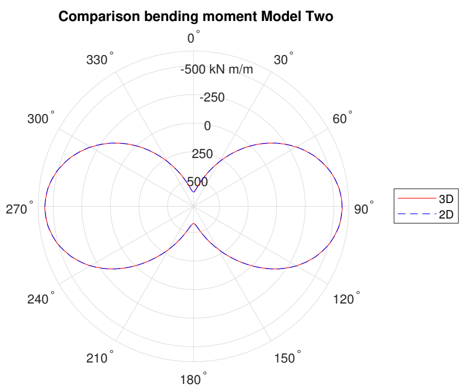

(b) Bending moments

Figure I.2: Results for the normal force and bending moment for model two in 2D and 3D

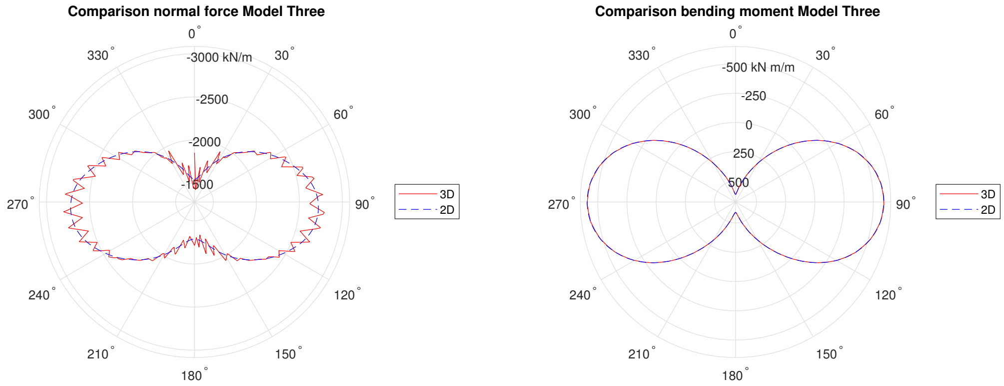

(a) Normal forces (b) Bending moments

Figure I.3: Results for the normal force and bending moment for model three in 2D and 3D

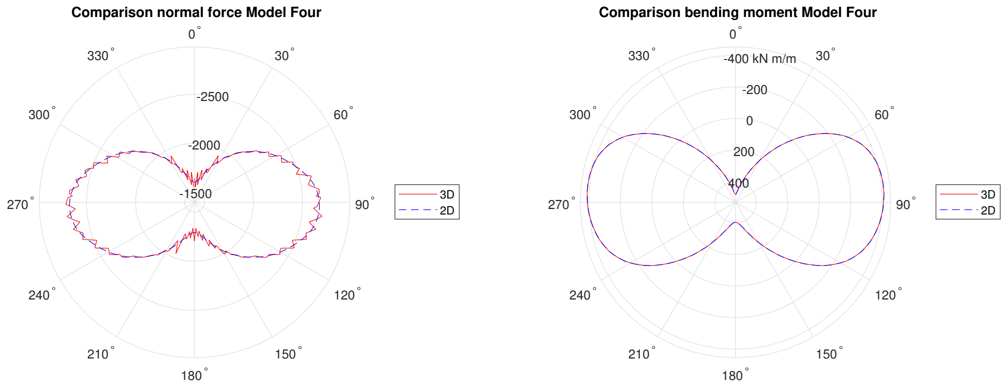

(a) Normal forces (b) Bending moments

Figure I.4: Results for the normal force and bending moment for model four in 2D and 3D

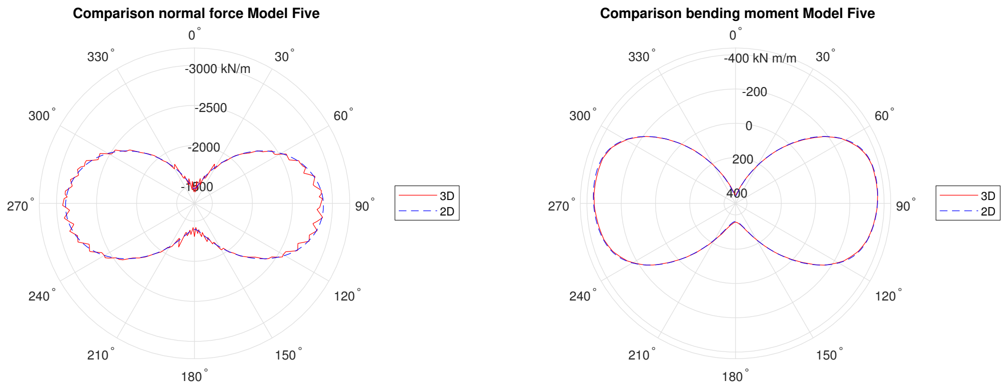

(a) Normal forces (b) Bending moments

Figure I.5: Results for the normal force and bending moment for model five in 2D and 3D

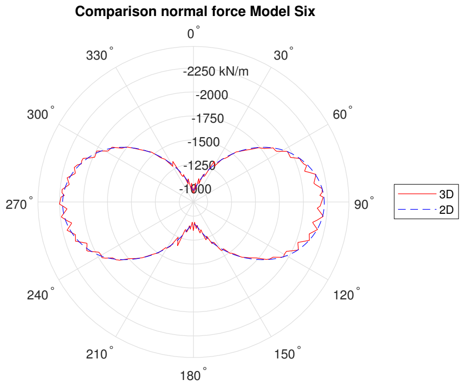

(a) Normal forces

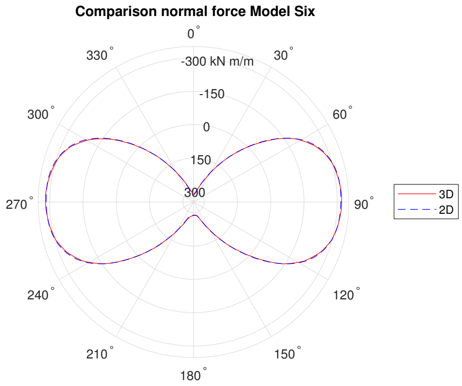

(b) Bending moments

Figure I.6: Results for the normal force and bending moment for model six in 2D and 3D

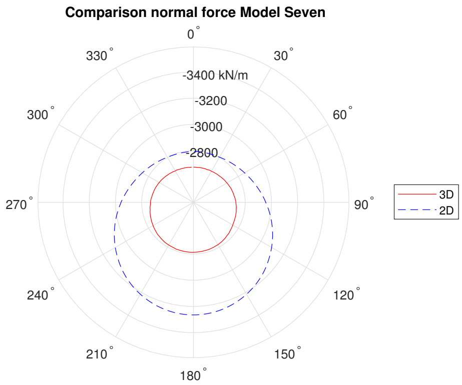

(a) Normal forces

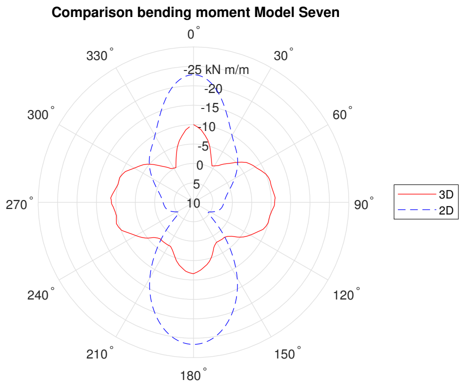

(b) Bending moments

Figure I.7: Results for the normal force and bending moment for model seven in 2D and 3D with drained analysis

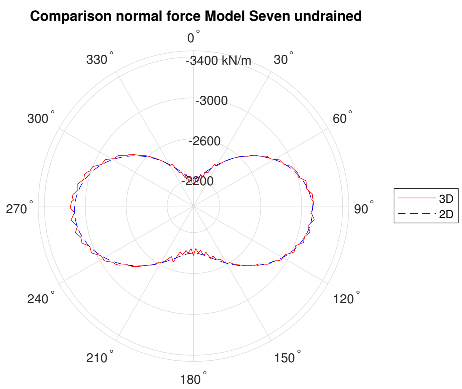

(a) Normal forces

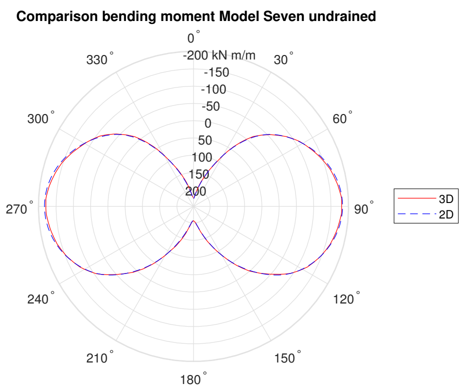

(b) Bending moments

Figure I.8: Results for the normal force and bending moment for model seven in 2D and 3D with undrained analysis

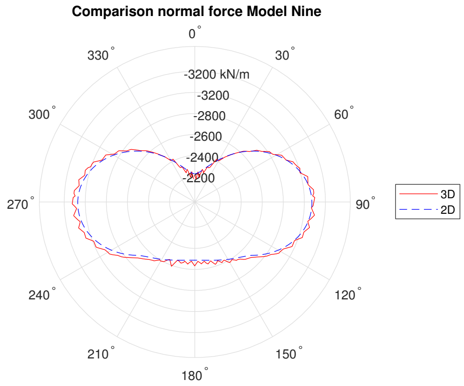

(a) Normal forces

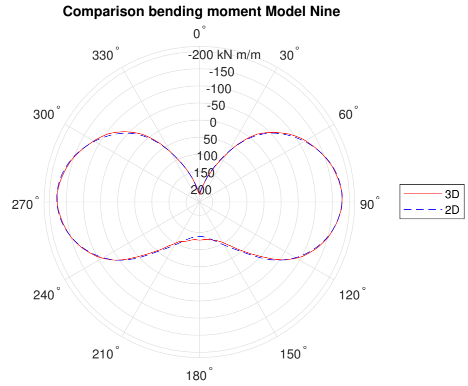

(b) Bending moments

Figure I.9: Results for the normal force and bending moment for model nine

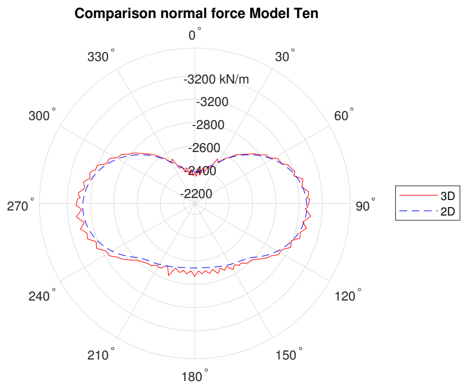

(a) Normal forces

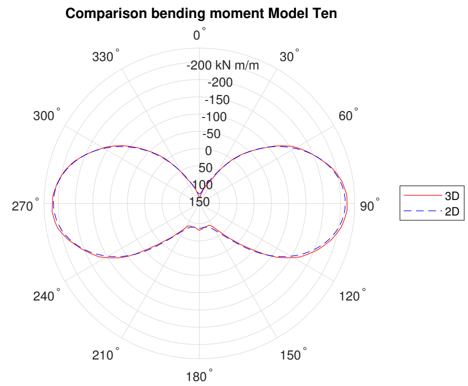

(b) Bending moments

Figure I.10: Results for the normal force and bending moment for model ten